The Dissertation Committee for Isaac Blaine Smith Certifies that this is the approved version of the following dissertation:

On The Spiral Troughs Of Mars

Committee:

John W. Holt, Supervisor

Alan D. Howard

Gary Kocurek

David Mohrig

Wonsuck Kim

Donald D. Blankenship

On the Spiral Troughs of Mars

by

Isaac Blaine Smith, B.S., M.S.

Dissertation

Presented to the Faculty of the Graduate School of

The University of Texas at Austin

in Partial Fulfillment

of the Requirements

for the Degree of

Doctor of Philosophy

The University of Texas at Austin

August 2013

Dedication

I want to dedicate this dissertation to my friends and family, especially my mom, who has shown me what it means to work hard for what you want.

Acknowledgements

This work was supported by many sources. I would like to thank NASA for generous contributions via grants NAG5-12693 and NNX10AO26G and the NASA Earth and Space Science Fellowship NNX10AT24H. Additionally, the Jackson School of Geosciences and Gayle White Fellowship at the University of Texas Institute for Geophysics supported portions of my research. Le Laboratoire de Météorologie Dynamique (LMD) in Paris, France served as an excellent host institution during one semester of off campus research. Some special people contributed to this work. I thank Charles Brothers and Scott Kempf for tireless support. Sarah Christian gave me a big leg up in looking at radargrams, and Gary Parker provided introduced me to the cyclic step model on which I base many of my interpretations. I also want to thank my committee members for supporting the work through classes and insight: Alan Howard, David Mohrig, Gary Kocurek, Donald Blankenship, Wonsuck Kim, and my advisor John W. Holt. This project was fascinating and rewarding. I owe much thanks to my advisor for pointing me in this direction, which has been a highlight of my life. Lastly, I want to thank my mom, father, and brother for supporting me along the way, especially my mom, who always encouraged me to dream big and look at the stars.

On The Spiral Troughs Of Mars

Isaac Blaine Smith, Ph.D.
The University of Texas at Austin, 2013

Supervisor: John W. Holt

The north and south polar layered deposits (NPLD and SPLD respectively) of Mars are 2 – 3 km thick and mostly ice, comprising nearly all of the known water reserves on Mars. They are commonly believed to hold a detailed record of recent (~10 – 100 Myr) climate within their layers. Dominating the surface of the NPLD, intriguing spiral depressions called troughs, exhibit a pinwheel appearance.

In late 2006, the Shallow Radar (SHARAD) instrument began making observations. SHARAD can detect internal structure within the PLD, making observations that are impossible with instruments that only inspect the surface. SHARAD data reveals a unique stratigraphic record associated with trough formation and migration. The troughs did not exist during deposition of the first half of NPLD accumulation but initiated some 1000 m below the current surface and have migrated as much as 100 km northward. Three processes are responsible for this migration: wind transport, insolation induced sublimation, and atmospheric deposition.

I synthesize work from ground penetrating radar, optical imagery, established analogs, and atmospheric modeling in order to derive a process model that describes trough formation and evolution, including migration. The NPLD spiral troughs belong to a larger classification of features called cyclic steps, which can exist in either erosional or depositional environments. On the SPLD, troughs and a variety of other features exist. While SPLD features are more complex than NPLD troughs, they exist due to the same three processes.

Table of Contents

List of Tables

List of Figures

Chapter 1: Onset and migration of spiral troughs on Mars

The landscape of the north polar layered deposits of Mars (NPLD) is dominated by a pinwheel array of enigmatic spiral troughs [*Cutts et al*., 1979]. The troughs have intrigued planetary scientists since the Mariner 9 spacecraft returned the first close-up image in 1972, but conclusive evidence of their origin has remained elusive. Debate continues regarding all aspects of the troughs, including the possibility that they have migrated [*Howard*, 1978, 2000; *Howard et al*., 1982; *Squyres*, 1979], their age in relation to the current NPLD surface [*Tanaka et al*., 2008], and whether they are fundamentally erosional [*Kolb and Tanaka*, 2001; *Tanaka et al*., 2008] or constructional [*Howard et al*., 1982; *Squyres*, 1979] features. The troughs are probably related to climatic processes [*Milkovich and Head*, 2005a; *Squyres*, 1979], yet the nature of this relationship has remained a mystery. Previous data characterizing only the exposed NLPD surface were insufficient to test these hypotheses. Here we show that the central spiral troughs initiated after deposition of three-quarters of the NPLD, quickly reached a stable morphology and migrated approximately 65 kilometers poleward and 600 meters in altitude over the past two million years or so. Our radar stratigraphy rules out hypotheses of erosional incision post-dating deposition [*Kolb and Tanaka*, 2001; *Pelletier*, 2004; *Tanaka et al*., 2008; *Winebrenner et al*., 2008], and instead largely validates an early hypothesis for constructional trough migration [*Howard*, 1978, 2000; *Howard et al*., 1982; *Squyres*, 1979] with wind transport and atmospheric deposition as dominant processes. These results provide hard constraints for paleo-climate models and a new context for evaluating imagery, spectral data, and now radar sounding data, the better to understand the link between orbital parameters and climate, the role of climate in shaping the polar

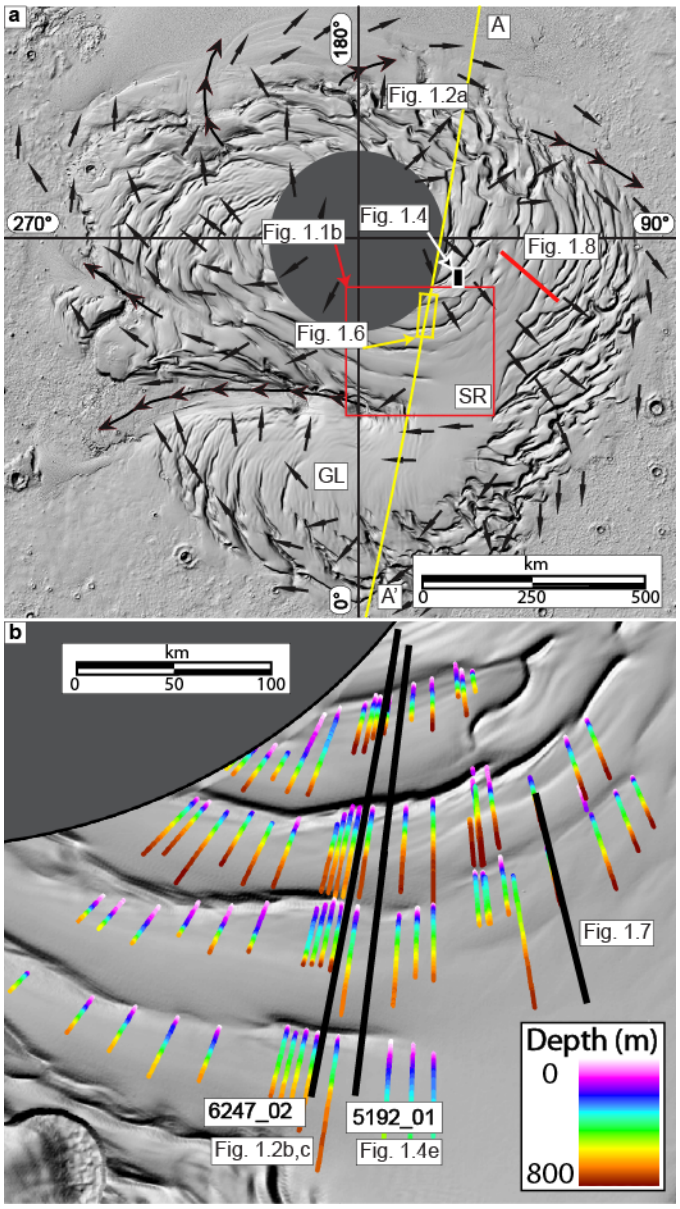

Figure 1.1: North polar layered deposits (NPLD) with locations of data. *a, Shaded-relief NPLD surface from MOLA elevation data [Smith et al., 2001] showing morphology of troughs, overall wind patterns from wind streak mapping [Howard 2000] (black arrows) and locations of other figures. b, Upward projection of mapped discontinuities. Colors indicate trough migration path (TMP) depth below surface. Location of orbit segments indicated in black.*

ice of Mars, and eventually, the age of the polar deposits themselves [*Cutts and Lewis*, 1982; *Fishbaugh and Head*, 2005; *Head et al.*, 2003; *Milkovich and Head*, 2005a].

The spiral troughs of the NPLD (Figure 1.1a) were found in Mariner and Viking imagery to have layers exposed on their equator-facing (northern) slopes, whereas their pole-facing (southern) slopes showed no such layers [*Cutts*, 1973b; *Howard*, 1978; *Soderblom et al.*, 1973]. This observation implied erosion on the equator-facing slope and deposition on the pole-facing slope, leading to a hypothesis of northward scarp migration [*Howard et al.*, 1982]. The process proposed to explain such migration involves uniform deposition over the region accompanied by preferential

erosion of the equator-facing slope due to solar ablation, along with wind transport of eroded material to the pole-facing slope by katabatic winds.

In contrast to this constructional migration scenario, a number of other hypotheses have been proposed that support spiral trough formation only after NPLD deposition. Such mechanisms include random erosion organizing into large-scale spirals [*Pelletier*, 2004], differential rotation between the inner and outer deposits during glacial flow [*Weijermars*, 1986; *Zeng et al*., 2008a], albedo contrasts from wind-deposited dust [*Ng and Zuber*, 2006a], along-trough wind erosion [*Cutts*, 1973b; *Tanaka et al*., 2008], accublation derived from upward flow beneath the troughs [*Fisher*, 2000]. The wide range of ideas put forth in the past three decades regarding these major features emphasizes how limited is our knowledge of fundamental processes governing polar ice on Mars.

Although they are essential to our current understanding of stratigraphy in the polar layered deposits, optical techniques allow only the interpretation of layers that have been exposed by erosion. Radar has been instrumental in mapping subsurface stratigraphy within ice sheets on Earth since the 1970s, and more recently, two orbiting radars began collecting data at Mars: Mars Advanced Radar for Subsurface and Ionospheric Sounding (MARSIS) [*Picardi et al*., 2005] on Mars Express and the Shallow Radar (SHARAD) instrument [*Seu et al*., 2007b] on the Mars Reconnaissance Orbiter. MARSIS was designed to probe deeply at the expense of resolution, while SHARAD, with a higher frequency and bandwidth (see Methods), has a vertical resolution of about 10 m in water ice and easily penetrates the ice-rich polar layered deposits [*Grima et al*., 2009; *Phillips et al*., 2008b] to reveal internal layering and structure. Layers observed in radar are assumed to exhibit the same slopes and general structures as those in optical data, on the basis of gross comparisons in troughs (Figures 1.2 and 1.6), theoretical

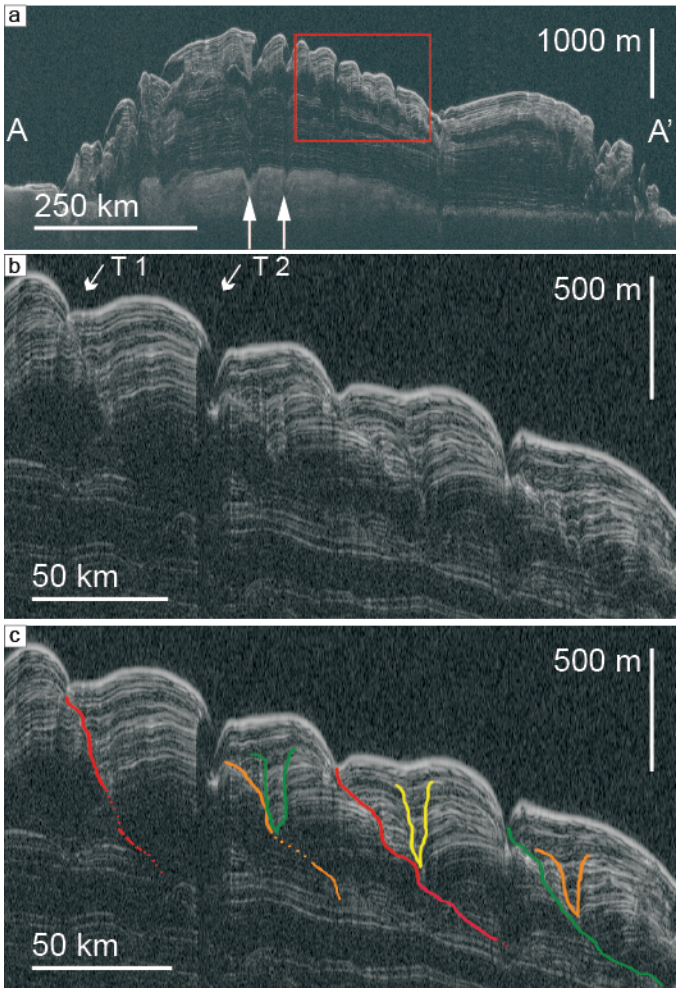

Figure 1.2: SHARAD data over troughs*. a, observation 624702 (location indicated with yellow line in Fig. 1.1a), with vertical axis converted from time delay to depth assuming dielectric constant of water ice. White arrows point to anomalies resulting from depth correction algorithm where MOLA topography is missing. Vertical exaggeration is ~90:1. b, Expanded view of troughs (box in 1.1a) showing discontinuities and V-Shaped structures in the upper 500 m. White arrows indicate troughs shown in Figure 1.6. c, Same as Fig. 1.2b but with interpretation of data to delineate structures.*

studies [*Nunes and Phillips*, 2006] and detailed correlations [*Milkovich and Plaut*, 2008].

Below the spiral troughs, sloping discontinuities visible in SHARAD data interrupt sub-horizontal layering in the uppermost section [*Phillips et al.*, 2008b] (Figure 1.2). These discontinuities have slopes between 0.33 and 1.65 degrees, penetrate to between 500 and 700 m below the surface, and, in most cases, intersect the surface at a trough (Figure 1.2b and 1.2c). The discontinuities are contiguous up to 65 km in length and always point down and to the south from the associated surface trough. In contrast, radar layers in the lower 1,500 m of the NPLD are usually continuous for many hundreds of kilometers (Figure 1.2a).

We examined troughs across the NPLD and in the south polar

layered deposits (SPLD) to assess variability. The majority of NPLD troughs have discontinuities that can be traced below the surface to approximately 600 m (Figures 1.2, 1.3e, and 1.7) or 360 m in some cases (Figure 1.8). Because of regional accumulation variations [*Holt et al*., 2010a], two discontinuities in the saddle region between Gemina Lingula and the main lobe (Figure 1.1) extend farther below the NPLD surface but are at the same stratigraphic level as the 600 m discontinuities. Because they are steep and reach the substrate, troughs closer to the NPLD margin often have no associated stratigraphic record in radar to evaluate. Like the NPLD, the SPLD are deposited layers of water ice and dust of varying concentration, are more than 2 km thick, and have large spiral troughs covering the surface. In radar, however, the SPLD show few reflectors near the troughs, making it impossible to assess migration with this technique. Optical interpretations find no evidence of mass transport or trough migration in the south [*Kolb and Tanaka*, 2001].

Also observed, but more limited in number, are V-shaped structures (Figure 1.2b and c) formed by a near-vertical alignment of inflections in downward bending layers. They are found adjacent to sloping discontinuities that reach a depth of 600 m, are contained within the uppermost, 400 m, and do not reach the surface. Undulations currently on the NPLD surface near 270° E and the western end of Gemina Lingula have topographic expressions that mimic these layers; see the orange horizons in Figure 1.3e.

In map view, an overall pattern of the discontinuities following the spiral shape of the troughs becomes apparent (Figure 1.1b). The less extensive V-shapes also follow this pattern. We interpret the spiraled, sloping discontinuities as positions through time of the south-facing scarps, or trough migration paths. In all cases the trough migration paths on the main lobe are deeper to the south, so the data support northward, upwind trough migration and a constructional origin of the troughs during deposition, as first

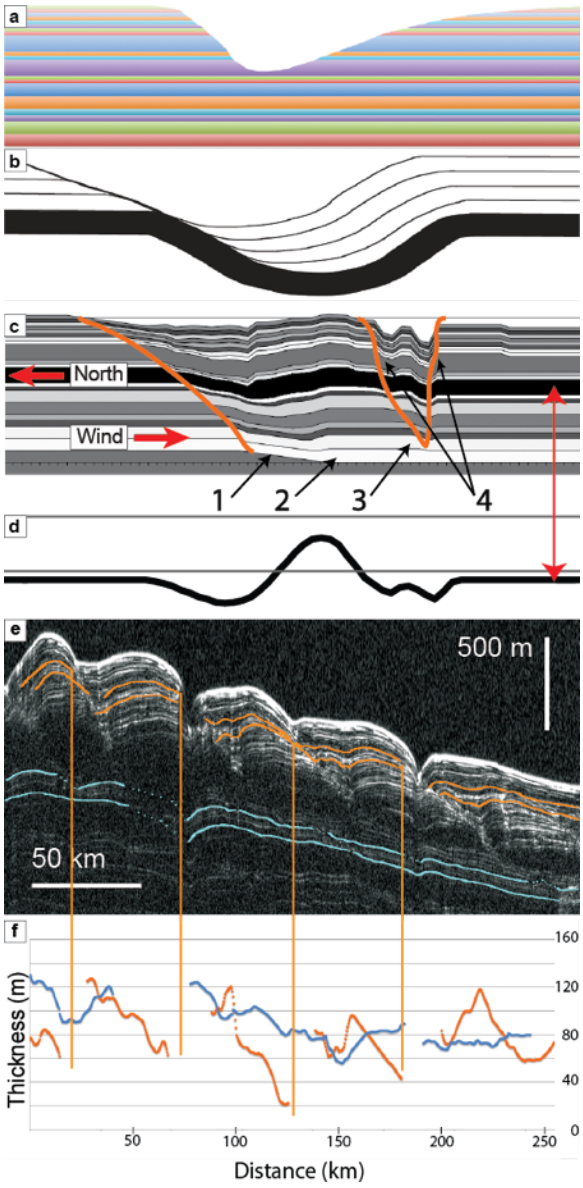

Figure 1.3: Stratigraphy and layer thickness changes resulting from different proposed mechanisms of trough formation/migration*. a, No trough migration. Layers are truncated by erosion but otherwise uniform in thickness and sub-horizontal. b, Trough migration caused by ablation of material on the equator-facing slope [Squyres 1979]. The trough migrates upward and northward, but layer thickness only varies on the south-facing slope. c, Wind dominated stratigraphy: 1. Scouring on south facing slope initiated at scarp, 2. Material transported southward assuming no material is lost to sublimation, 3. Small mound (or undulation) builds downwind, creating a secondary downwind face, 4. V-shape forms during subsequent deposition over the area between the leeward face of an undulation and further downstream. d, Relative thickness of black layer in c showing lateral change with respect to trough. e, SHARAD data from orbit 519201 (location indicated in Fig. 1.1b). Sub-horizontal layers (orange) are broken by sloping discontinuities and are vertically separated across the boundaries by approximately 150 m. Stratigraphic layers below the discontinuities (light blue) are more continuous and uniform in thickness. Vertical scale exaggerated ~90x. f, Plot of separation distance between reflector pairs shown in e. The change in thickness of the upper pair (orange) is similar to the pattern predicted by wind transport in d. For each trough, positions are indicated by vertical lines. Smaller variations in the lower layer (blue) may be related to regional deposition patterns or data processing algorithms.*

hypothesized [*Howard*, 1978; *Squyres*, 1979]. The troughs in Figures 1.2, 1.3, 1.4 and 1.7 are about 65 km north of, and 620 m above, their initiation point (560 m of deposition and 6 m of upslope migration), although the exact depth varies depending on location. Other interpretations of the trough migration path as faults or as resulting from flow are not supported by the data.

This new radar stratigraphy can be used to constrain the processes that have been proposed to govern trough migration [*Howard*, 2000; *Howard et al*., 1982; *Squyres*, 1979]: solar ablation, wind transport, and atmospheric deposition. Any could be dominant under different climatic circumstances. First, uniform deposition adds a fresh layer of material to the polar layered deposits over an existing trough, raising the overall surface elevation. Katabatic winds descending into the trough approximately perpendicular to their length scour the equator-facing surface and remove material to be deposited downstream onto the pole-facing slope, causing both slopes to move northward while thickening the downwind side (Figure 1.3c). Such winds and their ability to move material have been observed (Figure 1.4). In solar ablation, the slope most directly facing the sun is warmed the most, causing preferential sublimation and retreat of that slope from the sun [*Squyres*, 1979] (Figure 1.3b). Additional deposition forms new layers that drape the surface and are vertically offset across the trough.

The sum of these three processes gives rise to the trough migration path as a distinct feature that records the border between erosion and deposition, with its slope determined by the relative amounts of each. High deposition rates relative to erosion/ transport increase the slope (less migration), while the opposite scenario decreases the slope (more migration). Thus the trough migration path slope indicates the relative balance between these climate-driven processes over time.

In a depositional regime accompanied by wind-dominated erosion and transport, layer thickness should depend on distance from the upwind scarp [*Squyres*, 1979]. Layers will be uniform far from the trough but thinner along the upwind slope (cutting into lower layers if erosion exceeds deposition) and thicker on the downwind scarp [*Howard et al*., 1982]. Stratigraphic thickness variations measured from radar layers across troughs (Figure 1.3) are consistent with this scenario and hence with a dominant role for wind

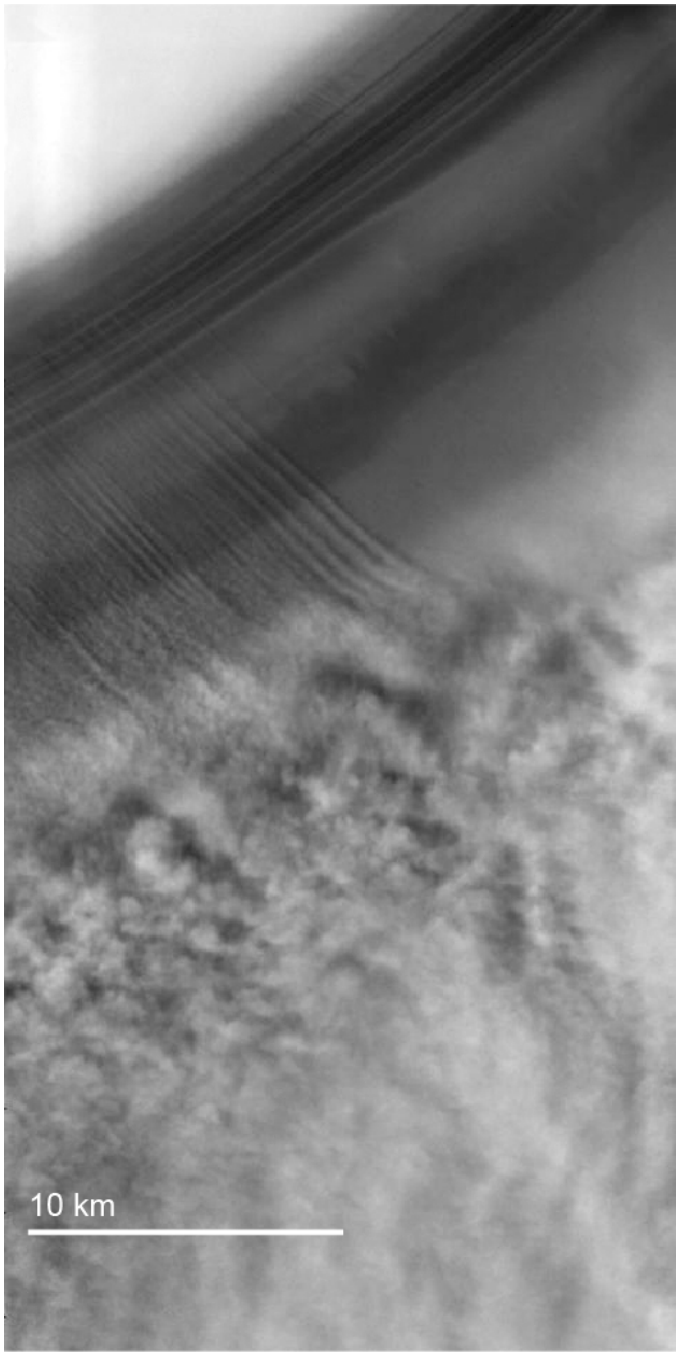

Figure 1.4: Image of trough cloud and effect of katabatic winds*. THEMIS image V1243200130, showing thin, katabatic flow scouring the south-facing slope of a trough on the main lobe and moving material southward and downwind where it is deposited. Location indicated in Figure 1.1a.*

erosion and transport. Mapped wind patterns (Figure 1.1a) are oriented roughly perpendicular to troughs, even where troughs are not aligned east–west.

Although solar ablation is plausible as the only cause of equator-facing slope retreat, layer thickness changes observed in the radar data do not match the uniform layer thicknesses predicted by solar ablation [*Squyres*, 1979] (Figs 3c and d). However, we cannot rule out some component of solar ablation in slope retreat. Late-stage trough incision into the NPLD (for example, erosive downcutting by along-trough winds) is not supported by the radar data, because that would result in the truncation of layers on both sides of the trough (Figure 1.3a), and equivalent layers would not be vertically offset.

A striking aspect of the radar data is that the stratigraphic layering representing older polar layered deposit surfaces is remarkably consistent from shortly after trough initiation until the present-day surface. Some instances in which layers on the equatorward slope were truncated (erosion/transport dominant) and then unconformably overlaid by a new layer that was preserved (deposition dominant) are observed (Figures 1.2 and 1.3), but the overall shape indicates that after initiation more than 560 m below the present surface, the processes governing trough morphology quickly reached a quasi-steady state that remained until the present or at least until very recently. Combining this with the evidence for a dominant role of wind in trough morphology and the mapped pattern of winds on the NPLD surface (Figure 1.1a), it is likely that katabatic winds directed by the Coriolis force acted on the troughs from their initiation until now, having an important effect on their shape and position, including the spiral pattern.

Average accumulation rates in the NPLD are estimated to be between 0.28 and 1.2 $mmyr^{-1}$ [*Fishbaugh and Hvidberg*, 2006a], and we use this to constrain trough age and migration rate. Using the 560–700-m trough initiation point, the main central troughs initiated between about 2.49 million years ago and 467,000 years ago and migrated on average 0.02–0.16 myr^{-1}. The 360-m initiation point of troughs further east implies a younger age of between about 1.29 million years and 300,000 years. These ages do not account for possible depositional hiatuses. Higher deposition rates (that is, a younger age) might result in migration observable over decades, assuming the process is still active.

Before the troughs initiated, deposited layers were mostly continuous and uniform, indicating that different steady-state conditions prevailed then. What changes occurred in the Martian climate that suddenly created conditions favorable to trough formation are still unknown. With these new observations, perhaps climate models that include accumulation, solar ablation, feedback from regional and local topography,

winds, and orbital forcing can better constrain these processes so that we can determine why the troughs began to appear on the NPLD only after three-quarters of its thickness was deposited.

METHODS SUMMARY

Theoretical [*Nunes and Phillips*, 2006] and empirical [*Milkovich and Plaut*, 2008] studies indicate that radar reflections result from contrasts in the dielectric properties of visible NPLD layers and therefore serve to represent the same geometrical relationships. SHARAD data shown here were processed with a focused synthetic aperture radar technique to improve along track resolution to about 300 m. Depth conversions assume a permittivity (real part) of 3.2, a value consistent with a composition of water ice at typical Mars temperatures. Layers and discontinuities are identified and mapped in time delay data, before depth conversion, using Schlumberger's GeoFrame seismic interpretation software.

CLUTTER SIMULATIONS AND LIMITATIONS OF DEPTH CORRECTION

While SHARAD can produce well-defined stratigraphy, data quality is influenced by acquisition geometry. In areas with large cross-track slopes, reflectors from surface topography to the sides (i.e. clutter) can arrive at the same time delay as reflectors from the subsurface directly below the spacecraft. Thus, the best geometry for observing stratigraphy beneath troughs occurs when the observation ground track is perpendicular

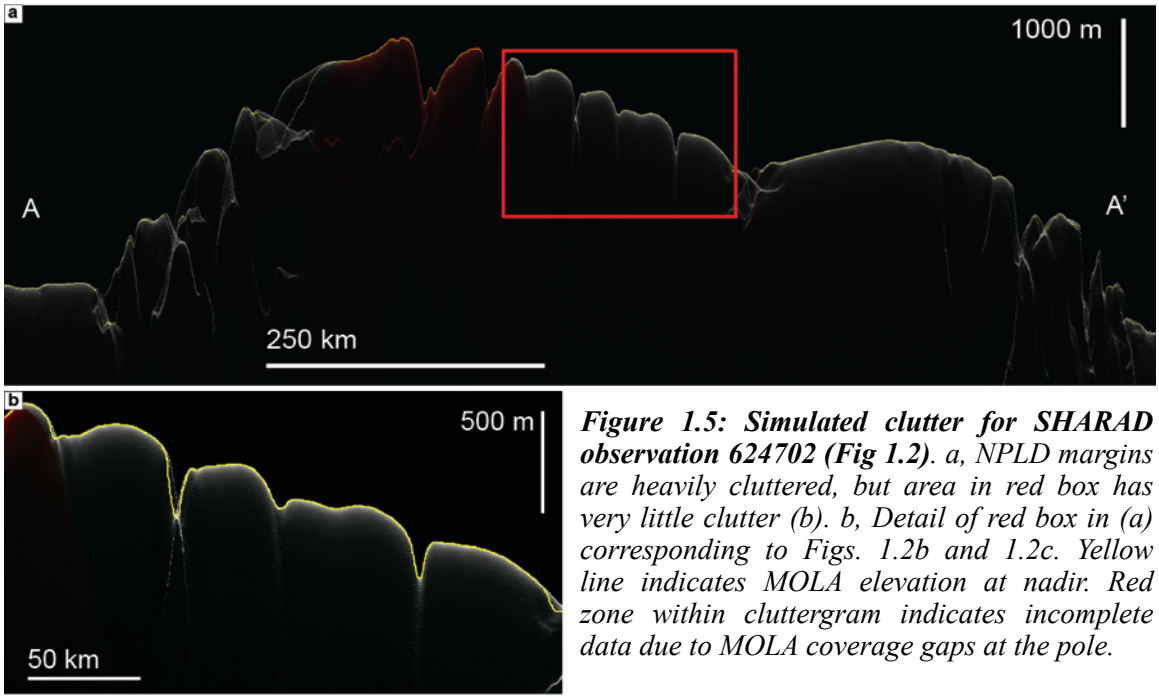

Figure 1.5: Simulated clutter for SHARAD observation 624702 (Fig 1.2)*. a, NPLD margins are heavily cluttered, but area in red box has very little clutter (b). b, Detail of red box in (a) corresponding to Figs. 1.2b and 1.2c. Yellow line indicates MOLA elevation at nadir. Red zone within cluttergram indicates incomplete data due to MOLA coverage gaps at the pole.*

to their orientation. Surface clutter reaches a maximum when the ground track runs parallel to the trough axes. The region between 0 and 90 degrees East longitude (Figure 1.1) on the main NPLD lobe is well suited for this analysis due to the largely clutter-free geometry (Figure 1.5).

Simulations created from elevation data show radar reflections that arise from the surface only and allow us to differentiate true subsurface reflectors from undesirable clutter (Figure 1.5). The clutter simulation was performed with a facet-based, incoherent scattering model [*Holt et al*., 2006] using spacecraft positioning and MOLA topography [*Smith et al*., 2001]. Furthermore, it is clear that the returns are from directly below the spacecraft, as indicated by the match between the first return and MOLA elevation at the nadir point in the simulation.

The depth correction algorithm aligns the radargram to the MOLA Digital elevation Model and assumes that the surface reflection is from directly below the

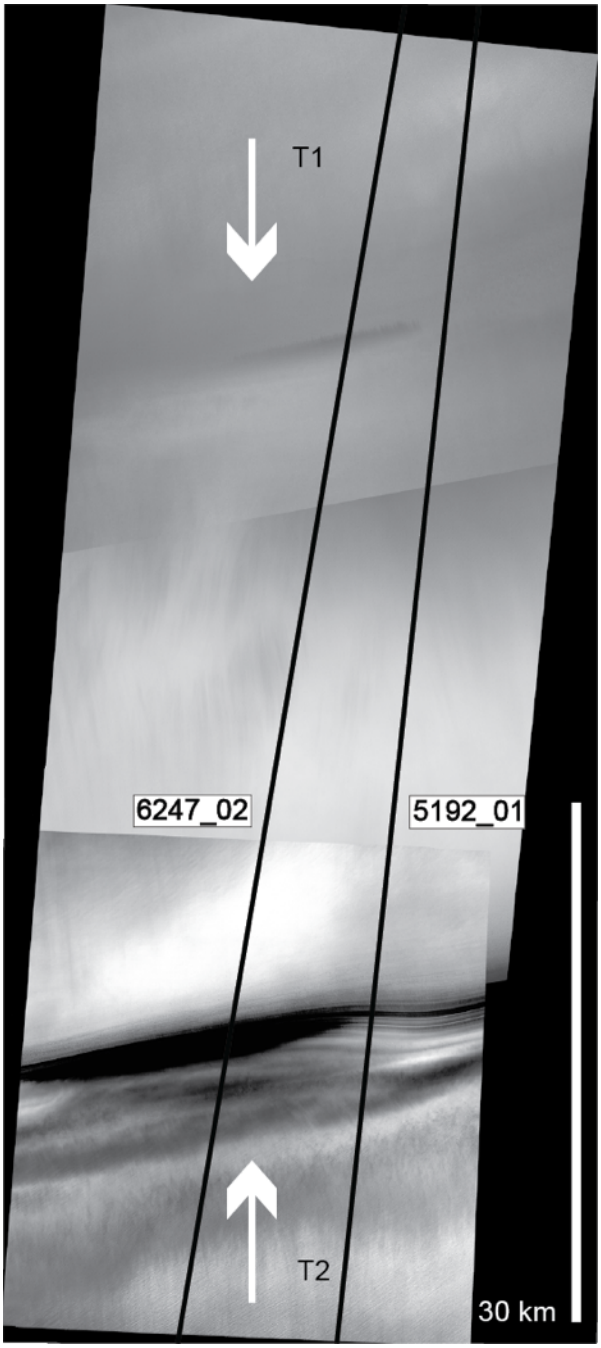

Figure 1.6: Surface expression of troughs from mosaic of Context Camera (CTX) images*: P20_008755_2665, P20_009005_2655, P21_009 66_2729. Location of mosaic indicated in Fig. 1.1; T1 and T2 identified in Fig. 1.2. North is up in this mosaic.*

spacecraft, which is not the case always. Near the center of the NPLD (higher than 88°) there is very little elevation data, and what exists above 87.1° it is interpolated from sparse data. Because of the missing data, we are not able to correctly place the location of first reflection, which can be distant from the nadir point. Also, clutter simulations based on MOLA elevations will be inaccurate. This region is highlighted in red in Figure 1.5.

COMPARISON WITH OPTICAL DATA

Figure 1.6 shows imagery of two troughs with different surface expressions. SHARAD observations 624701 (Figure 1.2b) and 519201 (Figure 1.3e) both fall within this mosaic. The lower trough has steep slopes and exposed layers, while the upper is almost completely covered. This is manifested in radar data that

show layers reaching the surface at the lower trough while the upper is covered (Figure 1.2). Thus the gross morphology of radar layering agrees with that observed in imagery, and either deposition or local erosion may dominate in neighboring troughs.

TERRESTRIAL ANALOGS IN ICE

In eastern Antarctica, large areas covered by dune-like features, termed megadunes, show radar reflector stratigraphy similar to that seen beneath the spiral troughs [*Frezzotti et al*., 2002]. These megadunes have shorter amplitudes and wavelengths than the spiral troughs but share a characteristic upwind migration pattern. Additionally, the dune crests align themselves perpendicular to the prevailing katabatic wind, which maintain uniform direction and speed [*Fahnestock et al*., 2000]. The dunes have long wavelengths and low amplitudes: 2 to 5 km and 2 to 4 m, respectively. This scales approximately 1:100 to the spiral troughs on the NPLD, which have ~50 km wavelengths and 320 to 400 m amplitudes for troughs shown in Fig 2.5. While these dimensions are much smaller, we feel that they are good for comparison. Megadunes in Wilkes Land, Antarctica, have estimated migration rates between 5 m and 25 m per year [*Black and Budd*, 1964, p.19; *Frezzotti et al*., 2002] , two orders of magnitude greater than observed on Mars in this paper and from rates predicted in optical imagery [*Howard et al*., 1982]. Megadunes must form during times of relatively low accumulation and steady wind velocities to be so well organized. That is the case where they are found: in the middle of the ice sheet, far from passing storms [*Frezzotti et al*., 2002]. A notable aspect of the megadunes is that they lie within regions where the slope is about 10 times that where dunes are not found: 0.10-0.15% vs. 0.013-0.022% [*Frezzotti et al*., 2002].

This has been cited as an important control on megadune genesis [*Fahnestock et al.*, 2000], likely due to increased wind speed. So far, insolation is not linked to megadune formation. Wind transport, however, plays a very important role. The troughs on Mars may not have formed under the same conditions, but they have behaved similarly since initiation. Upwind migration, repeating patterns, perpendicular alignment to regional winds, and mass transport characterize both of these systems.

ALTERNATE INTERPRETATIONS OF TROUGH STRATIGRAPHY

Faulting: Faulting of pre-existing layers would produce offset layers of equal thickness, a prediction unsupported by the radar data. Layering is also inconsistent with growth faults, as those would exhibit layers thickening uniformly toward the fault surface on the headwall, with maximum thickness at the scarp [*Nittrouer*, 2007]. This is not seen in the NPLD, where accumulation appears to vary more based on surface slope. Furthermore, radar layers just below the discontinuities are not offset, restricting potential faulting to the upper several hundred meters (an impractical strain scenario for such a uniform composition). There is also

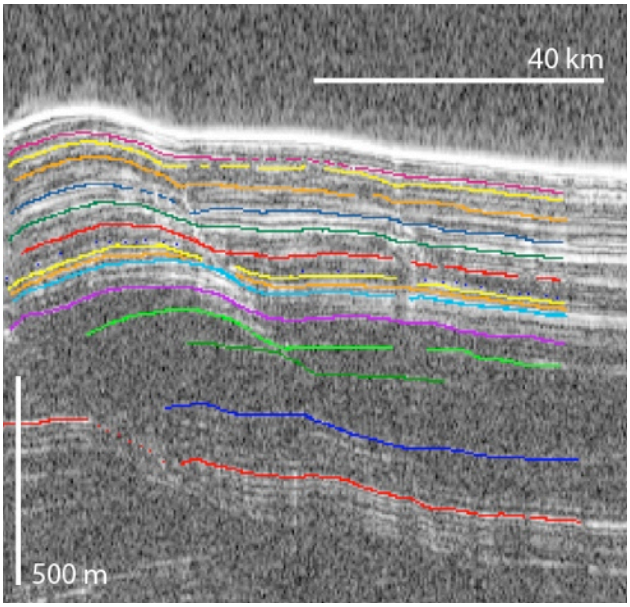

Figure 1.7: *Segment of radargram 616701 (location in Fig 1.1b). Stratigraphic reflectors traced across the TMP continuous, one variation of migration.*

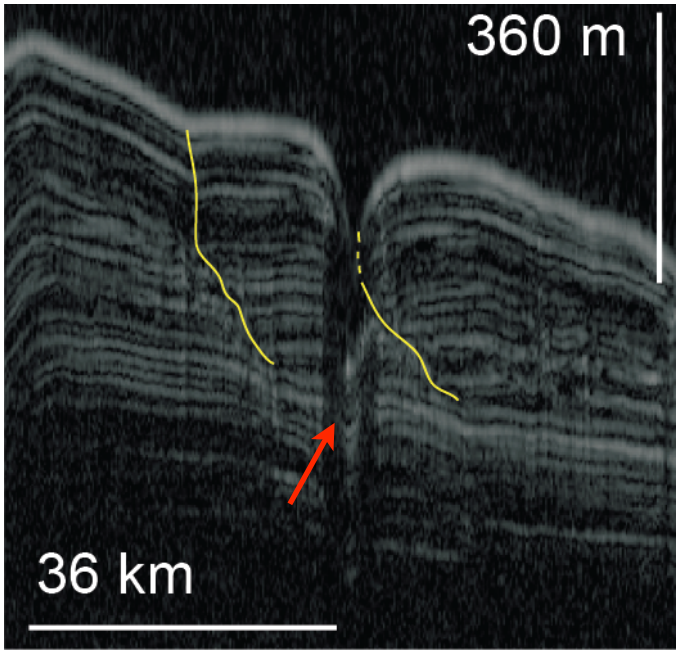

Figure 1.8: *Segment of observation 761602 (location in Fig 1.1a). TMP, indicated by yellow lines, are seen beneath troughs as in Figure 1.2, but layer thickness does not vary as much as below other troughs. TMP begin about 360 m below the surface here. Artifact, indicated by red arrows, is the result of steep slopes on the surface of the PLD and the depth correction algorithm. A TMP slope change, seen best on the left, indicates a temporal change in the ratio of deposition to transport.*

no evidence for an accommodation zone or pressure ridge below any trough, some of which are 600 km from the NPLD margin. Another argument against the faulting argument is that TMP slopes in observation 624702 (Figure 1.2c) and adjacent orbits range from 0.9 to 2.1 degrees and average ~1.2 degrees, values much too small to allow movement over 65 km. Steeper slopes, indicating less migration, are observed in the upper section of some observations 616701 (Figure 1.7) and 761602 (Figure 1.8), but in those section layers are continuous across the TMP, which does not evidence faulting. We find it unlikely that brittle deformation, in the form of faulting, can occur over slopes this shallow, with no accommodation, and over such a great distance.

Two further terrestrial examples with stratigraphic properties similar to the TMP including shallow slopes and layer offsets are found in the marine sediments of the Blake Ridge off the east coast of the United States[9] and the 'Humboldt Slide' near the Eel River in California [*Lee et al*., 2002]. Stratigraphic discontinuities in these sediments were originally interpreted as submarine failures [*Dillon et al*., 1998; *Lee et al*., 1981], but later, high-resolution seismic data as well as numerical and physical models revealed

them to be large-scale sediment waves created by preferential erosion of upstream slopes combined with deposition [*Holbrook et al*., 2002; *Lee et al*., 2002]. Discussion about marine sediment waves versus faulting continues [*Nittrouer*, 2007], however the data more strongly support the aggradational rather than the deformation hypothesis.

The radar data below many troughs on the NPLD show a strong correlation to the seismic data of sediment waves on Earth. In many cases (e.g. Figure 1.7) internal reflectors can be traced across the inflection point (TMP) showing them to be continuous beds. Figure 1.7 crosses the same trough as Figures 1.2 and 1.3e (location in Figure 1.1b) near enough to enable the connection of discreet reflectors but far enough that a different morphology (reflector continuity and lack of V-shape) is seen. Here we may eliminate faulting because the reflectors are continuous. They can then be extrapolated west towards 624702 and 519201. A differing ratio of processes (e.g., less wind relative to deposition) accounts for the morphology. Variations of insolation would make sense for the change in morphology if the troughs were at different latitudes, but Figure 1.7 contains the same trough as Figures 1.2 and 1.3e. It is, however, east of the other two observations, in a location of less regional slope. This indicates that the winds will accelerate less, pick up less material, and, therefore, cause less erosion. Furthermore, the slope of the TMP may be both concave up and concave down at different stratigraphic levels within the same radargram (Figures 1.2 and 1.7). This is the result of varying processes in a depositional regime and is not possible for normal faults, that only allow for linear or concave up discontinuities. Thrust faulting due to compression, allowing the concave down scenario, is unlikely given the stress regime, which would result in outward deformation, if possible.

Flow: The geometry of layers seen in radar data does not match that predicted in models of flow [*Fisher*, 2000], where layers bend upward below troughs due to less

Figure 1.9: Radar observations of troughs on SPLD. *a, Observation 563301. b,Observation 563101. Stratigraphic layers and discontinuities are rarely observed near troughs in the SPLD (yellow) leaving little evidence for trough migration. c. Basemap showing locations of (a) and (b) on MOLA-derived surface. Gray circle indicates missing elevation data.*

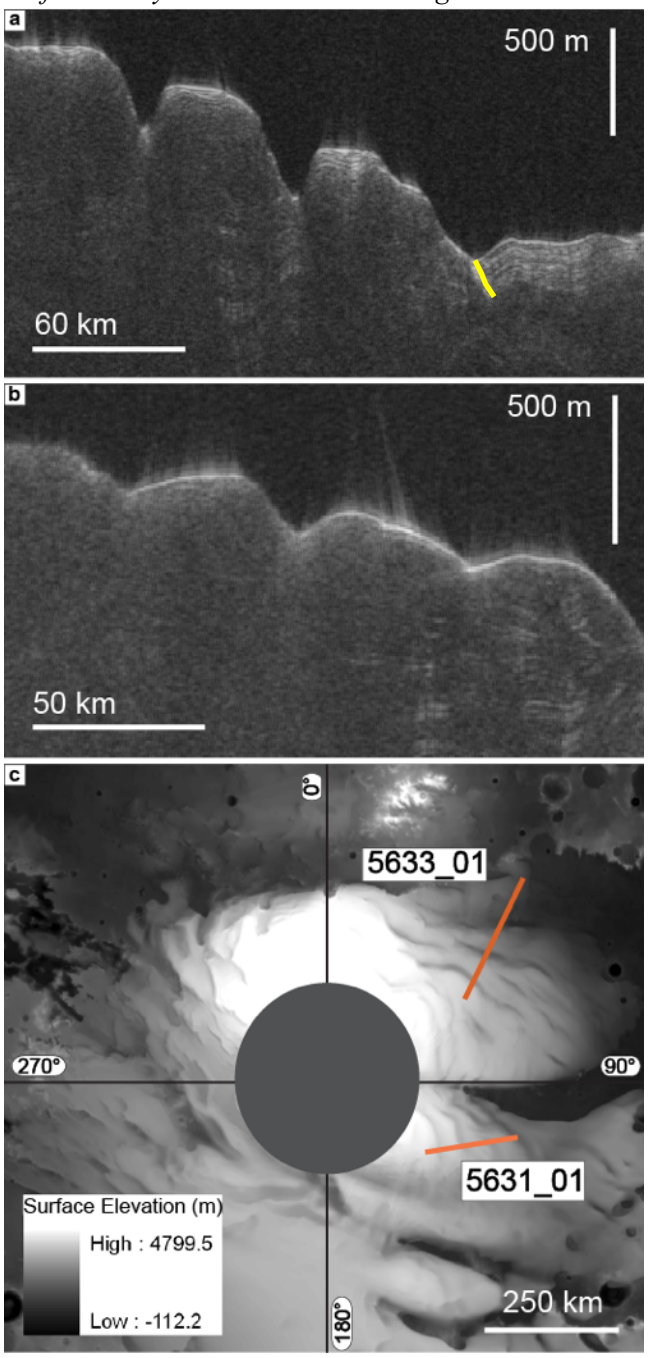

overburden. Instead, layers are sub-horizontal and of uniform thickness in the lower ~1500 m, and either conformal to the surface (i.e. downward bending) or truncated at troughs in the upper ~500 m. Modeling results compared to optical observations of layers over large distances indicate that flow has not occurred in the uppermost 500 m14, consistent with the radar observations.

TROUGHS OF THE SOUTH POLAR LAYERED DEPOSITS

SHARAD data in the SPLD show fewer layers relative to the NPLD, greatly limiting our technique there (Figure 1.9). In general, there is a discrepancy between morphology of the NPLD and the south polar layered deposits (SPLD) in laser altimetry [*Smith et al.*, 2001],

optical, and radar data [*Phillips et al*., 2008b; *Seu et al*., 2007b]. Some interpretations indicate that troughs in the south have not migrated and are late-stage erosional features [*Kolb and Tanaka*, 2001]. Possible explanations for a different trough history in the SPLD include lower carrying capacity of wind due to the 6.4 km higher elevation and associated lower air density and lack of deposition since approximately 5 Ma [*Herkenhoff and Plaut*, 2000]. Additionally, unlike the NPLD, inter-trough undulations in the south are missing [*Howard*, 2000], supporting the interpretation of there being less material to move.

Chapter 2: New Insights into the Spiral Troughs of the Northern Polar Layered Deposits, Mars from SHARAD Observations

1 Introduction

Layers of ice and dust cover the north polar region of Mars (Figure 2.1). The exposed stratigraphy of these "north polar layered deposits (NPLD)" has been studied for decades as a record of accumulation [*Howard et al*., 1982; *Murray et al*., 1972; *Tanaka et al*., 2008]. The layers record atmospheric deposition of ice and dust in varying ratios [*Clifford et al*., 2000; *Cutts and Lewis*, 1982; *Fishbaugh et al*., 2010; *Hvidberg et al*., 2012; *Laskar et al*., 2002; *Levrard et al*., 2007; *Toon et al*., 1980] and are widely considered to contain the best record of recent climate in the Amazonian [*Byrne*, 2009; *Fishbaugh and Hvidberg*, 2006]. Being one of the largest reservoirs of water ice on the planet, the polar layered deposits (PLD) are actively exchanging moisture with the atmosphere, and are therefore fundamentally tied to the global water cycle of Mars [*Head et al*., 2003; *Laskar et al*., 2002].

Many investigations have examined the layers of the NPLD with the goal of extracting the depositional and climatic history associated with ice accumulation. Layers are exposed primarily by the extensive spiral troughs and scarps [*Byrne*, 2009; *Fishbaugh and Hvidberg*, 2006; *Milkovich and Head*, 2005]. These exposures act as windows into the deposits, allowing for interpretations of how the NPLD developed. However, these troughs and scarps have provided the only means for accessing the stratigraphy that is

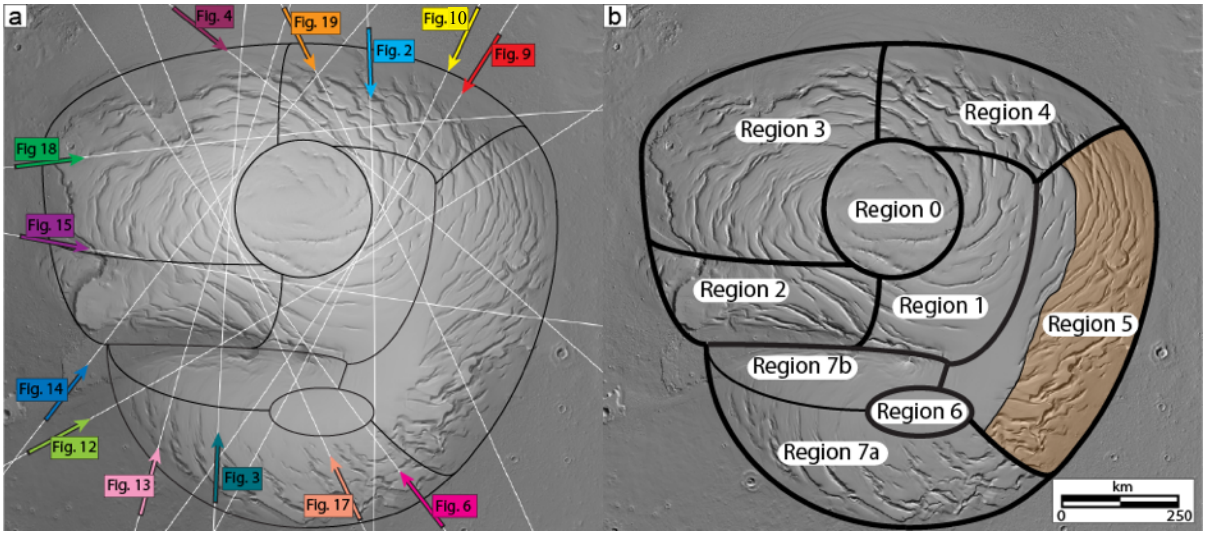

Figure 2.1: MOLA Hillshade of the NPLD with regions divided by characteristics*. a); ground tracks of observations in this paper. Figure 2 is radargram 1247002; Figure 3 is radargram 2162801; Figure 2.4 - 761602; Figure 2.6 - 725402; Figure 2.9 - 1252401; Figure 2.10 - 1247101; Figure 2.12 - 855602; Figure 2.13 - 2265701; Figure 2.14 - 2189301; Figure 2.15 - 1044302; Figure 2.17 - 2007101; Figure 2.18 - 1087101; Figure 2.19 - 1982701. b). NPLD troughs have many similar characteristics, but they vary by location. We divide the NPLD into eight regions based on surface morphology and subsurface structure.*

largely hidden in the subsurface, leaving room for multiple interpretations of NPLD development [*Fisher*, 1993; *Tanaka et al*., 2008].

Recently, radar sounding from the Mars Advanced Radar for Subsurface and Ionospheric Sounding (MARSIS) on Mars Express and the shallow radar (SHARAD) instrument on Mars Reconnaissance Orbiter have provided a new method of looking into the NLPD subsurface [*Picardi et al*., 2005; *Seu et al*., 2007]. SHARAD, in particular, has provided remarkable observations of NPLD stratigraphy and has proved valuable for determining the evolution of the NPLD [*Holt et al*., 2010; *Phillips et al*., 2008; *Putzig et al*., 2009].

It was recently recognized that layers exposed in the spiral troughs are affected by local processes both during and after deposition [*Smith et al*., in review]. Specifically, the interaction between trough morphology and winds determines how and where ice and dust accumulate. Any interpretation of stratigraphy must take into account this forcing.

Furthermore, the troughs have been an integral part of NPLD surface evolution since onset ~0.5 – 2.4 Ma [*Smith and Holt*, 2010]. Therefore, a better understanding of trough processes should result in a better understanding of the development of the NPLD.

Here we present the first comprehensive survey of troughs and related features using SHARAD. We analyze stratigraphy, compare to optical data, draw inferences on pertinent observations, and present hypotheses regarding the development of the NPLD with respect to the spiral troughs.

The troughs are not circumpolar features, and references to their equator and pole-facing slopes are inadequate. Therefore, to reduce confusion, we adopt the trough reference frame of *Smith et al.,* [in review] who referred to the trough high and low sides, which are independent of trough location or orientation on the NPLD. The high side is topographically higher than the rest of the trough (Figures 2.2e and 2.3b) and faces towards the equator. The opposing slope of the trough, the low side, is topographically lower than the high side and faces generally towards the north pole. High side slopes contain exposures of layers, while banded terrain is ubiquitous on the low side.

2 PREVIOUS OBSERVATIONS RELATED TO TROUGHS

After their discovery in Viking data [*Murray et al*., 1972], the NPLD spiral troughs and their stratigraphy have been studied in detail for more than 30 years [*Blasius et al*., 1982; *Cutts*, 1973; *Cutts et al*., 1979; *Howard*, 2000; *Howard et al*., 1982; *Smith and Holt*, 2010; *Squyres*, 1979; *Tanaka et al*., 2008; *Weijermars*, 1986]. *Howard et al*. [1982] made some of the very earliest observations about the spiral troughs based on a

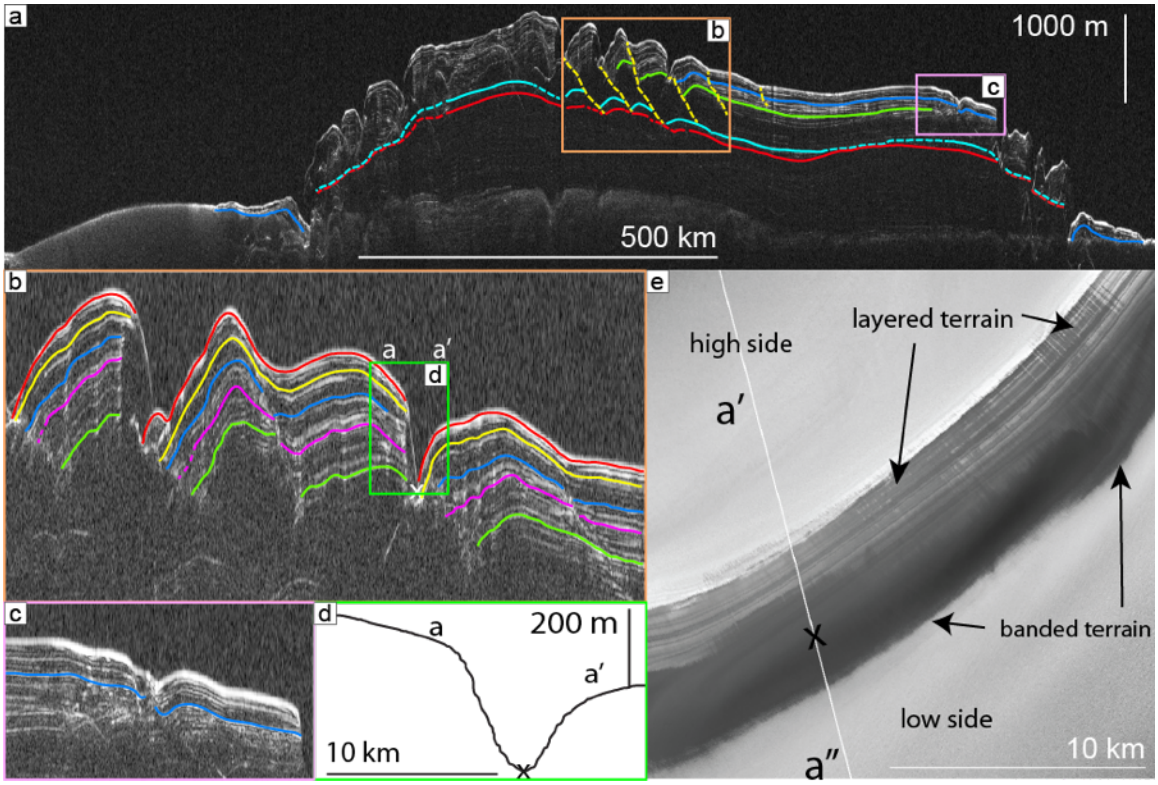

Figure 2.2: Radar and optical observations of troughs. a) Interpreted radargram 124702 displaying entire of NPLD *(Location in Figure 2.1). Several horizons are traced throughout the paper: red is R29 (TIS-1), light blue is R25, green is R17 (TIS-2), dark blue corresponds to the contact of ABb1 and ABb3 from* [Tanaka et al., 2008] (Contact1-3). *Yellow dashed lines indicate trough migration paths (TMPs). The three southernmost TMPs identified do not reach TIS-1, indicating that the troughs formed later. Boxes are for b) and c). Vertical exaggeration ~120x b) Portion of Radargram 1247002. Individual reflectors are offset at the TMP by as much as 150 m. Layers are thinnest at the trough high side wall. Layers thicken on the low side. X, a', and a" correspond to the same in d) and e) c) Un-interpreted portion of a) displaying bright reflector and unconformity associated with* Contact1-3. *d) Topographic profile corresponding to b) and e). Trough high and low sides are defined by elevation and are asymmetric in slope. e) Portion of CTX image P01_001595_2665_XN_86N319W observing a classical trough. Trough high side exposes fine layers. Wind streaks cover this surface, indicating direction of flow. Black X marks the lowest elevation of the trough as indicated in d). Downstream of the X, on the trough low side, banded terrain overlies layers.*

detailed survey of Viking imagery. They found that most troughs conform to a few generalizations: asymmetric accumulation of ice across the troughs, exposed layers facing roughly equatorward, and banded terrain that faces roughly poleward (Figure 2.2). Banded terrain is described as "irregular layering that unconformably overlies adjacent

terrain and has an albedo intermediate to the layered and inter-troughs regions" [*Howard et al*., 1982].

These observations led to the interpretation that the troughs migrate towards the pole, a result of erosion of the equator-facing slope and accumulation on the pole-facing slope. *Howard et al*. [1982] interpreted the contacts of accumulation and erosion as bounding surfaces associated with migration and estimated that 43 – 130 m of migration occurred during the time required for 10 m of accumulation.

Attempts to provide mechanisms for trough formation and to explain gross morphological characteristics followed the detailed stratigraphic work of *Howard et al*., [1982]. These later studies resulted in hypotheses that varied greatly as to the trough's formation: non-uniform accumulation [*Cutts et al*., 1979]; Coriolis oriented fractures from glacial surges [*Weijermars*, 1986; *Zeng et al*., 2008]; recycled ice from ablation [*Fisher*, 1993]; purely erosional cutting from wind and insolation [*Kolb and Tanaka*, 2001; *Rodriguez and Tanaka*, 2011]; lateral heat transfer within the surface [*Pelletier*, 2004]; incision due to ablation and then viscous relaxation [*Pathare and Paige*, 2005]; and atmospheric deposition of low albedo material causing spatially periodic and spiral sublimation [*Ng and Zuber*, 2006], among others. These models all successfully explained spiral depressions but implied stratigraphies in disagreement with those observed by *Howard et al*., [1982]. A test of each hypothesis with new instrumentation was necessary.

In 2006 SHARAD entered orbit around Mars. SHARAD has the capability of probing the subsurface of the NPLD for internal stratigraphy and structure associated with spiral troughs, and is therefore the perfect instrument to test the varied hypotheses. However, initial observations were inconclusive. *Phillips et al*. [2008] observed anomalies beneath the spiral troughs (Figures 2.2 and 2.3) but were unable to determine

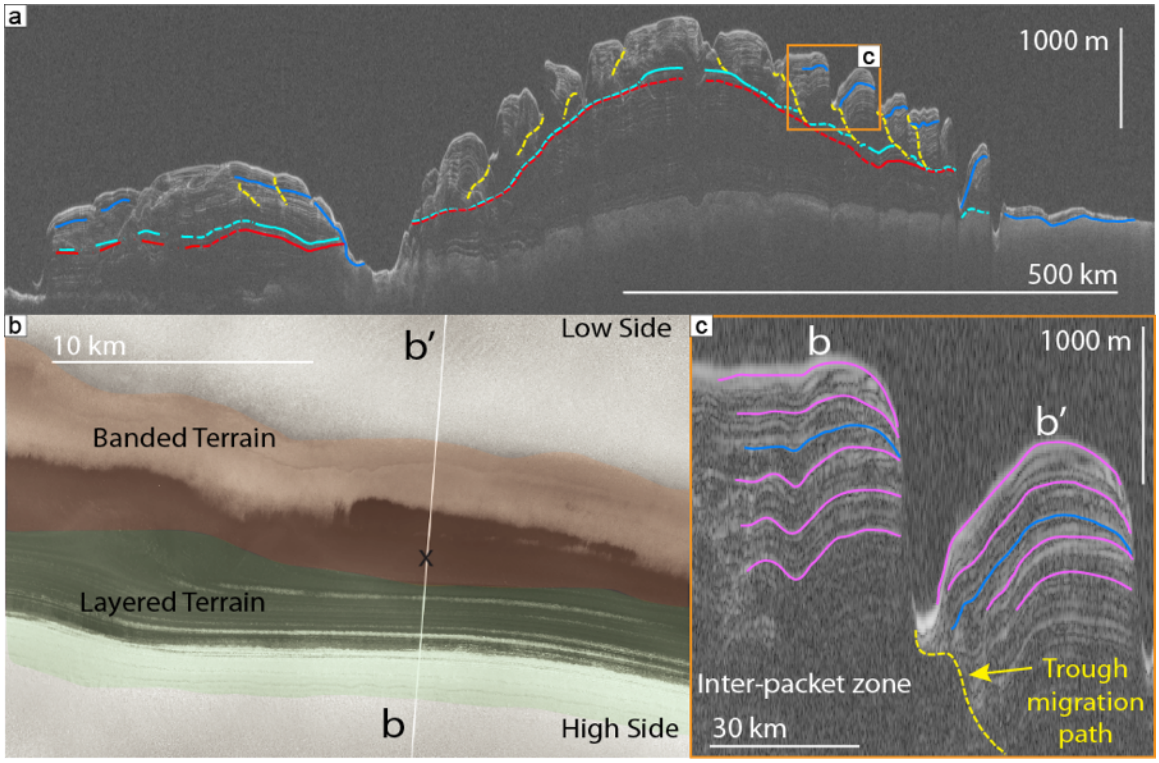

Figure 2.3: Radar and optical observations of troughs *(Location in Figure 2.1s). a) Interpreted radargram 2162801 of the NPLD converted to depth. Colored lines are the same as in Figure 2. Box indicates c). Vertical exaggeration is ~ 100 X. b) Portion of CTX image P01_001416_2665_XI_86N132W displaying layered (green) terrain on the trough high side. Banded terrain (orange) is on the low side of a trough. White line is ground track of SHARAD observation corresponding to c). Black X is lowest elevation of trough. c) Portion of radargram 2162801. Layers thin as they approach the trough from the high side. A TMP is easily delimited where low side layers onlap older surface of inter-packet material. The inter-packet zone (no radar reflectors) described by Putzig et al., [2009] is exposed in the lowermost ~100 m of the high side of this trough.*

whether they were real structures or artifacts in radar image generation. *Putzig et al.*, [2009] provided the first detailed examination of internal structure of the NPLD based on packets of reflectors. In the uppermost section described by them, labeled G, they noted the same features at *Phillips et al*. [2008] but offered no interpretation as to their formation.

A study conducted by *Smith and Holt* [2010] was the first to recognize the anomalies detected by SHARAD as the result of discontinuous reflectors. The highest

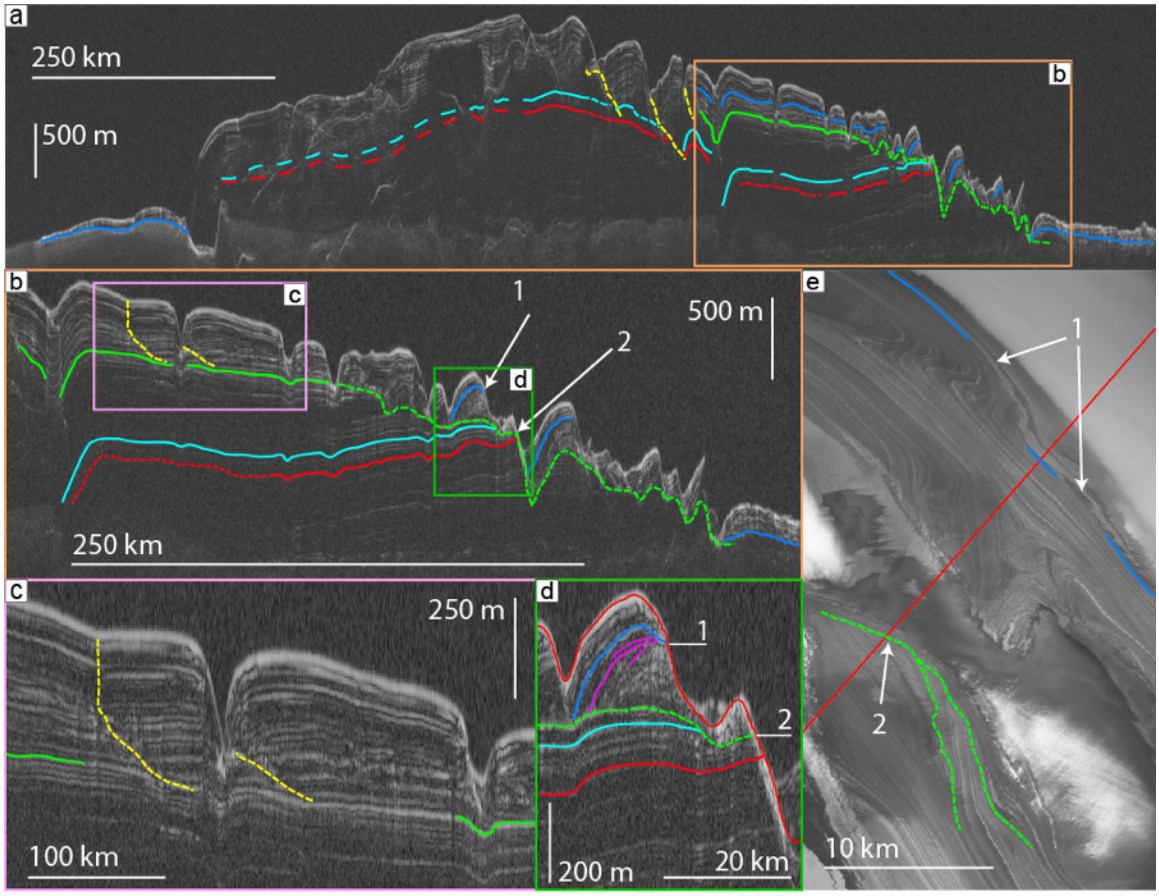

Figure 2.4: Radargram and optical observations of troughs a) Radargram 761602 observing Regions 4, 1, and 5. *Starting from the left, the* Contact1-3 *is visible near the NPLD border. Center left: Region 4 is riddled with clutter and not useful for analysis. Center: Region 1 troughs behave classically with TMP and thickness variations. Center right: Troughs form at R17 (green), stratigraphically higher than TIS-1 (red) troughs. A large erosion predated troughs in Region 5 (dashed green line). TIS-2 slope is 0.31°. Trough wavelength is ~20-30 km. b) Radargram from a) with fewer interpretations. TMP slope of two troughs (yellow) increases dramatically from 0.93° to 12° at* Contact1-3. *Arrows coincide with contacts displayed in d) and e). c) Portion of radargram 761602 indicated in b). Layer thickness variations demonstrate the former location of troughs. Bright reflector (R10) corresponds to the erosional surface TIS-2. d) Portion of radargram 761602 indicated in b). Two contacts are exhibited. One exposes older NPLD material, pre-TIS-1. The other is the RAP. e) Portion of CTX image P01_001529_2622_XN_82N288W displaying unconformities. A large angular unconformity is mapped on the surface and crosses ground track of d) [Tanaka and Fortezzo 2012]. Arrows indicate NPLD contacts (1) and unconformities (2) indicated in b). Exposed layers in lower section are NPLD material that predates TIS-1. Layered and banded terrains are easily identified. Wind streaks are visible indicating two directions.*

reflectors within the NPLD are offset vertically across these discontinuities by as much as 300 m (Figure 2.3), and the slope of each reflector varies by location with respect to a

trough. The 3D mapping of *Smith and Holt* [2010] demonstrated that the discontinuities were spatially correlated with the spiral troughs: connecting at the bottom of the troughs and having the same spiral pattern. Based on the spatial correlation, *Smith and Holt* [2010] interpreted the discontinuities as being genetically related to the spiral troughs and thus part of the stratigraphic record of their evolution.

Smith and Holt [2010] concluded that the observed discontinuities were bounding surfaces, formed during the deposition of migrating bedforms, in agreement with the observations of *Howard et al*., [1982]. The bounding surfaces, which they called trough migration paths (TMPs), indicate the former position (lowest point) of each trough where the eroded, layered terrain was onlapped by subsequent deposition of banded terrain.

TMPs begin at the bottom of troughs and extend hundreds of meters into the 2000 m thick NPLD. They are not all the same though. The troughs north of Chasma Boreale (Region 1, Figure 2.1) have TMPs that reach to more than 900 m, while troughs in Region 5 (Figure 2.1) only reach to ~350 m (Figure 2.4). This observation is in stark contrast to recently published studies that assumed or concluded that the troughs formed only after the entire NPLD were deposited [*Ng and Zuber*, 2006; *Pathare and Paige*, 2005; *Pelletier*, 2004; *Winebrenner et al*., 2008].

Smith and Holt [2010] detected variability in the slope of TMPs and argued that the TMP slope was intimately related to both migration and accumulation rates (Figure 2.5). These variations were found laterally within a single trough and between adjacent troughs. They concluded that the ratio of migration to accumulation was not constant in time and that, on average, 70 – 115 m of migration occurred during the accumulation of 10 m of ice, reducing the uncertainty of *Howard et al.,* [1982].

Based on SHARAD stratigraphic analysis and wind streak mapping by *Howard* [2000], *Smith and Holt* [2010] suggested that three processes determine the slope of the

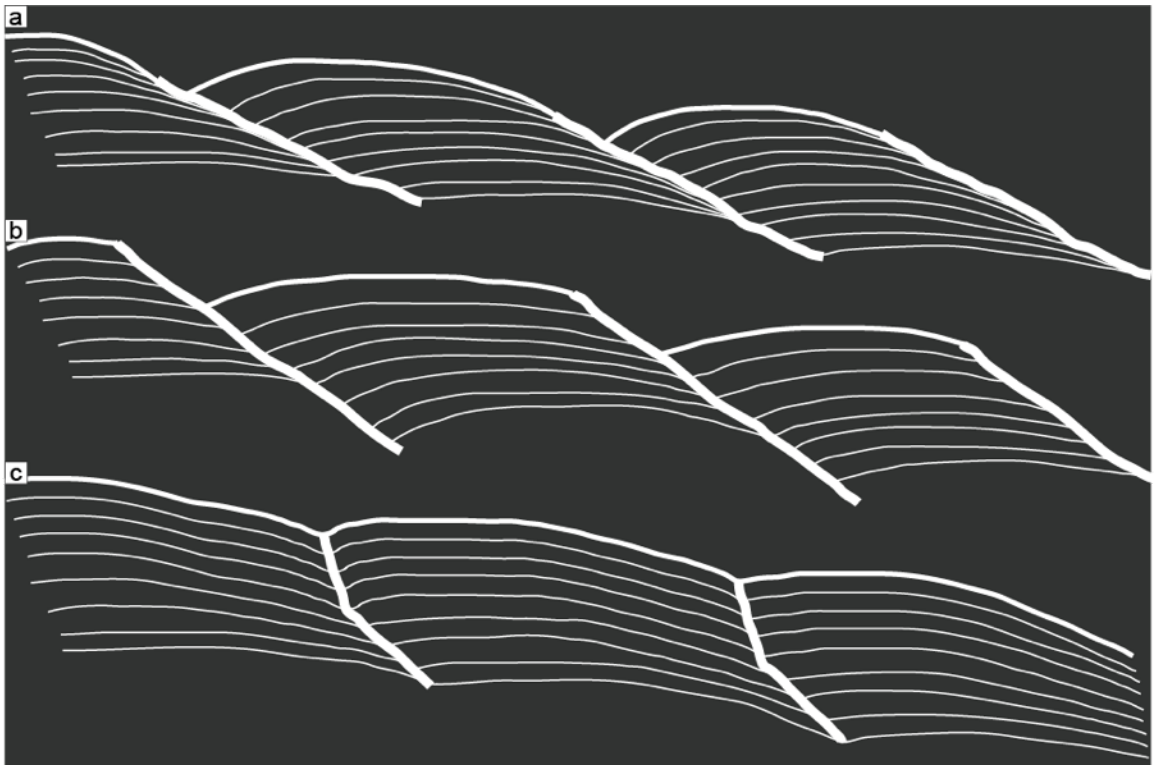

Figure 2.5: Animations of trough migration given different scenarios. a) Trough migration involving approximately equal parts of solar induced sublimation, wind enhanced erosion, and atmospheric deposition. *Troughs have identifying characteristics: thinned layers on the high side of the TMP and thicker layers on the low side. Migration is relatively rapid, and the TMP slope is low. b) Trough migration with enhanced insolation relative to wind transport. Layers are exposed on the high-side walls, and TMP is very pronounced. Individual layers are discontinuous and offset significantly. Layers have same thickening and thinning pattern across the TMP as in a). Reducing the winds to have no influence would result in layers that are uniform in thickness. c) Trough migration involving enhanced accumulation. Given sufficient deposition, layers are not eroded. Layers are continuous, and a true bounding surface does not form. Nevertheless, the troughs migrate. As with a) and b) layers are thickest on the low side of the TMP and thinnest on the high side. About halfway up the section deposition and the TMP slope increase.*

TMP: removal and transfer of ice by wind, insolation-induced sublimation, and atmospheric deposition. Each process influences the slope independently. The TMP slope increases during periods of either high accumulation, low sublimation, or reduced winds. Conversely, the slope decreases during periods of low accumulation, enhanced sublimation, or increased winds (Figure 2.5). All three factors likely varied continuously and co-dependently.

Another important observation came out of the first spiral trough 3D surveys: a pattern of layer thickness variation as first observed by *Howard et al*., [1982]. Besides discontinuous reflectors, the separation of reflectors (a proxy for layer thickness) on either side of the TMPs varies as determined by distance from the TMP. Nearly ubiquitously, reflectors approaching from the high side decrease in separation (layer thinning) as they near a TMP, and reflectors approaching from the low side progressively increase in separation (layer thickening) (Figure 2.2). As demonstrated by *Smith et al*. [in review], the thickening and thinning of layers is indicative of transport of ice across the trough. This detection contradicted several hypotheses predicting troughs stratigraphies related to ice flow and incision. In particular, the stratigraphies of recycled ice of *Fisher* [1993] and accublation *Fisher* [2000] were not detected by SHARAD.

Topographic undulations exist on the NPLD and are often located adjacent to the low side of spiral troughs [*Howard*, 2000]. Undulations are wavelike ridges and swales [*Cutts et al*., 1979] and have been interpreted to be the result of many possible processes: *Pathare and Paige* [2005] suggested that the undulations resulted from the viscous relaxation of former spiral troughs; *Squyres* [1979] interpreted them as the remnants of trough migration; and *Cutts et al*. [1979] concluded that they resulted from ice cap advance and retreat. More recently, undulations have been tied to depositional patterns associated with katabatic flow, similar to the troughs [*Smith et al*., in review].

3 METHODS

3.a SHARAD intro

SHARAD has been operating since late 2006 [*Seu et al*., 2007]. The instrument is a radar sounder that sends a chirped, 80 μs pulse from 15 to 25 MHz and records reflected energy versus time. Reflections are the result of contrasts in the real part of the permittivity, ε, which modifies the velocity of the signal. Within water ice, SHARAD has a theoretical vertical resolution of ~8.4 m [*Seu et al*., 2007].

Multiple pulses of energy are coherently summed onboard MRO. After relay to Earth for further processing, pulse compression, synthetic aperture focusing, and corrections for ionospheric distortion are performed [*Campbell et al*., 2011]. After processing, SHARAD resolves targets down to 0.3 – 1 km along track and 3-6 km cross track [Seu et al., 2007].

Since reaching Mars, approximately 2,200 observations of the NPLD have been collected. These observations provide very tight spatial coverage useful for analysis. Given the SHARAD footprint of ~3 km, this density effectively gives higher spatial coverage of observations at high latitudes than the horizontal resolution of the instrument.

With the wealth of data, we utilize both repeated and crossing observations to increase confidence in interpretations. Repeated observations are important for checking against artifacts of processing or low signal strength, things that may hamper an individual observation. Crossing observations are useful for eliminating ambiguous interpretations. By examining from multiple orientations, our view of subsurface geometries is improved. Furthermore, multiple observations of a target help to separate surface clutter from scientifically interesting subsurface reflections, a critical first step of interpretation.

3.b Mitigating clutter

SHARAD has a dipole antenna that radiates in a modified torus. The distance of SHARAD above the surface (~300 km) is sufficient to create a radiation pattern on the surface that is effectively a plane wave. Although the first Fresnel zone is ~3 km diameter, surface reflections may return from anywhere in the antenna pattern. Hence the point directly below the spacecraft, or the nadir point, is only a portion of the return signal. Surface reflections resulting from locations far away from nadir point are considered "clutter" due to the fact that they can appear as subsurface reflections with a similar time delay.

Clutter cannot be removed from a radargram, but it can be mitigated. By comparing predicted clutter in a synthetic radargram to actual SHARAD observations, one can determine which part of the signal is from the subsurface [*Holt et al*., 2008]. The synthetic radargram, or "cluttergram," is calculated from surface topography, and we use Mars Orbiter Laser Altimeter (MOLA) digital elevation models [*Smith et al*., 2001]. The cluttergram only shows what reflections the instrument will receive from the surface (Figure 2.6). Reflections in the radargram that are not present in the cluttergram are considered subsurface reflections. Their presence of subsurface reflections on additional, nearby tracks is further confirmation (the clutter changes position depending on the track geometry).

Orbital geometry has a strong influence the amount of clutter received and the location of the first reflection. For our survey, favorable geometries are those where the spacecraft ground track aligns nearly perpendicular to the strike of a trough. This results in "first return" surface reflections near the nadir point. More oblique angles are less favorable, and radargrams from orbital track geometries aligning parallel to troughs are

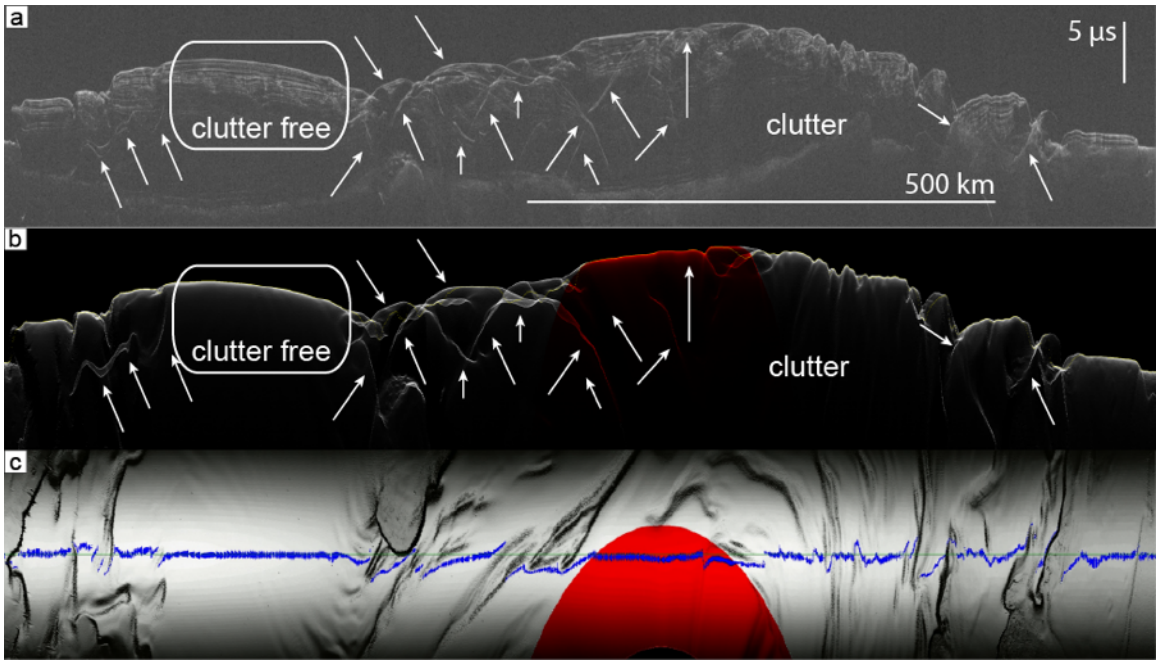

Figure 2.6: Radargram – synthetic radargram comparison. Observation 725402. *a) Portion of NPLD radargram 725402 in one way time. Arrows indicate clutter. One clutter free section exists and is discussed in Figure 2.20. b) Simulated radargram matching a). Clutter dominates the central portion of this image due to poor geometric alignment. Near the NPLD margins clutter is not as dominant, allowing for better interpretations. Yellow line indicates NLPD surface topography along track. Red shading indicates region with reduced clutter simulation due to missing topographic data. c) Shaded topography along the orbital track of radargram in a). Brightness indicates strength of reflections from the surface. Green line is ground track of spacecraft during this observation. Red area has little topographic data and is poor for clutter prediction. Blue shapes indicate the width of a single radar pulse Fresnel zone and location of first reflection. First reflection is farthest removed from nadir point then the ground track is oriented at low angles to troughs.*

often unusable (Figure 2.6). In our survey we employ clutter mitigation techniques for all observations and present radargrams that are most favorable for interpretation.

3.c Interpretation of 2D horizons and cross-correlating reflectors

As of yet, reflectors cannot be directly correlated to visible layers [*Milkovich et al*., 2009], but they can be used as proxies of the geometry of layering [*Christian et al*., in

press]. Reflectors, as observed by SHARAD, are therefore accepted to be profiles of paleo-surfaces of the former NPLD.

One of our goals for interpreting SHARAD radargrams is to recreate subsurface structure of the NPLD. This requires many steps. After mitigating clutter, the next step is to interpret or "pick" reflectors. NPLD reflectors are often continuous for hundreds of kilometers. To track these reflectors, we employ a method similar to that performed by *Putzig et al*., [2009] within a seismic interpretation software package. We chose Schlumberger's GeoFrame to track the coordinates of our "picks." Picks are interpretations that correspond to a single horizon or reflector (Figure 2.7). By following the reflectors we keep track of the x, y, and t coordinates of each pick and record that point for future reference.

Due to the range resolution and sampling of SHARAD, a reflector may be spread over several pixels. To determine with greatest precision the location of that reflector we rely on GeoFrame to find the brightest pixel within 50 nanoseconds of the human-chosen picks. This "autopick" tool allows for more accurate and faster interpretations.

Even with autopick, there is still subjectivity in choosing a reflector. Reflectors are often discontinuous at some or multiple points across the NPLD. A human interpreter must bridge the gap to create a complete horizon. We analyze multiple, crossing radargrams to complete this step. GeoFrame offers the capability of displaying two or more intersecting radargrams at the same time and at the same vertical scale (Figure 2.7), so that in many cases the gap can be circumvented entirely. This method allows us to confidently correlate a reflector in one radargram to the same reflector in another, even if separated by a large discontinuity or by hundreds of kilometers.

Few reflectors extend to the NPLD margin. Many disappear due to erosion or pinching out (Figure 2.2), and only the current surface and the lowest boundary, between

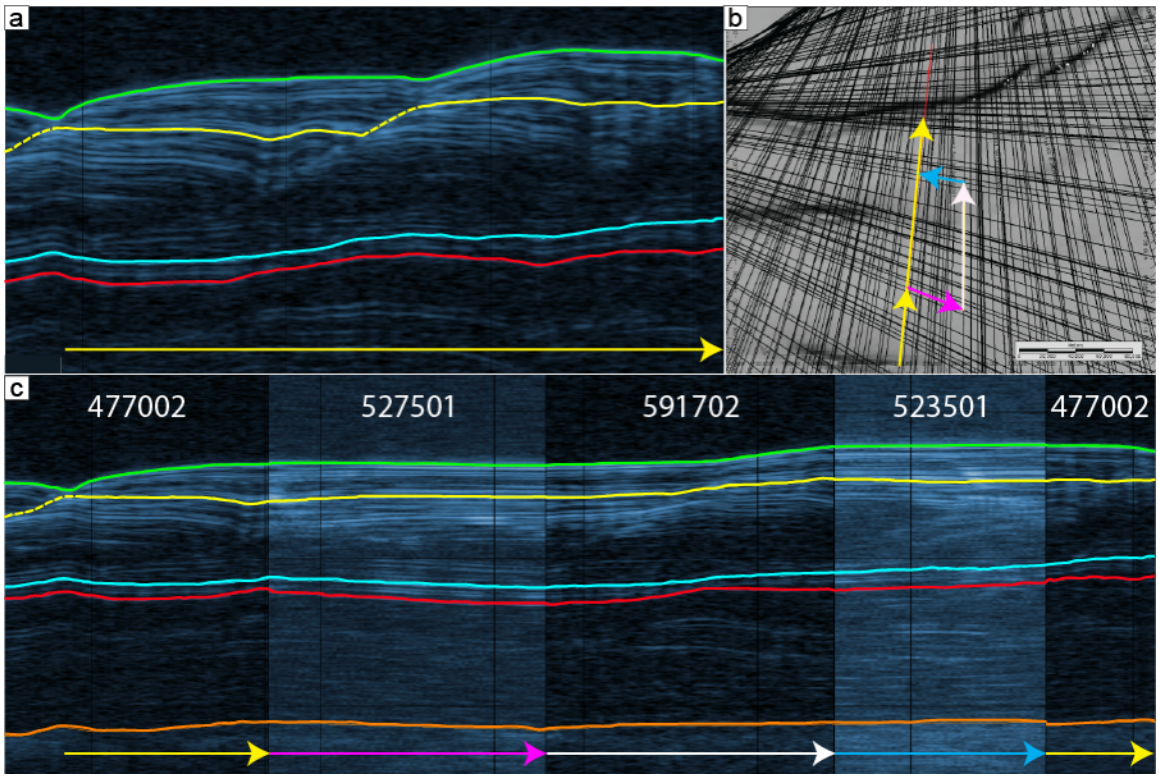

Figure 2.7: Technique for avoiding discontinuities. *a) Section of radargram 477002. Three reflectors are interpreted: red is reflector R29 (TIS-1); blue is R25; and yellow is internal reflector during trough migration. Yellow line crosses TMP and is therefore discontinuous (dashed). b) Map view of alternate route for connecting the yellow reflector across a TMP. Arrows indicate detour around TMP to avoid the discontinuity. c) Connected radargrams 477002, 527501, 591702, and 523501. The yellow line is no longer discontinuous because east of 477002 the trough has migrated less, and the reflectors are continuous.*

the NPLD and the basal unit, are continuous across the entire cap. Therefore, it is impossible to map every reflector (or paleosurface) entirely without extrapolation. Because there is no other technique for estimating the surface represented by a single reflector that disappears in places, we extrapolate as sparingly as possible. Reflectors below and above the eroded or invisible reflector provide constraints for estimating extrapolated surfaces.

Finally, we map the TMPs in order to study their variability in slope, vertical extent, etc. TMPs are by definition identified by discontinuous reflectors, making them generally more difficult to trace. However, when geometries are favorable, TMPs are

straightforward to detect. Once mapped, the locations and properties of the TMP can be analyzed for variability.

3.d Geospatially rectifying and creating surfaces

Once interpretation is complete, calculating the location of an individual reflector on a trace is critical for obtaining accurate x and y coordinates. Frequently, the reflection that reaches SHARAD first is not from directly below the spacecraft. This is especially true in regions with measurable surface slopes. Using in-house software, we create facets of topography based on MOLA elevation [*Smith et al*., 2001]. The facets are analyzed, and the corresponding angle, or aspect, relative to SHARAD's signal is calculated. If a simulated signal is the first to reflect back to the receiving antenna we call it a "first return". The x and y coordinates of the first return are then moved to this facet (Figure 2.6c). The benefit of this technique is that the geometry determined by radar more closely reproduces that of the actual layers [*Christian et al*., in press].

The physical location of reflectors is critical to our analysis, and our picks must be converted from the time based radargrams to depth. The t coordinate recorded by SHARAD is converted into z by employing Equation 1.

$$d = \frac{c}{\sqrt{\varepsilon_r}} * t$$

Equation 1

Where d is depth, c is the speed of light, t is time as recorded by SHARAD, and ε_r is the real part of the permittivity or dielectric constant of the material under question. We employ an ε of 3.15 calculated for NPLD ice [*Grima et al.*, 2009]. In this way we position each reflector in space beneath the first return.

Finally, once the coordinates of each pick are properly rectified they are converted to a latitude, longitude, and radius point with in-house software. These coordinates are imported into a GIS program such as ESRI's ArcMap for gridding. We interpolate each point into a raster grid using the natural neighbor algorithm in ArcMap. With this raster it is possible to study many properties of the surface, including topography, slope, aspect, and vertical separation from another surface.

To better convey polar geometries in this paper, we primarily display depth-corrected radargrams for figures. These images have been converted from time to depth by making assumptions about the dielectric properties of the NPLD. However, depth correcting inherently distorts the image, so our interpretations, as described in Section 3c, are done within the less processed time domain images. This reduces accumulated errors.

4 RADAR OBSERVATIONS

4.a Regional Variability

Previous trough studies utilizing SHARAD have focused primarily north of Chasma Boreale and near the margin at 90° E [*Smith and Holt*, 2010, 2011], but troughs elsewhere exhibit many of the same qualities, providing more sites for investigation. In

order to understand trough and ice accumulation around the cap, we extend the survey of *Smith and Holt* [2010] to include the majority of the NPLD and offer a more holistic characterization of trough structure and variability than prior work.

We divide the NPLD into eight regions based on a combination of surface morphology and SHARAD observations (Figure 2.1). Morphologically, the regions differ in several factors. Region 1 primarily exhibits classical troughs as described by *Howard et al.,* [1982] and *Smith et al.,* [in review]. Some troughs in Region 1 have minor topographic undulations, but they have low profiles and are not extensive. Region 2 and 3 contain many central promontories or steps on the trough high side. Troughs in these regions tend to be deeper than those in Region 1 and expose more layers on the high side. Region 3, along with Region 7, contains many well-developed topographic undulations with accompanying stratigraphic record. Regions 0, 4, and 7a are difficult or impossible to observe with radar but exhibit some classical and non-classical traits. Region 5 corresponds to the eastern extent of Gemina Scopuli. The troughs here are younger than elsewhere on the cap, having formed much higher stratigraphically. Region 6 has no surface troughs but exhibits buried troughs and evidence of southward migration, contrary to observations in other regions. We discuss these differences and commonalities in detail in the following sections.

4.a.1 Troughs in region 1

Region 1 (Figure 2.1) has previously been studied in detail due to favorable geometries and relatively continuous, bright reflectors. The wealth of good observations

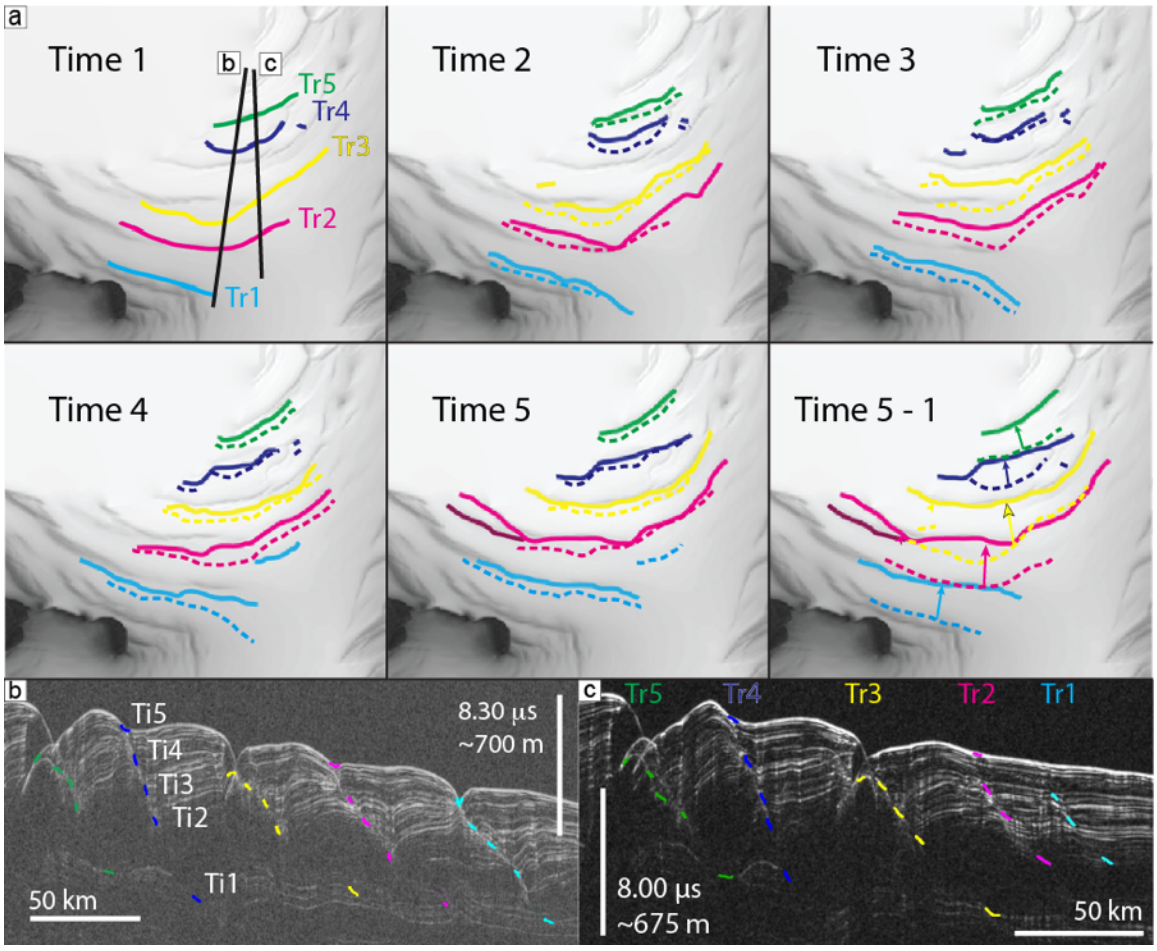

Figure 2.8: Plan view map of trough migration. *a) Plan view of NPLD topography with overlain trough locations at various time steps. Solid lines indicate an individual trough at each point in time. Dashed lines are trough positions at previous time step. b) Annotated portion of radargram 933202. Five TMPs are mapped for their intersection with individual reflectors. Yellow is trough initiation point; light blue is time step 2; dark blue is time step 3; magenta is time step 4; red is time step 5 (current surface). Some of the spiral troughs did not form until after the sequence had begun. For one trough there exists a TMP but no surface expression. c) Annotated portion of radargram 706402. Same as in b) except each trough has clear beginning point and surface expression.*

and stratigraphy that is straightforward to compare with predictions of *Howard et al*., [1982] makes Region 1 an ideal location for basing comparisons with other troughs.

Few other places on the NPLD offer this quality of observations, so we take the opportunity to analyze trough migration by mapping the location of five troughs at distinct stratigraphic levels. To observe migration in three dimensions, we tracked five

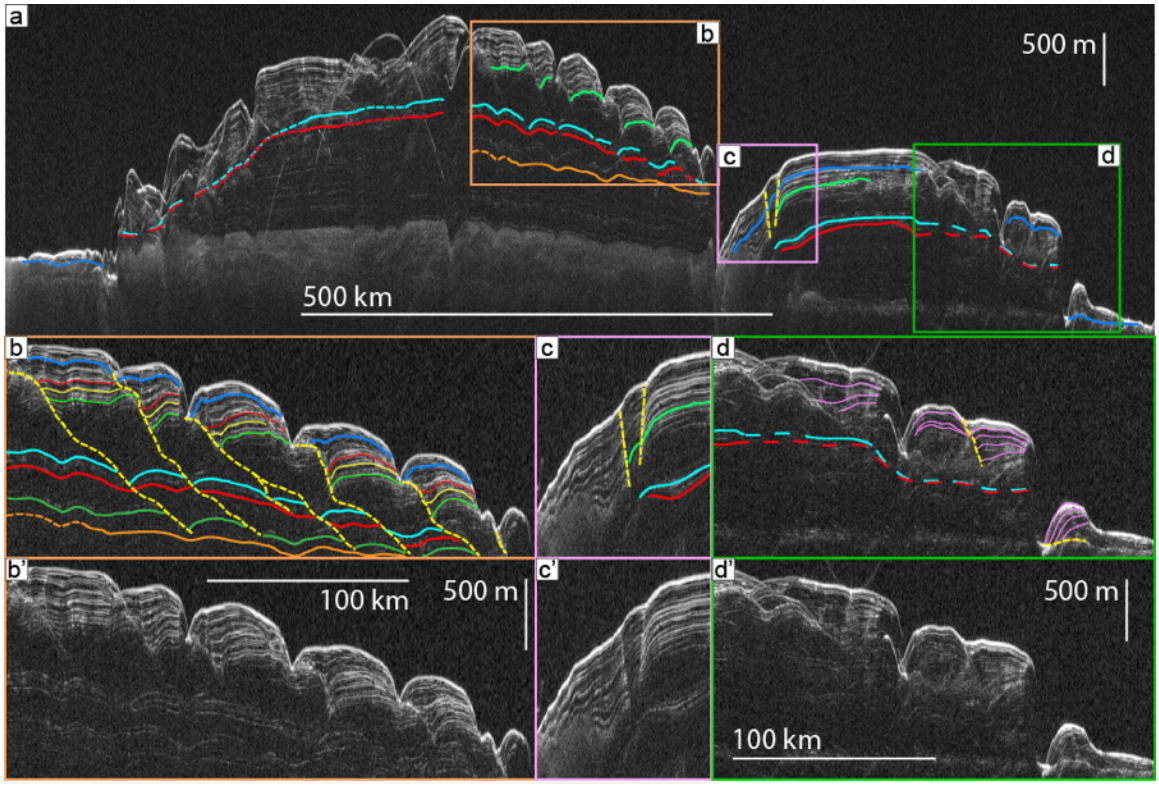

Figure 2.9: Radargram 1252401 depicting troughs observations in Regions 1, 3, 5. *a) Entirety of 1252401 with interpretations in color: R29 (red), R25 (light blue),* Contact1-3 *(dark blue). b) Section of 1252401 north of Chasma Boreale at Region 1. Troughs in Region 1 have easily identified TMP that extends below TIS-1. Reflectors below TIS-1 (red) are offset (green), signifying that the oldest troughs on the NPLD existed earlier than previously thought [Smith and Holt, 2010]. Troughs have migrated as many as 90 km since initiation, 1100 m beneath the current surface. This observation has only been detected in Region 1. c) Observation of Region 7b south of Chasma Boreale. R25 and* Contact1-3 *align with angular unconformities. d) Region 5 observation near NPLD margin. Troughs observations are difficult to make due to poor geometry. Layer thickness variations exhibit trough migration properties (magenta lines), including thinning on the high side and thickening on the low side. One TMP may be discernible (dashed yellow line).*

reflectors for their intersections with the TMP within tens of radargrams. The coordinates of each reflector's intersection with a TMP were recorded and converted to positions based on the techniques described in Section 3. We chose progressively higher stratigraphic reflectors for sequencing the location of each intersection. The reflectors include the current surface, bright reflector R25 (light blue line in all radar figures), and three others in between (Figure 2.8b,c).

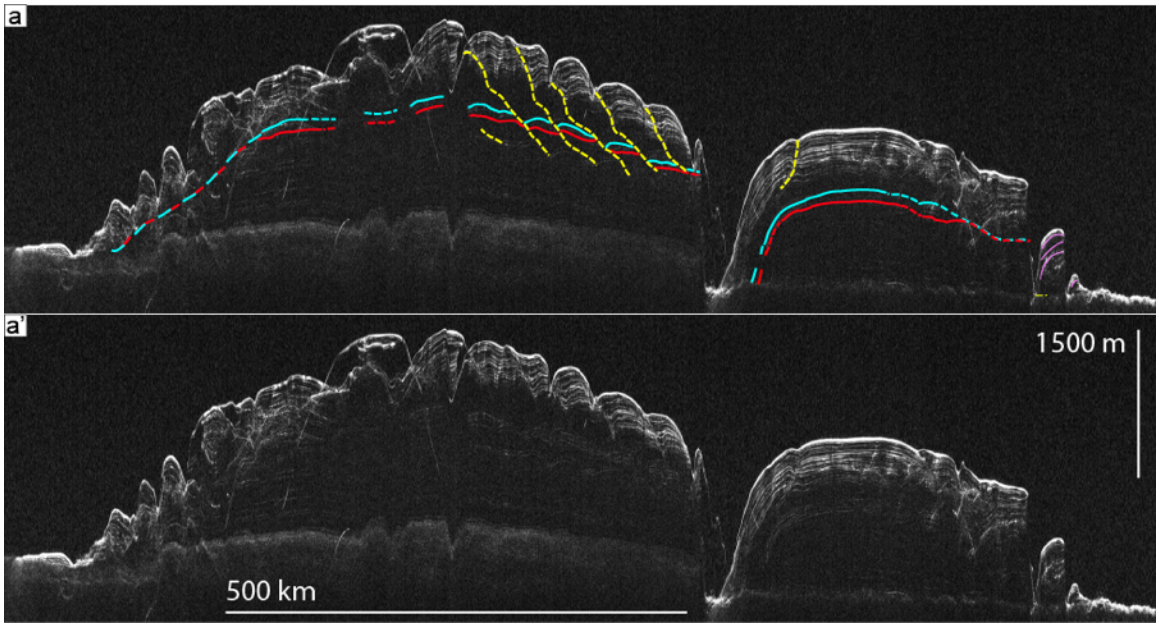

Figure 2.10: Radar observation 1247102 of NPLD in Regions 4, 1, and 7. *Region 4 trough have are poorly observed with this geometry. Region 1 troughs have V-shapes and TMP like in Figure 2_12524. Region 7b has immature trough. R29 and R25 intersect the bedrock in Region 7b. Troughs in Region 7a have migrated horizontally due to bedrock bases. Low side reflectors are indicative of migration.*

Projecting the intersection points into map view demonstrates the troughs position and orientation. In this way we observe each trough's relative (horizontal) motion through time (Figure 2.8a). The troughs generally migrate poleward, but lateral migration is faster in some locations than others. Specifically, between time steps 2 and 3 near the center of our tracked position the magenta trough migrated farther. Between time steps 4 and 5, the light blue trough moved very little on the western end but migrated significantly on the eastern side. An additional extension of the light blue trough appears between time steps 3 and 4, indicative of trough growth horizontally.

Smith and Holt [2010] observed that TMPs of troughs in Region 1 reached depths of 550 – 700 m, often intersecting R25. R25 is often discontinuous at that intersection, revealing that the troughs already existed at that stratigraphic level.

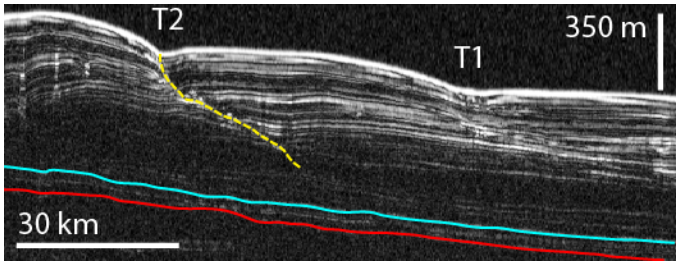

Figure 2.11: Portion of radargram 598301 demonstrating two types of migration. *Trough 1 has well defined TMP due to large reflector offset and truncated surfaces. Trough 2 is more poorly defined, and layers are not discontinuous. Instead, the reflector slope inflection indicates former trough location. Both troughs initiated stratigraphically higher than reflectors R25 (light blue) and R29 (red) but are part of the same progression as other troughs in Region 1. Trough 2 is immature compared to other troughs.*

Below R25, another bright reflector, R29 (shown as red in all figures containing radargrams), exists that is more extensive over the NPLD than R25. R29 is also more continuous with respect to TMP; i.e., it intersects TMP less often than R25 (Figures 2.9 and 2.10). These few TMP reach down to about 1 km, over 50% deeper than measured by *Smith and Holt* [2010]. One trough in Figure 2.9b has migrated ~100 km, farther than the 65 km previous reported for troughs in this region.

Even though troughs in Region 1 exhibit classical migration, there is variability that can be detected by geographic comparison. One such case is where the TMP is not a true bounding surface (e.g., the reflectors are not discontinuous). Near the easternmost portion of Region 1, the high side of some troughs were only thinned and not fully eroded. Even though the reflectors are not truncated, a stratigraphic inflection indicates the former location of those troughs (Figures 2.2b, 2.8c, and 2.11). Furthermore, the TMPs of T1 and T2 in Figure 2.11 do not reach R25. Instead, evidence of their initiation is stratigraphically higher than that of other troughs in this region and corresponds to the extension of Troughs 1 and 2 between time step 2 and 3 of Figure 2.8.

Most troughs in Region 1 exhibit pronounced accumulation asymmetry in addition to migration, similar to the stratigraphy indicated by Figure 2.5a. Also observed in Region 1 are V-shaped reflectors that are found on the low side of TMPs. *Smith and Holt et al*. [2010] detected these V-shapes and characterized them as an inflection in

layers approximately 10 km wide near the top and affecting reflectors ~300 m deep. These geometries were thought to be unique to Region 1.

4.a.2 Troughs in region 2

Region 2 troughs have much in common with Region 1 troughs. On the surface they display the same layered and banded terrain. Their wavelengths are approximately the same. However, these troughs also have more complex morphologies. Troughs of Region 2 are generally deeper and have W-shaped cross sections. We call the W-shaped troughs compound troughs (Figures 2.12b and 2.13b).

Figure 2.12b spans Region 1 and Region 2. At the highest latitudes (Region 1) classical migration is displayed. Further south, near Chasma Boreale (Region 2), the troughs are deeper – as much as 1 km. TMP are visible, and indicate that the two lowest troughs in Figure 2.12 have migrated 16 and 24 km, respectively. Thickness variations associated with migration are visible. Specifically, on the high side of each trough the layers thin as they approach the surface. We also detect a familiar V-shape geometry at the same two lowermost troughs in Figure 2.12b (magenta reflectors).

Continuing west, Figure 2.13b has strong evidence of migration. Near the mouth of Chasma Boreale, at 315° E, one trough is much farther north than its initiation point and has a well-delineated TMP that extends ~30 km horizontally. While migration is readily apparent, layers near the TMP have reduced variation in thickness compared to those in Region 1. Even with reduced variation, layers of each trough thin as they approach the surface on the high side.

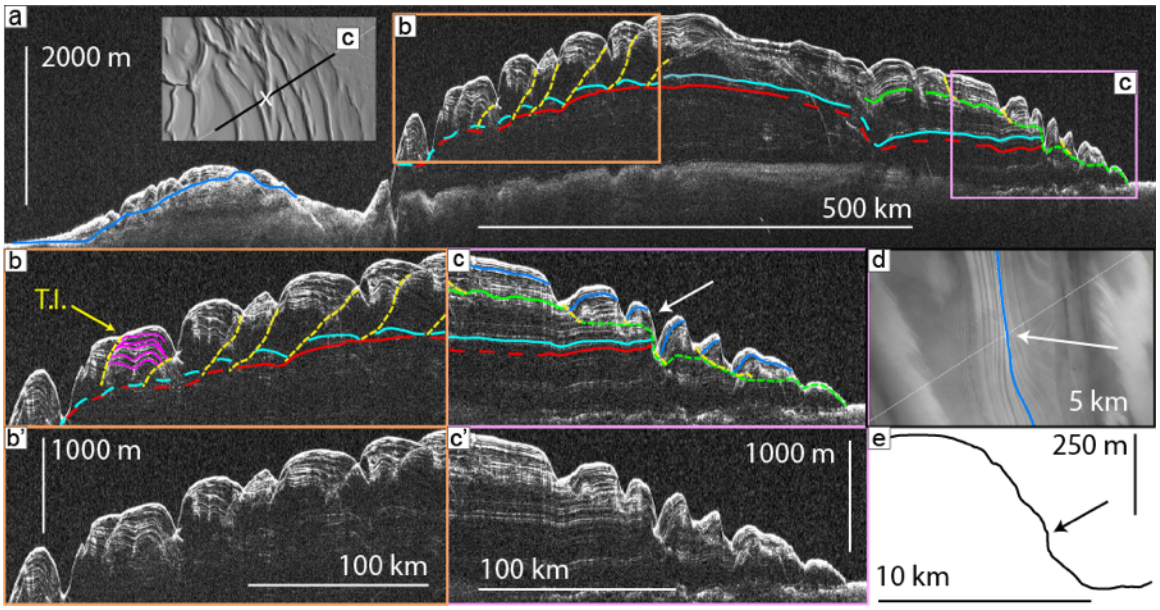

Figure 2.12: Radar observation 855602 of NPLD*. a) NPLD context for Regions 1, 2, and 5, and TIS-1 (red line). Inset is hillshade section of Region 5. Black line indicates ground track of b). White X indicates location of unconformity. b) Region 5 Troughs. Similar to Figure 4_761602, TIS-2 is exhibited stratigraphically higher than TIS-1, R29. Regional slope of TIS-2 is 0.39°, and trough wavelength is ~20-30 km. R25 (blue) and R29 (red) are truncated at the surface. White arrow identifies unconformity in c) and a)-inset. c) Portion of CTX image P20_008991_2644_XI_84N267W. White line is ground track of radargram 855602. An unconformity mapped by Tanaka and Fortezzo [2012] is identified by a white arrow. d) Region 1 and 2. Troughs in Region 1 have easily identified TMP. Farther south, in Region 2, the TMP are less easily identified. W-shaped troughs are exhibited.*

Even though they exhibit migration, troughs in Region 2 are also more complex than those in Figure 2.1. The furthest left troughs in Figures 2.12b and 2.13b are compound, having central promontories. This topographic surface profile was not observed in Region 1 and represents the first deviation from the classical trough described above. Farthest south in Figure 2.13, SHARAD detects two additional buried promontories. These topographic highs have been covered by ~250 m of ice and dust during migration. One promontory exhibits horizontal layering, in contrast to the sloping layers deposited above and to the sides, an indicator of the geometry of deposition before they were eroded.

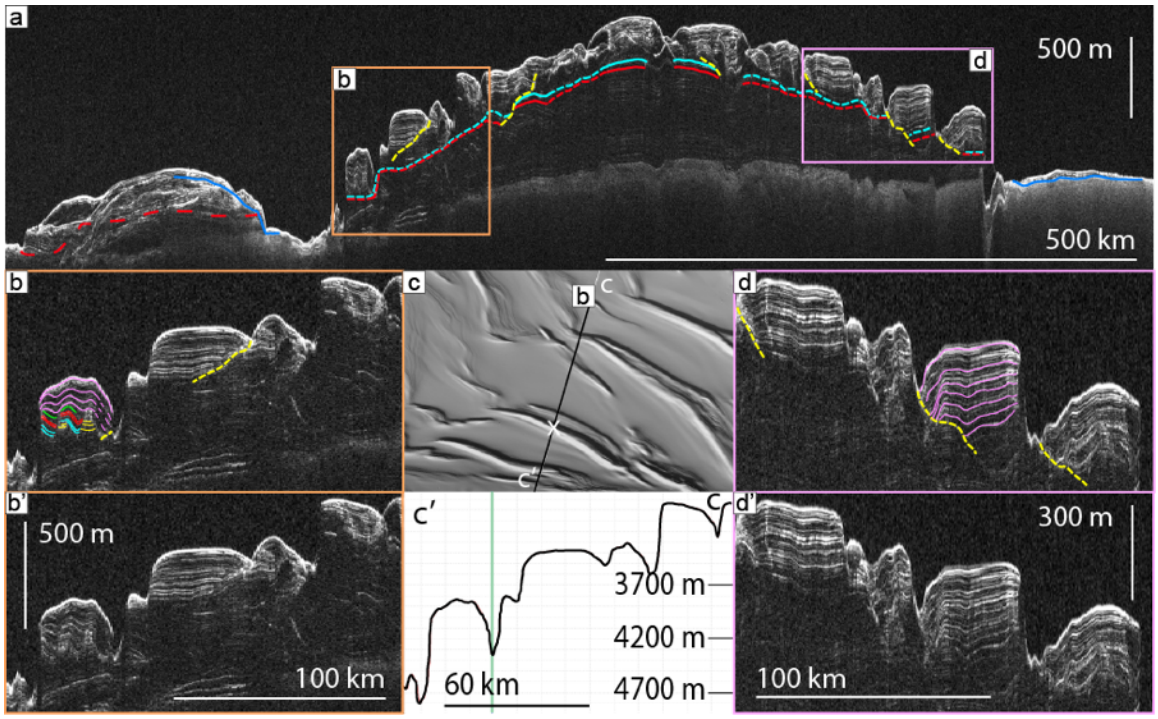

Figure 2.13: Radar observation 2265701 of NPLD. *a) NPLD context for Regions 2, 3, and TIS-1 (red line). Inset is topographic profile of b) and c). Blue line coincides with X in c). b) Troughs in Region 2 exhibit TMP (dashed yellow lines) and only minor thickness variations. They also exhibit a W-shaped morphology with central promontory. The deepest portion of the trough has onlapping deposition from younger material, evidence for migration. Buried undulations are not exposed on the surface (magenta). It is possible that the undulations overly former trough promontories, making double, or triple W-shaped troughs. c) Hillshade of Region 2 with ground track of 2265701. White line indicates radar observation ground track and topographic profile of inset in a). Trough has W-shape. The lowest point is marked by a black X. Trough is ~700 m deep. e) Portion of radargram 2265701 in Region 3. Troughs defined TMP but minor thickness variations.* Contact1-3 *extends ~150 km beyond the NPLD.*

4.a.3 Troughs in region 3

Like Region 2, Region 3 offers more diversity from the classical troughs of Region 1, including highly variable wavelengths and trough depths. Troughs are deeper nearest the NPLD margin, sometimes reaching 1 km. Topographic undulations dominate the inter-trough plateaus of this region.

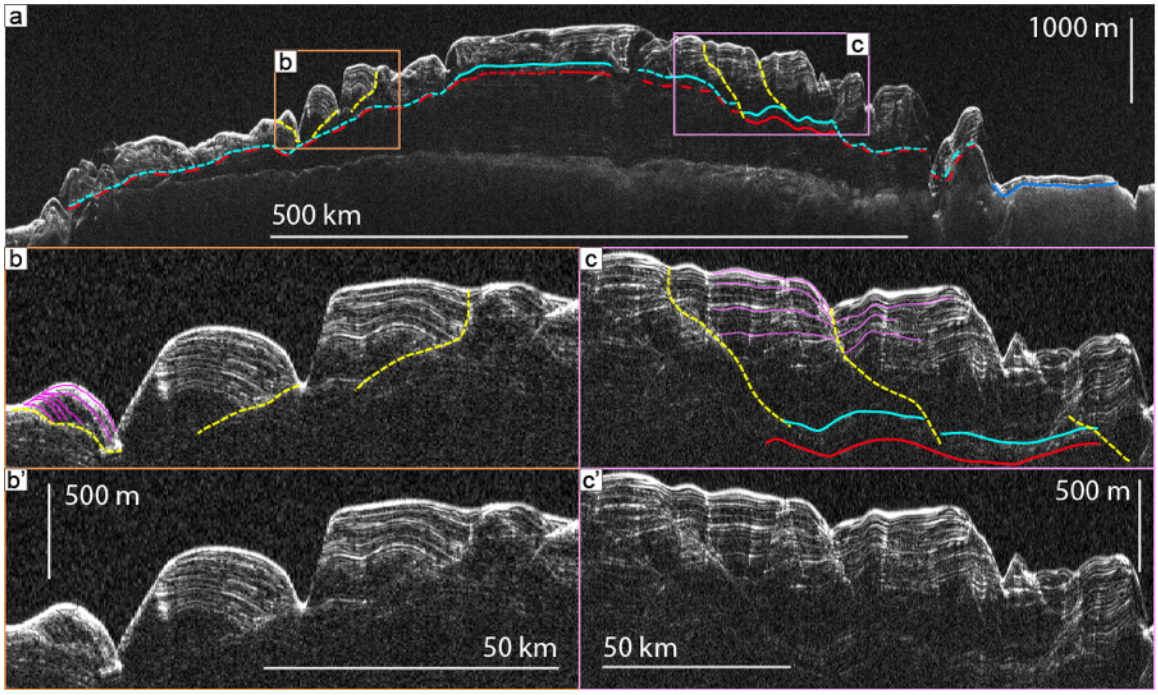

Figure 2.14: Radargram 2189301 observations of NPLD Region 2 and 4. *a) NPLD observation. b) TMPs exhibited. Well delineated TMP north of Chasma Boreale in Region 2. Troughs former location is easily determined. Approximate level of R25 is indicated (dashed light blue line) c) TMP near 205°. Trough has northward migration (yellow), but nearby undulation has southward migration (green) d)* Contact1-3 *demonstrated at NPLD margin.* Contact1-3 *is ~ 110 m thick and extends for ~100 km.*

At 289° E, near the boarder with Region 2, two latitude troughs display well defined migration paths that extend downward towards R25 (Figure 2.14b). Left to right, the troughs have migrated 17 and 19 km during ~500 m of accumulation. In general these northern troughs have similar features to the troughs in Region 1, but they deviate from the classical trough because they display reduced thickness variations. At lower latitudes the troughs have very low amplitudes (Figure 2.14a). One trough shows anomalous stratigraphy: low side layers that dip poleward more than observed previously and a downward sloping TMP (Figure 2.14b). This trough migrated 19 km.

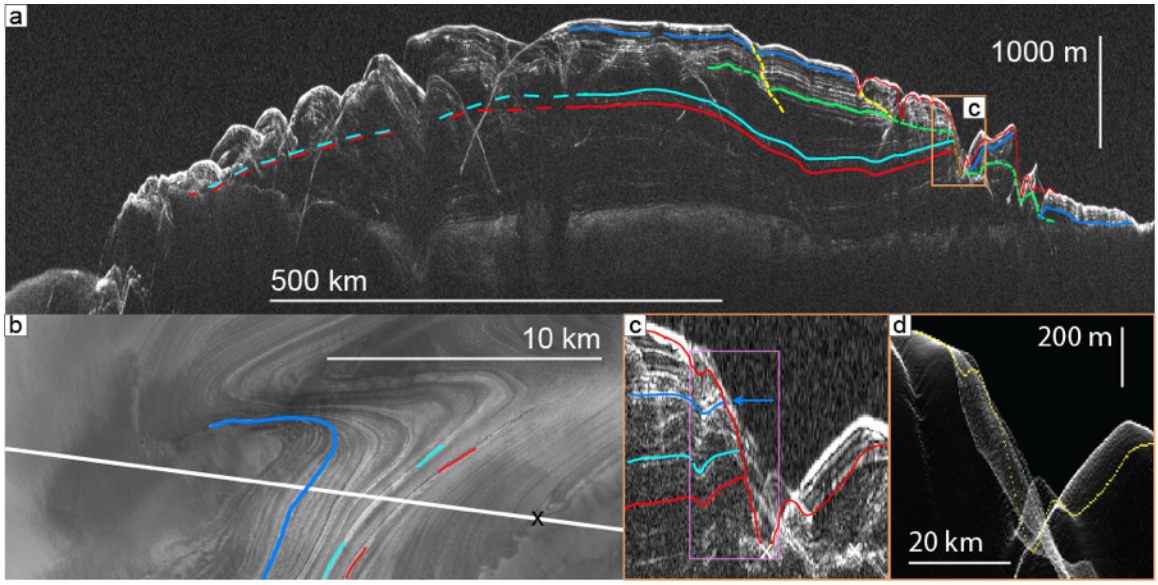

Figure 2.15: Radar and optical, and topographic observation of NPLD. *a) Radargram 1044302: Observation crosses boundary of Regions 2 and 3, where very little detail is evident. In Region 5 there is clear evidence of erosion (TIS-2). A bright reflector (R17) corresponds to TIS-2 and is easily traced (green). Reflectors R25 and R29 reach the surface on the high side of a trough. One TMP is detected (dashed yellow).* Contact1-3 *(dark blue). MOLA topographic profile (red). b) Portion of CTX image P01_001437_2622_XN_82N298W at 60.4°E, 82.5°N. An unconformity mapped by Tanaka and Fortezzo [2012] is identified by a blue line. Two prominent sets of layers may correspond to reflectors R25 and R29. Black X corresponds to bottom of trough d) c) Annotated portion of radargram 1044302. Reflectors R25 and R29 extend to meet the surface (red from MOLA). Reflectors above the topographic surface are clutter as detected in e). d) MOLA topographic profile of white line in b). X, 25, R29, and unconformity correspond to those mapped in b) and c).*

At about the same longitude, 296°E, Figure 2.15 demonstrates how poor geometry influences detection of TMP. Clutter obfuscates observations at each trough in Region 3, making mapping of the migration impossible.

Further west, at 227° E, 86.5N, another trough displays the characteristics of migration (Figure 2.3): a well-defined TMP, sloping layers, and thickness variations. The TMP is particularly easy to identify here because the low side layers are adjacent to a section with low reflection. There can be no mistake of interpreting layers as continuous across the TMP. However, the stratigraphy observed in Figure 2.3 differs from classical troughs in Region 1. Instead of significant thinning on the high for the entire section, the

layers only thin in the top ~110 m. Reflectors below that are sub-parallel. Layers in the lowest ~350 m of this trough very too little to detect.

Figure 2.13d also clearly exhibits trough migration in several places. Below ~250 m of reflectors, R25 and R29 are discontinuous across the TMP. This indicates that the trough existed prior to R29. Magenta colors also reveal subdued V-shaped reflectors that characterize this trough, similar several troughs in Region 1. This trough migrated ~30 km during ~250 m of accumulation.

A trough resides at 252°E and 84.5° N that has been the subject of debate regarding migration (Figure 2.16a) [*Rodriguez and Tanaka*, 2011]. This is a compound trough that displays a central promontory, around which layers can easily be traced in optical imagery. While this trough is not unique on the NPLD, it and others have been interpreted to form during only in-situ erosion, without migration. However, a closer look reveals evidence for migration both in optical and radar data.

The promontory adds complexity to this trough, but all of the classical characteristics of migration are visible, including high side erosion and layered terrain. In this case, the W-shaped profile means that the high side is compounded and longer than a simple trough. The lowest portion of this trough, between a' and a'', is ~400 m lower than the central promontory at a', and layered terrain are visible down to the lowest point of the trough. On the low side, banded terrain (a telltale sign of migration) is observed at a". Analysis of SHARAD data supports the optical observations (Figure 2.16b). Exposed, thinning reflectors on the high side are contrasted by thickened, pole-tilting reflectors on the low side. A short but otherwise clear TMP is readily observed.

Besides the visible central promontory of the trough in Figure 2.16 there is a second, buried promontory. This promontory has approximately the same dimensions as the one on the surface but has a reduced surface expression due to being buried beneath

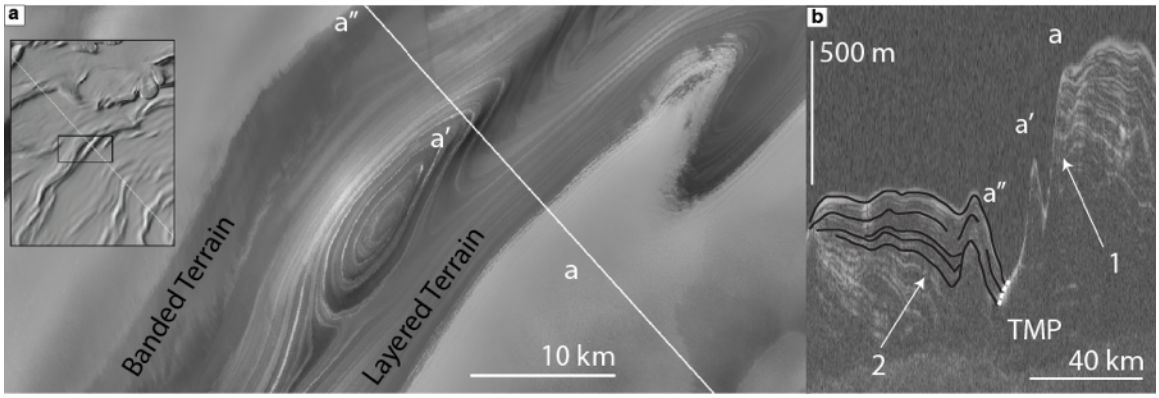

Figure 2.16: Observations of W-shaped trough, inter-packet Material, and TMP. *a) Portion of CTX image B01_010014_2644_XN_84N107W near spiral trough. Optical imagery depicts complex trough with central promontory giving the trough a W-shaped cross section. Visual layers are traced around promontory, complicating interpretations. Left of image is banded terrain, as described in Cyclic Step model of trough migration [Smith et al., in review]. White line corresponds to radar ground track in b). "Inter-packet material," observed in b) is outcrops between a' and a". Inter-packet material contains layers and is of low to intermediate albedo. b) Portion of radargram 556602 as indicated by ground track in a). Besides W-shape, trough exhibits features of the classic trough model: TMP and layer thickness variations. TMP results from banded terrain onlapping a formerly eroded surface. Beneath the overlying, low side deposits exists a buried promontory of approximately the same size as the exposed one at higher elevation. The layers drape this feature, which impacts the current surface. Inter-packet material (low reflectivity) is exposed on the lower portion of the W-shaped troughs. Putzig et al., [2009].*

~150 m of ice and dust. Additionally, the surface peak above the buried promontory is more than 1.5 km north of the buried peak, indication of migration.

Region 3 is rich in topographic undulations. *Smith et al*. [in review] suggested that undulations were related to trough formation but did not include stratigraphic analysis in their interpretation. Here we demonstrate that some undulations have detectible signatures in the uppermost NPLD. Furthermore, they are found to be stationary through time or migrate: either towards or away from their associated trough.

Figure 2.17 captures two sets of undulations in Region 3 near 245° E and 85-87° N. Strikingly, both sets have long-lived stratigraphic expressions that extend hundreds of meters into the subsurface. One set (Set A) reaches 500 m beneath the current surface, down to approximately R29. Another set of undulations (Set B) existed between 500 and

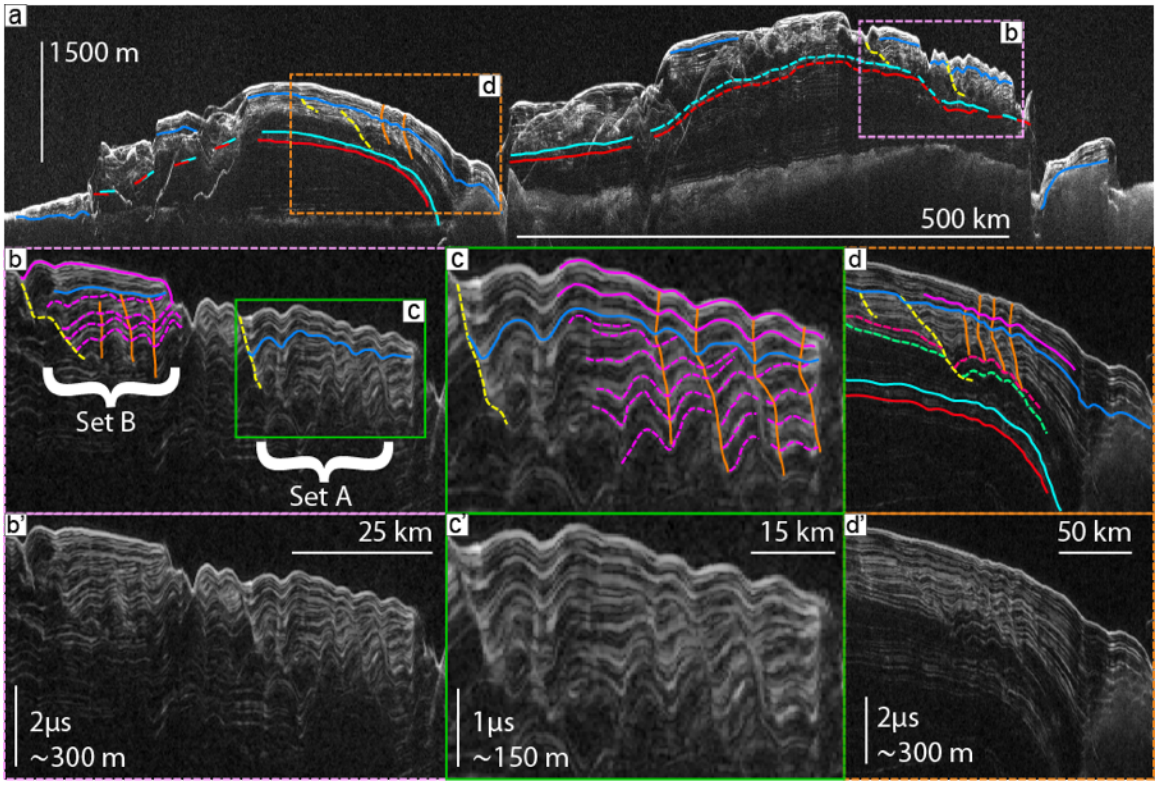

Figure 2.17: Radargram 2007101 observation of NPLD in Regions 3 and 7. *a) Radargram 2007101 crossing NPLD with interpretations in color: R29, R25,* Contact1-3. *Boxes indicated b) and d). Observation also crosses Regions 1 and 2, but poor geometry makes observations impossible. b) Section of radargram 2007101 in Region 3. Stratigraphic evidence for undulations is found in two locations: Set A and Set B. Set A undulations are expressed at the surface and have records as many as 300 m beneath the surface. Set B undulations also meet at 300 m beneath the surface, but are buried ~ 85 m beneath the surface. RAP separates the two units. c) Expanded view of box in b). Undulations migrated approximately one wavelength before reversing direction at* Contact1-3. *Prior to* Contact1-3*, it is likely that erosion has exposed layers within these undulations. d) Section of radargram 2007101 in Region 7b. TMP and undulations exist, but the TMP are buried at* Contact1-3. *Undulations reverse direction at* Contact1-3 *but are not buried. R25 and R29 intersect the bedrock at a relatively high angle, illuminating the discontinuity between Gemina Lingula and the main lobe. Note, b) c) and d) are displayed in time. a) has been converted to depth. Dashed boxes are approximate.*

90 m depth but were subsequently buried. Between 500 and 90 m beneath the surface both sets show pronounced northward migration, as much as 6 km. Starting at 90 m, each set experienced erosion and then change properties. Set B undulations were completely buried. Approximately 80 m of ice draped them, so that there is no surface expression. At approximately the same stratigraphic level, Set A undulations change

migration direction from northward to southward (Figure 2.17c). Independent of migration direction, both sets of undulations' wavelength remain approximately constant throughout accumulation, at ~9 km.

4.a.4 Troughs in region 4

Observations of troughs in Region 4 (Figure 2.1) are more difficult to make with SHARAD than in previous regions. Commonly, the orbit of MRO suffers from bad observation geometry, resulting in a lot of clutter in each radargram. Furthermore, this region has undergone large-scale erosion and deposition prior to the current surface, and when a good radargram exists, subsurface structure is difficult to interpret.

Figure 2.18 details the amount of clutter visible in a radargram with moderately favorable geometry. The highest latitude troughs have some stratigraphy for interpretation, and we detect discontinuous reflectors R25 and R29. We interpret the

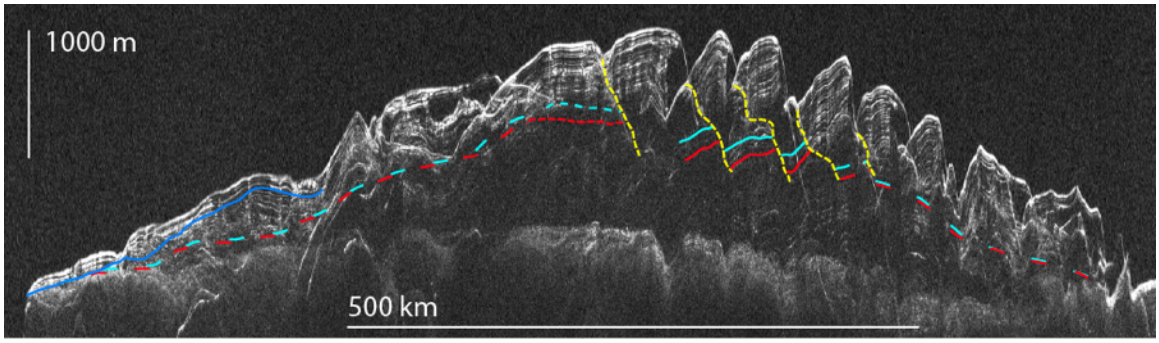

Figure 2.18: Radagram 1087102 observation of NPLD in Regions 3 and 4. *Poor geometry results in significant clutter and difficult interpretations. At high elevations TMP are delineated by the discontinuity of R25 and R29, indicating the age of these troughs. At low elevations reflectors are difficult to interpret and may have been removed by erosion.* Contact1-3 *is marked in Region 3 near the margin.*

location of migration paths for the highest latitude troughs, but the lower troughs are impossible to interpret with confidence.

In another modestly favorable geometry, Figure 2.10 crosses Region 4, but, again, clutter is very prominent. Internal reflectors show poleward tilted low side deposits and some thickening. High side reflectors thin as they approach a trough wall. Little else can be observed in this region.

4.a.5 Troughs in region 5

Region 5 is unique when compared to the other regions. First, the troughs are relative late-comes, having initiated stratigraphically higher than those of other regions. Second, the slope on which Region 5 troughs initiated was the result of erosion.

Reflectors R29 and R25 can be traced throughout Region 5, but neither reflector exhibits discontinuities associated with trough migration paths or other thickness variability (Figures 2.4b, 2.12c, 2.15, and 2.19). Instead of containing trough structure, R25 is continuous and has a convex up shape indicating the paleo-chasma detected by *Holt et al.,* [2010]. Above R25, the paleo-chasma was filled in with as many as 600 m of ice before evidence of trough existence is observed (Figure 2.4).

Stratigraphically above R25 and subsequent deposition, an angular unconformity cuts layers near trough initiation. Layers beneath the unconformity are truncated without thinning, but layers above the unconformity often meet at strong angles associated with onlap and trough migration. Thus, the first sign of trough stratigraphy in Region 5 is immediately subsequent to the eroded surface (Figures 2.12 and 2.4).

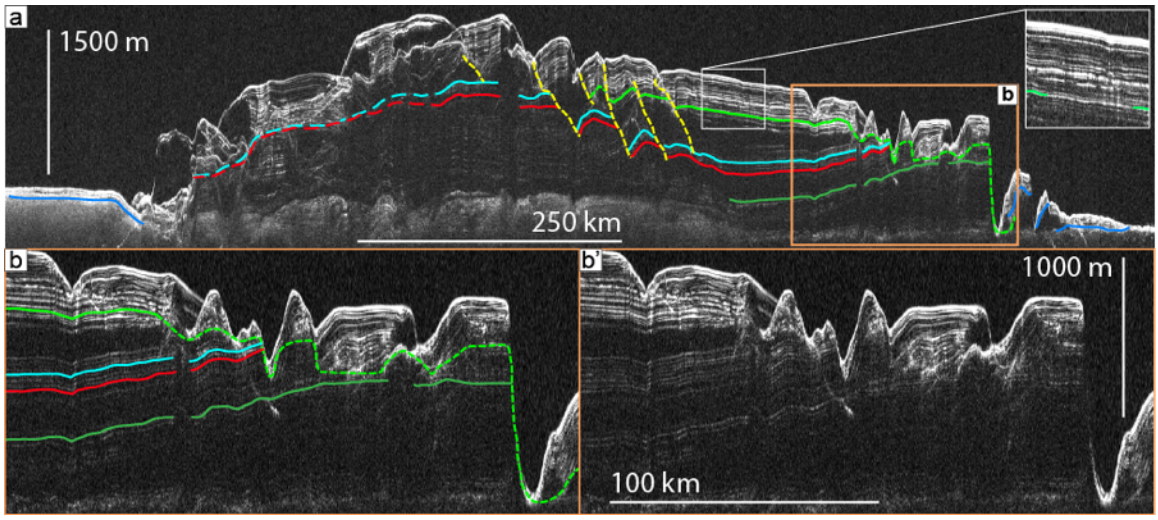

Figure 2.19: Radargram 19827 observation of NPLD in Regions 4, 1, and 5. *Region 4 is difficult to interpret due to poor geometry. Region 1 troughs have easily identified TMP and discontinuous reflectors. Region 5 shows the TIS-2 erosion and paleochasma that predated troughs. Inset demonstrates the relative brightness of R17, corresponding to the TIS-2 erosion. b) Expanded view of radargram 19827. R25 and R29 reach the surface at a trough. Another reflector (R40) is exposed at a 1 km high scarp.*

The erosion associated with trough initiation is very extensive. It spans the entire longitudinal breadth of Region 5, more than 650 km, from 18° to 104° E (Figure 2.1b), corresponding to the eastern portion of Gemini Scopuli [*Tanaka and Fortezzo*, 2012]. Tracking this erosion eastward from ~100° E is difficult due to clutter and complex depositional history associated with Region 4. Westward of ~20° East, at the Region 7a boarder, the scarp angle becomes too low to differentiate from horizontal layering. Latitudinally, the unconformity extends from higher sections of the NPLD at ~84°N to beyond the margin. The northernmost extent of erosion parallels the highest latitude troughs throughout Region 5, giving it a somewhat linear appearance (Figure 2.1b). The troughs have since migrated northward to their current location (Figures 2.12c and 2.20).

Many unconformities have been identified within Gemini Scopuli [*Tanaka and Fortezzo*, 2012]. We take this opportunity to explore the intersections of R25 and R29 with the surface in hopes of finding exposures of older, pre-trough NPLD material. It is

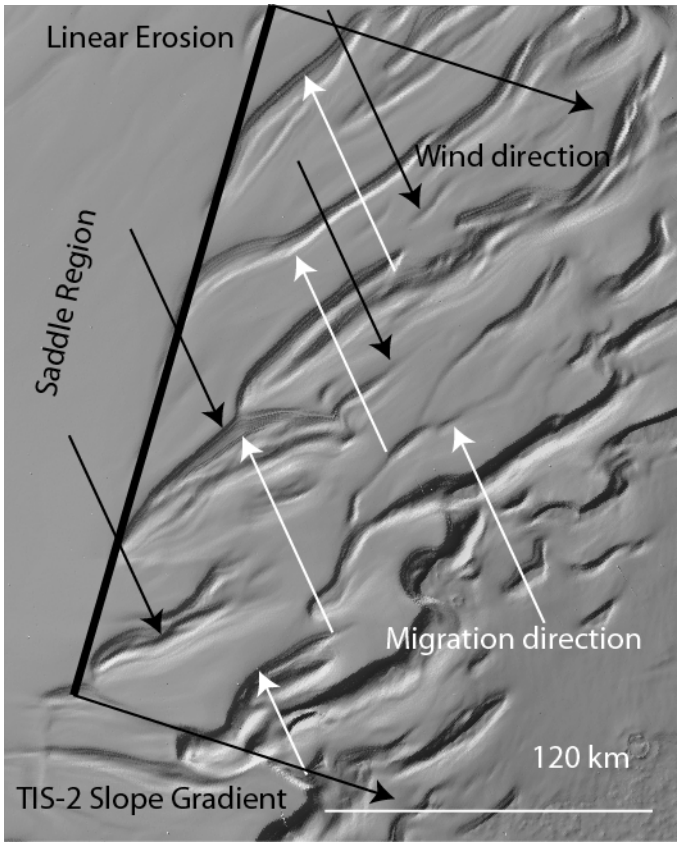

Figure 2.20: Expanded view of Region 5. *Wind directions (from Smith et al., [in review] align anti-parallel to migration direction of troughs. However, the highest slope gradient related to TIS-2 is in another direction. Winds are steered by topography and the Coriolis force.*

notoriously difficult to co-locate exact points between optical imagery and SHARAD. Often, the vertical and horizontal resolution of the radar is the limiting factor, and only an argument based on measured slopes and spatial frequency of layers [*Christian et al*., in press] or roughly on position [*Milkovich et al*., 2009] can be made. While this is generally true, exposures on the NPLD are sometimes large enough that an isolated unconformity can be co-located between the instruments.

Within a trough, at 70.2° E, 82.3° N, there exists an exposure of the NPLD approximately 17 by 9 km with ~300 m of relief (Figure 2.4e). This area is large enough that a radargram footprint can confidently be placed within the boundary. Optical imagery of the trough reveals an unconformity (Unconformity #2) on a trough high side slope [*Tanaka and Fortezzo*, 2012].

As seen in radar at the same location, R29 approaches the surface (Figure 2.4d). Reflector R25, however, is truncated by an unconformity that corresponds to the elevation of Unconformity #2 in Figure 2.4e. There is some clutter in the radargram, but

the combination of radar reflectors reaching the surface and exposed layers in optical data indicate that the surface is not mantled. Below Unconformity #2 the entire section contains layers that appear uniform in albedo and thickness, harmonious with the radar reflectors, which also appear relatively uniform at this location. We interpret this evidence to signify that R29 reaches the surface somewhere between Unconformity #2 and the bottom of the trough

Higher on the trough slope, there is a distinct change in layer properties near white arrow #1 (Figure 2.4e). Stratigraphically below the contact, layers are regular and have no evidence for wind streaking. Above the contact, layers are smoother, except where they appear to be scoured by winds. SHARAD detects an unconformity at approximately the same elevation (Figure 2.4d). As with Unconformity #2, we interpret this to be evidence for a single unconformity in optical and radar data.

SHARAD's resolution, particularly the horizontal dimensions, is not sufficient to locate exact x, y points of an unconformity. However, we explore locations with distinct, isolated stratigraphic contacts. Finding unconformities in otherwise undisturbed layers is a promising method for interpreting the structure of the NPLD. We perform this correlation at other locations. As with in Figure 2.4, radar reflectors in Figures 2.12, 2.15, and 2.19 indicate that within some troughs an unconformity separates relatively young material from material that predated R29. Thus, old NLPD material is exposed on the surface within certain troughs.

4.a.6 Troughs in region 6

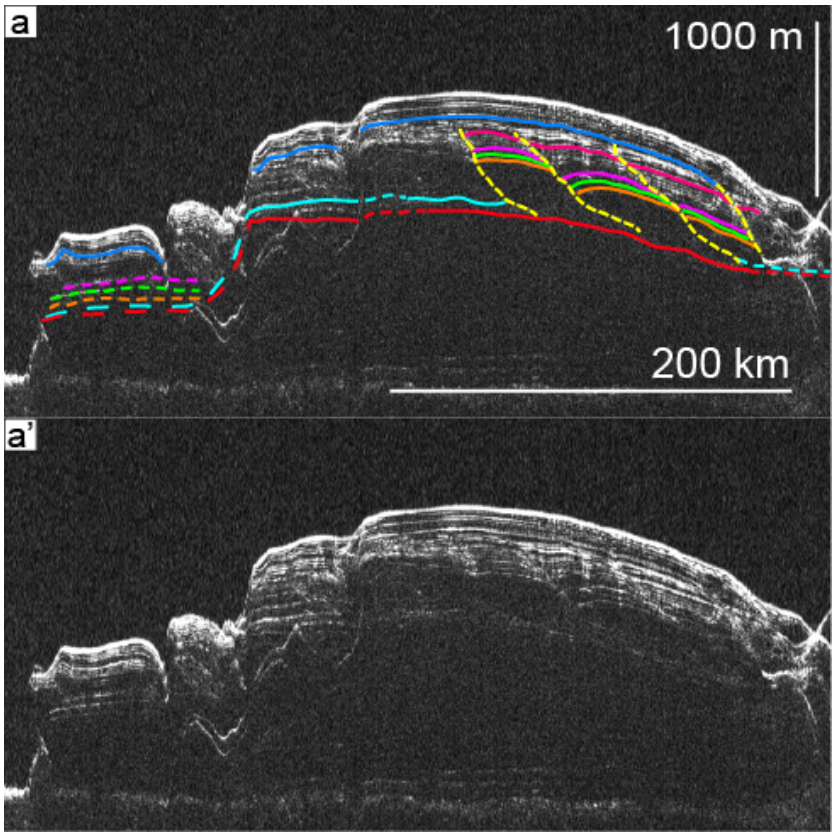

Figure 2.21: Expanded view of radargram 725402 from Figure 6_synthetic*. Troughs in Region 6 were formerly at the highest elevation of an earlier Gemina Lingula. They formed around TIS-1 at R29 and have characteristic wavelengths of ~50 km, comparable to troughs in Region 1. These troughs have two abnormal qualities in that they migrated away from the pole and were subsequently buried by 100 m of ice. No expression of troughs in Region 6 exists on the current surface.*

Region 6 at first glance does not belong on the list of locations containing troughs. The surface, as measured by MOLA [*Smith et al*., 2001], is one of the smoothest places on the NPLD, and there is no indication at all of trough related stratigraphy. Yet, SHARAD observations with favorable geometries detect TMPs in the subsurface (Figures 2.17 and 2.21).

Here we present the first clear evidence of buried troughs on the NPLD. Figure 2.21 displays radar reflectors indicating the classic characteristics as troughs in Region 1: TMPs, and asymmetric accumulation across the TMP. Two distinct troughs with wavelengths of ~50 km are present, and some indication of a third exists. Three migration paths are evident during ~600 m of deposition. Throughout accumulation, the highest trough migrated ~40 km. The next two troughs migrated ~65 and 60 km,

respectively. Region 6 troughs have comparable stratigraphies to those in Region 1, including wavelengths and approximately contemporaneous onsets with R29.

There are two main differences between these troughs and those previously observed in this paper. First, the troughs, at their maximum elevation, are completely buried by ~110 m of parallel, sub-horizontal reflectors. Across that boundary the troughs transition from being very easily detected to nonexistent. At about the same stratigraphic level, the TMP disappears. Second, the TMPs in Figure 2.21 indicate that the troughs migrated southward prior to burial. Only one other instance of loss of TMP inflection at a trough has been found on the NPLD (Figure 2.2), making this location a surprise and unique.

4.a.7 Troughs in region 7

Region 7 shares characteristics with other regions, including extensive undulations, as in Region 3; marginal troughs and scarps similar to Region 5; and unfortunately, Region 7 shares a poor geometry for observation with Region 4. Because of the poor geometry, most troughs are difficult to observe and interpret with SHARAD (Figure 2.9c). Furthermore Region 7 is not as extensive as other regions, so no more than two troughs can be interpreted within a single radargram (Figure 2.10). Nevertheless, some general observations may be made.

To begin, we subdivide Region 7 into two portions. Region 7a encompasses the troughs on the Gemina Lingula southern margin also associated with Gemini Scopuli. Many of these troughs are deep enough to reach the bedrock that lies beneath the NPLD (Figure 2.10) and are sometimes called scarps in the literature [*Pathare and Paige*, 2005].

Region 7b borders Chasma Boreale to the south. Troughs here are less mature than in other regions but still exhibit characteristics of migration (Figure 2.9c). Topographic undulations exist in both sub-regions, but few have sufficiently good geometries to be detected by SHARAD (Figure 2.17d).

In Region 7a, Figures 2.9c and 2.10 exhibit poleward-facing deposits on the low side of each marginal trough, mantling the previous low side. Reflector separation is difficult to measure, but contrary to what is found elsewhere, reflectors appear to thin as they approach the bottom of the trough from the low side. Nevertheless, some classical asymmetry is detected in layer thickness at higher elevations (Figure 2.9d). In Figure 2.10 no thinning on the high side is detected, but interpretation is easier on the low side, where layers appear to thicken with increasing distance from the bottom of the trough – again, contrary to observations of classical troughs.

Troughs in Region 7a frequently reach the bedrock, adding complications to our interpretations. TMPs usually slope downward from the bottom of a trough, but this is impossible with a non-erodible bed. In this light, we detect horizontal TMPs that reaches the bedrock at each trough, something unique to marginal troughs in Regions 7a and Region 5.

On the northern side of Gemina Lingula, in Region 7b, minor troughs are observed. We define a minor trough as having a small cross section and distinct TMP (Figures 2.9c and 2.10). These are distinguished from undulations primarily because they are individual, instead of in groups. Good geometry observations in Region 7b are more readily come by in 7a, and we can detect migration throughout the section. Detected TMPs reach from the surface down to some level higher than R25.

Migration of the minor trough in Figure 2.10 is traditional in the sense that the trough observed has migrated uphill, or upstream to the winds. In Figure 2.9c, on the

other hand, the two minor troughs migrated non-traditionally: one has a rare, vertical migration; the other has always been migrating down slope.

4.b. Trough initiation surfaces and slopes

Region 1 has the best record of trough evolution on the NPLD, and troughs there make good standards for comparison. Looking from east to west these troughs show variability in the timing of initiation, from prior to R29 (Figure 2.9) to post R25 (Figure 2.11). No one stratigraphic level can be considered the formation surface. Nevertheless, there is only a small amount of evidence for trough-related stratigraphy below R29. Thus, R29 predates most of the troughs in Region 1 (and elsewhere on the NPLD). Because of the proximity of R25 to the initiation of most troughs outside of Region 5, we refer to R25 as trough initiation surface one (TIS-1), or the mapped surface closest to the time at which most NPLD troughs formed.

To understand the structure of the NPLD around the time of trough initiation, we track surface TIS-1 to its extent. Because TIS-1 is either continuous or broken by only small segments, layer analysis is straightforward for much of the NPLD (Figures 2.2 and 2.15). However, in some sections regions, specifically at the boundary of Regions 1 and 5 near 90° E (Figure 2.12), large offsets and weak radar reflections make connecting R25 difficult. To compensate, we look for radargrams that connect the reflector (Figure 2.15) and apply the cross-correlation technique discussed above to circumvent the disconnected segments.

This method results in an incomplete survey. TIS-1 extends to the NPLD margins in only a few locations. In certain areas, specifically south of 86° in Regions 3 and 4,

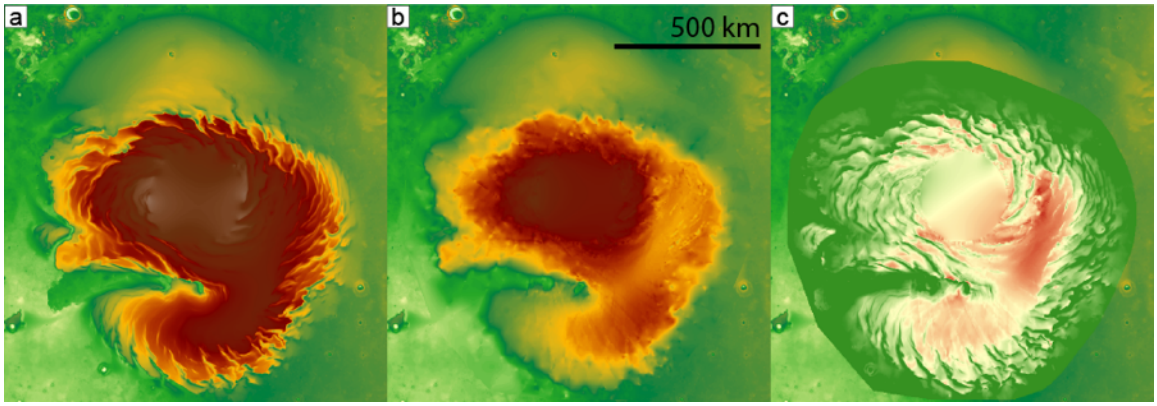

Figure 2.22: Topography and accumulation of NPLD. *a) current topography from MOLA [Smith et al., 2001] b) Topographic map of TIS-1 for comparison with the current NPLD. The NPLD has developed significantly since formation of the troughs began, especially in Regions 5 and 7. c) Accumulation (thickness) map between current MOLA surface and TIS-1. Red is thickest. Green is no or little change. The buried chasma received the greatest amount of accumulation. Troughs are visible because of extreme non-uniform deposition. Locally, the lowest points of troughs have received the least accumulation, while the highest points in the inter-trough region have received the most. Near 270° E, where the former and current highest points of the NPLD are, relatively little ice has accumulated. Abalos Mensa developed since troughs formed, as described in [Brothers et al., 2012].*

R25 is not observed and has likely been removed by erosion. Using methods described in Section 3 for creating surfaces, we extrapolate R25 towards the margin (blue dashes in figures containing radargrams) to estimate the size and shape of the NPLD at the time of TIS-1 (Figure 2.22b).

By comparing the current MOLA surface (Figure 2.22a) to that of TIS-1 (Figure 2.22b), several observations are readily apparent. Chasma Boreale existed at that time but was much shallower than it is currently. The paleo-chasma discovered by *Holt et al*. [2010] east of the saddle region still existed but was partially filled in. The highest elevation on the NPLD (with mapping limited to latitudes south of 88° N) was not centered at the pole. Instead it was nearest 270° E, in agreement with current topography and topography of the early NPLD [*Putzig et al*. 2009].

The topography generated for reflector TIS-1 gives the capability of estimating the volume of the NPLD near the time that troughs initiated. Around the time of trough

onset, we find that approximately $7x10^{14}$ cubic meters of ice and had already been deposited. The basal units and lower section of NPLD1, as described by *Tanaka and Fortezzo* [2012], comprise the total volume of ice around the time of trough onset.

We subtract the elevation of TIS-1 from the MOLA surface to determine the pattern of accumulation and the volume of ice that has accumulated since trough onset (Figure 2.21c). $\sim 3x10^{14}$ cubic meters have been deposited in that time. This volume is approximately half of the volume that was deposited prior to TIS-1. Because of the aforementioned erosions in Regions 3, 4, 5, and 7, the volume we calculate for accumulation since TIS-1 is necessarily a minimum estimate.

Since troughs began forming, the greatest accumulation has occurred at the boundary of Regions 1 and 5, at the site of the buried chasma. At this location over 1000 m of ice have accumulated. Other locations that have accumulated significant volumes of ice are between troughs (highest local points) and Gemina Lingula, which has acted as a second depocenter. Additionally, Abalos Mensa has completely developed, in agreement with the conclusion that this location acts to receive ice being blown off the margin of the NPLD [*Brothers et al.*, 2013].

The locations that have received the least amount of accumulation are at the bottoms of present day troughs. They have the lowest local elevation, some close to the elevation of TIS-1. Because all of the troughs have completed development after TIS-1, the troughs appear in the difference map (Figure 2.22c). Of note, the previous highest elevation of the NPLD, near 270° E has received relatively little accumulation since trough onset.

For comparison between regions, we calculate the average slope of TIS-1 (Table 2.1). This is easiest in Region 1 because of continuity. The initiation slope angle of

TIS-1 for Figures 2.2 and Figure 2.10 are 0.15 and 0.16, respectively. The average slope for all observations in this region is therefore 0.19°.

In Region 2, R29 and R25 were both partially eroded during the formation of the troughs (Figures 2.12b and 2.13b). By using geologic clues, we estimate the approximate location of R29 to calculate the initiation slope (Table 2.1). The initiation surface for troughs in Region 2 varies by longitude, and the average value is 0.27°, higher than in Region 1.

It is difficult to determine the exact initiation point of all of the troughs in Region 3. While evidence of the troughs being the same age is lacking, the observations available give us some confidence that the troughs of Region 3 initiated near TIS-1 (Figures 2.14 and 2.17). However, TIS-1 is discontinuous in several observations, probably due to erosion and or migration of troughs. The initiation of some troughs, below, at, and above TIS-1 is similar to interpretations of Region 1, and we take R29 to be an approximate stratigraphic level about which the troughs formed. We estimate the slope of the initiation surface to be on average 0.27° (Table 2.1), similar to Region 2 and larger than Region 1. There is increased variability when compared to TIS-1 in Region 1 and reduced variability from Region 2.

Region 4 troughs likely formed prior to the deposition of R29 (Figure 2.18), but without useful crossing observations, we are unable to confidently place the initiation of many troughs. Calculating an initiation slope in Region 4 is difficult, but we can set a lower estimate from Figure 2.10 from the dashed R29. We find the slope to rise ~1100 m over ~150 km, for an angle of ~0.39°.

Region 5 and Region 7a correspond to the mapped area Gemini Scopuli. These regions are different from the rest of the NPLD in that the troughs formed stratigraphically higher than TIS-1. In these regions, R29 and R25 are only interrupted at

margins, where they are exposed on the surface, and trough related stratigraphy is not present at that level. However, there is clear evidence of widespread erosion in Region 5 (Figures 2.1b and 2.4) that immediately predates trough formation and coincides with a reflector we can R17. Because all Region 5 troughs initiated at this level (R17 and the unconformity), we call it trough initiation surface two (TIS-2).

TIS-2 is continuous across the entire extent of Region 5, and its slope varies by location. Eastern and central portions were eroded more strongly than those of the far west, near Region 7a, where either the surface becomes impossible to distinguish clearly (Figures 2.17 and 2.21) or very steep scarps show the removal of all marginal ice (Figure 2.19). In areas where the slope can be determined, we find that the initiation slope varied longitudinally from 0.27° to 0.39°. The average slope of this region was 0.32°, significantly higher than the slopes measured elsewhere except for Region 4.

Observations of the erosion associated with TIS-2 are confined to Region 5 (Figure 2.1b), yet another observation sheds light on the NPLD at that time. R17 is an exceptionally bright reflector (Figures 2.4, 2.15, 2.12, and 2.19) and is extensive throughout Region 5. It is located ~360 m beneath the current surface and can be traced into other regions. Outside of Region 5 R17 is usually less bright (Figures 2.2, 2.8b), but we have not connected R17 beyond Regions 5 and 1. Bright reflectors exist at approximately the same stratigraphic level in other regions, and future work will determine if R17 is as bright elsewhere or coincides with an unconformity outside of Region 5.

Spatially, Region 6 is less extensive than other regions. Being smaller, radar observations that have good enough geometries for measuring the initiation slope are rare. Nevertheless, TMP are traceable down to a level between R25 and R29, consistent with many troughs in Region 1. Also similar to Region 1, the troughs of Region 6

initiated on a relatively low slope of 0.13° that rises 340 m along a 165 km run. The wavelength of Region 6 is about 50 km, again similar to that of Region 1.

Determination of where the troughs initiated in Region 7 is more difficult. Because of the poor geometries of radargrams in Region 7a and lack of distinct initiation surface, there is no strong reflector or unconformity to trace. Troughs on the southern margin initiate within a zone that is either obfuscated by clutter or within an inter-packet material. Even when geometries are somewhat favorable, TMP are not easily distinguished from clutter. Minor troughs in Region 7b all initiated subsequent to R25 (Figures 2.3, 2.9, and 2.10).

4.c Inter-packet

Besides the central promontories within troughs of Region 3, another aspect is of interest. In a detailed SHARAD survey, *Putzig et al.,* [2009] observed a pattern of packet / inter-packet sections of reflectivity in the NPLD (Figure 3 of *Putzig et al.,* [2009] and 2.3 and 2.16). Packets are thin (200 – 500 m) sections that have numerous, bright reflectors. Inter-packet are vertically extended sections in which SHARAD detects little or no reflectivity. Previously there has been no observation of this inter-packet material reaching the surface, and hypotheses about its properties have remained untested.

Figure 2.16b exhibits a ~400 m exposure of the inter-packet material that reaches the surface just south and down slope of the central promontory. In optical data, between a' and a" (Figure 2.16a), a comparison with radar can be made. The exposed material is highly layered and of medium to low albedo.

Another exposure of inter-packet material is found at 227° E, 86.5N (Figure 2.3c). On the high side of the trough, towards the bottom, a zone of few and dim reflectors reaches the surface. The lowest bright reflector is approximately 150 m above the trough floor and 350 m lower than the inter-trough height. Similar t in Figure 2.16a, radar detects few reflectors in the lowest 150 m, but visible layering is observed in optical imagery (Figure 2.3b). At the resolution presented in optical data, the inter-packet region detected by SHARAD in both Figures 2.3 and 2.16 has no visible surface change from the higher packet material. Additionally, inter-packet material is exposed in Region 2 (Figure 2.14b and 2.12b).

5 DISCUSSION

5.a. Comparison of the regions

In order to understand the processes that affect trough morphology we compare troughs in 8 distinct regions (Figure 2.1). We separate the regions based on morphological and stratigraphic variations as well as the availability of quality radar observations. In general, the troughs of every region have similar characteristics, including repeated wavelengths, asymmetric accumulation, exposure of layers on the high side, and banded low side exposures. They all agree with the observations of *Howard et al.,* [1982] to varying degrees and meet the criteria of cyclic steps for stratigraphy and migration [*Smith et al.*, in review]. Things that separate troughs between

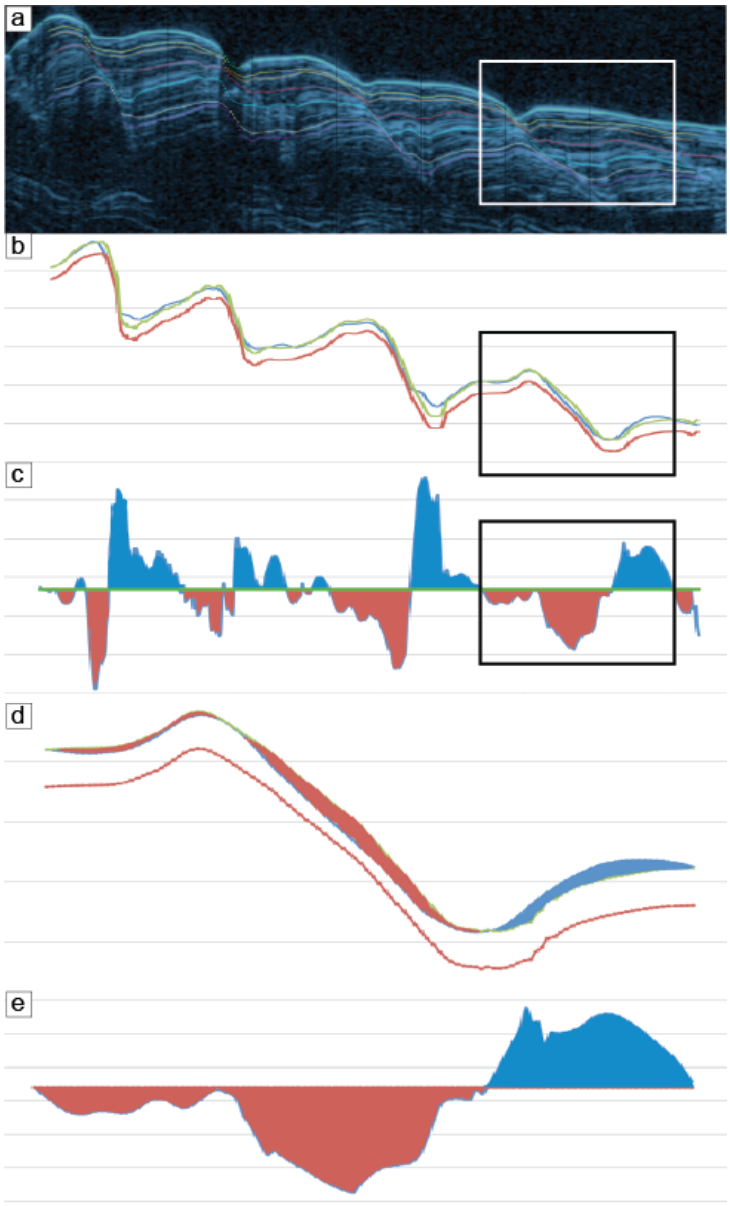

Figure 2.23: Idealized scenario of trough migration compared to reality in Region 1. *a) Portion of radargram 477002 with interpreted reflectors. White box matches those in b and c, which expand into d and e, respectively. b) two chosen reflectors (blue and red) compared to an idealized reflector (green). The average thickness between blue and red was found. That value, above the red reflector, is the height of the green. Comparing the elevation of green with that of blue, we calculate deviations from the average in c. c) Plot of the deviations between blue and red. d) zoom in from b. Red area indicates where mass is expected but not observed. Blue is where excess mass is detected. e) Plot of thickness from d. We compare the 2D volume of removed ice from the trough high side, 1.83 km^2, to excess ice on the trough low side, 1.71 km^2, and find that the excess ice volume is approximately 90% of the removed ice on the high side. 10% of the removed material from the high side is lost at this trough.*

regions include age of initiation, neighboring undulations, relative maturity, cross sectional morphology, and bedrock bases, among others.

Our comparison begins in Region 1 because it is the most uniform and easily analyzed region. The troughs here are favorably oriented for detailed study with radar, and they generally have uniform morphology and wavelength. Additionally, the troughs in Region 1 are well described by the observations of *Howard et al*., [1982] and the

cyclic step model [*Smith et al*., in review]. Based on that agreement, we categorize them as classical troughs and make them the basis for comparison around the NPLD.

Several characteristics define a classical trough. Layers are nearly always exposed on the high side slope, indicating greater erosion than deposition. In the subsurface, radar detects thinned layers as one approaches the high side surface. The low side of each trough exhibits banded terrain mantling previous deposits (Figure 2.1e); reflectors on the low side reveal thickened layers approaching the TMP (Figure 2.1b). This asymmetric accumulation, relative to the average across multiple troughs, signifies transport and migration (Figure 2.23).

Classical troughs demonstrate substantial effects of wind, insolation, and accumulation (Figure 2.5), but besides these observations, Region 1 troughs conform to the other observations that generalize NPLD spiral troughs: surface slope asymmetries, albedo contrasts on each side of the trough, regional wavelength uniformity, orientation perpendicular to mapped and modeled wind patterns [*Smith et al*., in review].

These same traits are observed in other regions, but they exhibit more variety. For example, we find that troughs in every region exhibit both banded and layered terrain, evidence for migration. However, compound troughs dominate Region 2 and part of Region 3. Regions 3 and 7 have extensive topographic undulations. Troughs in Regions 5 and 7a often reach the bedrock substrate and migrate horizontally. Region 6 troughs are nearly identical in wavelength and initiation date as Region 1 troughs, but they migrated southward and have subsequently been buried. Regions 4 and 0 are difficult or impossible to observe with SHARAD. Nevertheless, they are closely related to those in Region 1 and are fundamentally classical troughs.

Region 2 troughs reside at the western end of Chasma Boreale on the Main Lobe. The troughs, upon first glance, connect on the surface to those in Region 1, but they are

distinct in several ways. Region 2 has a higher regional slope (.27° vs. 0.14° for Region 1). Furthermore, the troughs here are significantly deeper (up to 1 km vs. ~400 m) [*Pathare and Paige*, 2005]. Compound cross sections also distinguish Region 2 from Region 1 (Figure 2.13). The combination of being deeper and having a compound cross section causes these troughs to expose many more layers on the high side than a Region 1 trough. While it is clear that the W-shaped troughs are erosive in principle, they exhibit strong evidence of migration with banded terrain and thickened reflectors on the low side.

We offer three hypotheses to explain the formation of compound troughs. The first hypothesis is that the central peaks are the result of a more resistive layer, protecting just the deposits at the elevation of the central portion. In this scenario, layers above and below would erode faster than the resistive layer, creating benches or steps. However, if the central promontory were the result of a protective layer, it would indicate a local protection, parallel to the trough, but linear. Eroding a portion of the resistive layer (within the higher leg of the W) but not the central peak is improbable. Furthermore, neighboring troughs have central promontories, but the respective layers and elevations are different. This would require many local, individual, highly resistive, trough parallel layers at different stratigraphic levels, something we find implausible. One resistive layer that intersected many troughs would be more likely. We do not favor this hypothesis.

The second hypothesis is based on wind patterns. It is plausible that erosive winds created the promontories and that promontories are topographic undulations like those on the current surface. This would require an erosional formation mechanism for some undulations, supported by evidence in the literature [*Hand*, 1974]. For the trough in Figure 2.16, the undulation scenario appears likely. Here, the high side of a trough would retreat. At approximately one half (undulation) wavelength downstream there would be little or no erosion. Further downstream, another undulation or promontory

may exist, something we detect (Figures 2.16 and 2.13b). Problematic with this hypothesis is that while most undulations appear to be constructional, forming in a depositional environment, these are the result of erosion. We prefer this hypothesis to the first, but more work is required to understand the flow conditions required.

The last is more speculative. The troughs in Region 2 have large cross sections. We argue that the observations of compound morphology and wider cross section may be consistent with a changing wind regime that affects the wavelength of the troughs. In other words, a shortening wavelength of cyclic steps may cause erosion at the higher portion of the W-shape. In this scenario an increasing regional slop that produces faster winds would resort in a shortened distance between katabatic jump [*Smith et al*., in review]. This hypothesis offers promise, but determining its accuracy requires future work with atmospheric modeling.

At low latitudes, Region 3 shares compound trough morphology with Region 2. However, at higher latitudes, Region 3 is more similar to Region 1. Figure 2.3b demonstrates migration of a simple trough. When compared to troughs at the same latitude in Region 1, the trough is deeper and has smaller layer thickness variations, potentially a sign of reduced wind erosion relative to insolation (Figure 2.5b). As of yet there is no compelling argument for enhanced insolation or significant deviation in accumulation here, so the deeper troughs are likely a consequence of reduced intensity winds. Reduced winds will cause less thinning on the high side and are less likely to redeposit ice at the bottom of the trough [*Smith et al*., in review].

Other evidence supports this interpretation. Region 3 is set apart from others by profound and prolific topographic undulations (Figure 2.1 and 2.17). Undulations are hypothesized to result from undular shaped katabatic jumps near troughs (Figures 4c and 5b from *Smith et al*., [in review]). Undular clouds form during reduced wind

environments that measure Froude numbers between 1.4 and 1.7. Froude numbers are directly proportional to wind velocities, and lower numbers indicate reduced intensity winds. One other factor is that the migration distance for troughs in Region 3 is shorter than those in Region 1. Reduced migration implies reduced transport from lower intensity winds.

The stratigraphy of two nearby sets of undulations is telling (Figure 2.17b). These sets formed at approximately the same time and migrated approximately one wavelength upstream during ~300 m of deposition, after which both experienced distinct changes approximately 85 m beneath the current surface. Set A changed migration direction towards the south; Set B was buried. Because regional slope and local topography changed little when the undulations reversed, we find it likely that atmospheric conditions are a likely cause for the change.

The existence of deeper troughs, reduced asymmetry in layer thickness, and prolific undulations in Region 3 all suggest that winds have lower intensity than in Region 1. However, the slope on which Region 3 formed is greater than that in Region 1 (Table 2.1). Katabatic winds generally accelerate more on steeper slopes, resulting in more intense winds. So why do we find geomorphic evidence for weaker winds in a region with a steeper slope? Perhaps the wind regime in Region 3 is more variable than other regions or larger scale atmospheric properties are in effect. More atmospheric modeling is required to answer this question.

SHARAD has poor radar returns with lots of clutter in Region 4, making interpretation difficult. The troughs nearest the pole (and Region 1) offer the best observations of trough migration, through sloping layers that vary in thickness. The offset of R29 at intersections with TMPs indicates that these troughs are some of the oldest on the NPLD (Figure 2.18), but little more can be determined.

Region 5 stands alone when compared to other regions. These troughs formed on an eroded surface we call TIS-2, coinciding with R17, as many as 600 m higher in elevation than TIS-1. The troughs are therefore significantly younger than those in the other regions.

The reason for late onset troughs in Region 5 maybe be simple. Prior to the erosion of TIS-2, the surface slopes in Region 5 were insufficient to allow strong katabatic winds. The large paleochasma detected by *Holt et al.,* [2010] dominated this Region 5, and regional slopes oriented towards the pole (Figures 2.12 and 2.22), restricting and decelerating winds. At some time after significant infill, Regions 5 and perhaps 7 experienced large-scale erosion, corresponding to Gemini Scopuli. In Region 5, material was eroded laterally between ~20 - 120° E, over 600 km (Figure 2.1b). This erosion provided much steeper surface slopes than previously existed, sufficient for katabatic jumps to form. Another plausible explanation is that atmospheric conditions changed at the time of erosion, finally allowing katabatic jumps to form. Evidence for concurrent trough migration in other regions may dispel this hypothesis, and we favor the increased slope interpretation. Lastly, troughs may have existed on the steeper margin of Region 5 prior to TIS-2 erosion. A record of those possible troughs would have been lost.

Perplexingly, the erosion associated with TIS-2 is not readily apparent over the entire NPLD, provoking further questions about regional vs. cap-wide processes. In many radar observations a bright reflector R17 coincides with the stratigraphic level of TIS-2 (Figures 2.4, 2.9, 2.12, and 2.19), but at large distances from Region 5 the reflector has no outstanding characteristics. Perhaps the existing trough processes in other regions stabilized the NPLD morphology and the troughs survived the erosion.

On a more speculative note, it is tempting to interpret TIS-2 erosion as having coincided with the erosional of central promontories found in Regions 2 and 3 or that it

may be contemporary with a decrease in TMP slope found in the upper sections of many troughs in Region 1 (Figure 2.9). Future work will attempt to substantiate or disprove these ideas.

Region 5 troughs migrate upwind, not necessarily upslope. This is evident when one considers the wind direction (modeled and mapped by [*Howard*, 2000; *Massé et al*., 2012; *Spiga et al*., 2011]), which is dominantly steered by the Coriolis force when relief is low. The troughs nearest the saddle region, between the main lobe and Gemina Lingula, have an atypical structure (Figure 2.20). Initially, the troughs formed parallel to the erosion of TIS-2, but over wind acted on them from another direction, and they migrated sub-parallel to TIS-2 erosion, resulting in the elongated, rotated appearance.

Region 6 troughs exemplify all of the characteristics of classical troughs, but they differ based on two major observations: radar reflectors clearly indicate migration away from the pole, and these troughs are buried beneath ~125 m of ice. Except for minor undulations (~10 m or relief), Region 6 is one of the smoothest locations on the entire NPLD (Figure 2.21). The undulations on the surface form from easterly winds, incongruent with mapped TMP. Furthermore, modeled wind intensities and directions for present day cannot support the formation of troughs in Region 6, so a previous wind regime is the most likely cause of these troughs (see Figure 14 from [*Spiga et al*., 2011] or Figure 13 from *Smith et al*., [in review] for modeled wind patterns in modern northern spring).

Region 7 corresponds to Gemina Lingula, and we subdivide it into two groups based on the orientation of topographic relief. Region 7a contains troughs that exist on the NPLD margin in the western section of Gemini Scopuli. They orient more to the west than troughs in Regions 1 – 5 due to the non-polar source of winds on Gemina Lingula [*Spiga et al*., 2011]. These troughs often have bedrock bottoms, which do not preserve

lower ice related stratigraphy and have been called scarps for this reason [*Pathare and Paige*, 2005]. While the distinction between scarp and trough is blurred in Region 7a, these features exhibit the same characteristics as migrating troughs, and we interpret them as special case troughs.

Unfortunately, Region 7a, like Region 4, presents difficulties for radar observations. Ground track geometries of SHARAD have poor orientation to the strike of the troughs and undulations. Clutter is therefore significant, and messy radar returns complicate interpretations. It is possible, however, to offer some interpretation, and we find limited evidence of trough migration with one detected TMP (Figure 2.9). The reflectors on either side of the TMP show thinning and thickening associated with transport. Additionally, low side layers on the marginal scarps/troughs tilt towards the pole. With some minor variations from classical troughs, this evidence supports the interpretation of migration.

On the north side of Gemina Lingula we define Region 7b. Here we observe poorly developed, minor troughs (Figures 2.17d, 2.10). These troughs are much smaller in cross section than troughs from other regions, and only slight deflections in the radar indicate their TMP. Yet, they show clear signs of migration. One such immature trough has even migrated downwind (Figure 2.9c), contrary to the classic model. We interpret this as a unique feature, possibly a hybrid of a trough and an undulation.

5.b Relative ages of troughs

Stratigraphic analysis of radar reflectors is useful for determining the relative age of the spiral troughs, and SHARAD provides the necessary tool for this detection. The

exact stratigraphic level of initiation for each trough is not easily detected, but we can say with confidence that the majority of troughs on the NPLD initiated shortly after the deposition of reflector R29. A few troughs formed previous to R29, at 1100 m beneath the surface (Figures 2.9 and 2.18). Most of the troughs on the NPLD had completed formation by the time R25 was deposited. Outside of Regions 5 and 7, only a few examples are confirmed to be younger than R25 (Figures 2.8c and 2.11), and these are lateral extensions of existing troughs. We call all of these Generation 1 troughs.

The increase in number of troughs, from just a few when R29 was deposited to a majority of the troughs by R25 tells of initiation that was more gradual than punctuated. Instead of a single onset for Region 1 troughs, as previously hypothesized [*Smith and Holt*, 2010], Generation 1 troughs formed as initial conditions became favorable. This entire process took place during the deposition of ~600 m ice from ~1100 m to ~500 m beneath the current surface. Prior to ~1100 and after 500 m no troughs formed in Regions 0, 1, 2, 3, 4, and 6.

There is no need for every trough to form at the same time, and given static atmospheric conditions, the cyclic step model of trough formation accommodates the gradual onset of troughs due to increased surface slope [*Smith et al.*, in review]. The single requirement of trough formation is that katabatic jumps form. This implies that conditions for katabatic jump became more favorable as the regional surface slope increased during deposition.

Utilizing estimated accretion rates of NPLD ice, we find an estimate for the amount of time required for all Generation 1 troughs to form. ~600 m of ice were deposited during Generation 1, and accepted accumulation rates vary from 0.28 to 1.2 mm per year [*Fishbaugh and Hvidberg*, 2006; *Herkenhoff and Plaut*, 2000]. We use 0.5

mm per year for our estimate; the actual ages will be better determined in future work. Approximately 1 My elapsed during all of Generation 1 trough's formation.

Region 5 troughs initiated significantly later than those in other regions on an erosional surface called TIS-2. This initiation was a much more punctuated than for Generation 1, and contrary to in Region 1, where troughs formed over a long period, Region 5 troughs all appear to form at or on R17. We call these Generation 2 troughs.

For Region 7a, stratigraphic analysis is not yet sufficient to determine an age for the troughs. However, context may provide necessary clues. Region 7a shares a boarder with Region 6. The opposing sense of migration between the two regions must be reconciled. Is it possible that the marginal troughs of Region 7a formed so close to the buried, Generation 1 troughs at the same time? We find this unlikely. More probable is that Region 7a troughs share a common initiation period with Region 5 and TIS-2. Forming later, and in a different wind regime, would relieve any inconsistency in TMP orientation. This is consistent with geologic interpretations that Gemini Scopuli is a single region with a uniform date of origin.

The minor troughs of Region 7b formed after Generation 1 troughs, but the exact timing cannot be correlated to Generation 2.

5.c Uppermost NPLD section

It is likely that several units detected in this survey relate stratigraphically to those presented from geologic mapping of the surface [*Tanaka et al*., 2008]. *Tanaka et al*., [2008] describe contacts in the uppermost NPLD between the ABb1 and ABb3 units of the NPLD (Figure 2.4 white arrow #1). ABb1 is the major constituent of the NPLD,

being 1500 m thick in most places. ABb3 is described as a recently deposited unit, only tens of meters thick and overlying most of the NPLD.

Results from our mapping with SHARAD suggest that an unconformity or disconformity in the uppermost NPLD is consistent with the boundary described between ABb1 and ABb3 of *Tanaka et a.,* [2008] (Figure 2.4e and 2.4d). This delineation is found by SHARAD in many parts of the NPLD (Figures 2.2c, 2.3, 2.9, 2.12, 2.15, 2.17, 2.18, 2.21). *Tanaka et al.,* [2008] described the unit as being "tens of meters thick," but we are able to refine that estimate upward between troughs. The unit ABb3, if consistent with the layers above this unconformity, varies from a maximum thickness of 85 m in Region 3 to as many as 115 m thick in Region 5. It thins to tens of meters at each trough, matching the observations of *Tanaka et al.,* [2008] as predicted by the cyclic step model [*Smith et al.*, in review]. Except at troughs and scarps, this younger unit covers a significant portion of the NPLD.

Region 1	0.20	2197801	
Region 1	0.22	1207501	
Region 1	0.22	1294501	0.19
Region 1	0.15	1247002	
Region 1	0.16	1247102	
Region 2	0.22	1844601	
Region 2	0.26	1280202	
Region 2	0.23	1837301	0.27
Region 2	0.41	1321501	
Region 2	0.25	1818202	
Region 3	0.27	1321501	
Region 3	0.25	2268301	
Region 3	0.26	2356401	0.27
Region 3	0.31	725402	
Region 4	0.17	1087102	
Region 4	0.43	1247102	0.31
Region 4	0.34	1252401	
Region 5	0.27	1280202	
Region 5	0.30	1837301	0.32
Region 5	0.31	761602	
Region 5	0.39	855602	
Region 6	0.12	725402	
Region 6	0.14	923202	0.13

Table 2.1: List of estimated initiation slopes by region and radar observation number. *Region 6 has the lowest average slopes followed by Regions 1, 2, 3, 4, and 5.*

Exposures of the unconformity display the contrast between ABb3 and ABb1 that was observed by *Tanaka et al.,* [2008] (Figures 2.4, 2.12, and 2.15b).

5.d Wavelength dependence on regional slope

Troughs between different regions are known to display variability in wavelength [*Pathare and Paige*, 2005]. Good examples of the differences are between Region 1 and Region 5, which have wavelengths of 40-50 and 20-30 km, respectively. The cyclic step model predicts that wavelength is dependent on the regional slope, on which troughs form [*Smith et al*., in review].

Smith et al., [in review] concluded that the spatial frequency of troughs is determined by the initial spacing of katabatic jumps prior to trough formation. Katabatic jumps require sufficient acceleration to reach high Froude numbers, so greater acceleration results in shorter wavelength. Because Froude number is proportional to horizontal velocity, accelerating winds will become Froude supercritical more quickly on a steeper slope. After forming, the initial wavelength is preserved because newly created deposits act to trigger subsequent katabatic jumps near the slope break at the lowest elevation of each trough.

Based on these conclusions, the troughs in different regions should have different initiation surface slopes. We find this to be generally true. For comparison we measure the regional slope of trough initiation in various radargrams for each of Regions 1, 2, 3, 5, and 6. Regions 0, and 7 were left out due to no or poor determination of initiation slope (Table 1). Regions 1, 2, 3, 5, and 6 have slopes of 0.19°, 0.27°, 0.27°, 0.32°, and 0.13° respectively.

Wavelengths in each region are not entirely unique, so we estimate ranges. Plots in Figure 6 of *Pathare and Paige* [2005] were useful in this analysis for counting the number of troughs in each region. Region 1 has a characteristic wavelength of 40-50 km; Region 2: 35-40 km; Region 3: 35-50 km; Region 4: 30-35 km; Region 5: 20-35 km, 6: ~50 km. There is a loose correlation between increasing slope and decreasing wavelength, but local slopes also play a role in triggering katabatic jumps. Some regions, like Region 3 and Region 5 are large enough that their initiation slope varies longitudinally, muck like how wavelengths.

Other factors besides initiation slope are important in wind speeds, and should be considered. For example, some paramaters that affect katabatic winds are absolute temperature, temperature gradients, surface pressure, and surface albedo (driving temperature gradients). Changing obliquities will affect each of these variables. Modeling of the atmosphere at different obliquities is beyond the scope of this survey paper and will be included in future studies.

5.e Variation in migration

With a complete survey it is possible to compare the different styles of migration detected in each region, and we find evidence for several types of migration. Compared to other regions, Region 1 and 6 troughs have the greatest asymmetry in accumulation. This is a direct result of a relatively high proportion of wind transport relative to insolation (Figures 2.2, 2.5a). In Region 3, where evidence supports reduced intensity winds relative to insolation, asymmetry is present, but reduced in comparison (Figures 2.3, 2.5b). In Region 5 a drastic increase in TMP slope provides evidence for increased

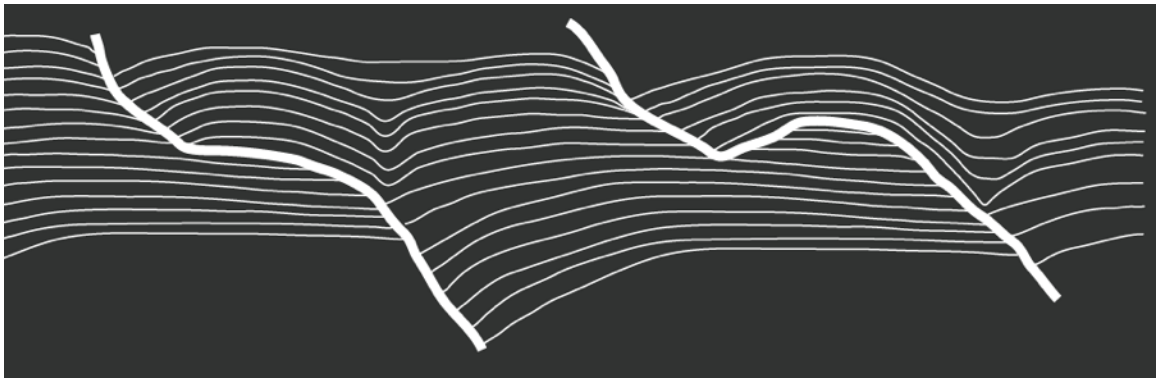

Figure 2.24: Cartoon depiction of trough migration with central promontories and step on the high side slope. *Low side accumulation behaves normally until accelerated accumulation. Afterward, a fresh layer will blanket both the low side and a portion of the high side. This creates a depression and a V-shaped reflector as detected by Smith and Holt [2010].*

deposition relative to insolation and transport (Figure 2.4c). In this rare case the TMP slope associated with a trough at 16°E, 82.5°N increases from 0.92° to 12.4° at ~160 m beneath the current surface (Figures 2.4c and 2.5c).

There are other styles of migration observed on the NPLD that are not so simple. *Smith and Holt* [2010] detected anomalous "V" shaped stratigraphies at three troughs in Region 1 (Figure 2.9b) and interpreted the Vs as being related to the topographic undulations on much of the NPLD. While the features were interesting, they were limited in distribution in the initial survey. We update the findings of *Smith and Holt* [2010] to discover V-shaped deposits in other regions, including Region 2 (Figure 2.12b) and Region 3 (Figures 2.13d and 2.16).

We find that the V-shapes are the result of rapid deposition over a central promontory or step (Figure 2.24). In the case of a central promontory, sediments onlap the low side normal conditions. When deposition outpaces erosion, a continuous blanket of ice will be deposited that mimics the underlying topography, and reflectors detected by SHARAD will reveal this geometry. That pattern may persist throughout hundreds of

meters of deposition. In some places the V-shapes still exist on the surface (Figures 2.13d and 2.16b). In others they are eventually buried completely (Figures 2.13b).

As discussed above, promontories in Region 3 may be related to erosional undulations, consistent with interpretations of *Smith and Holt* [2010] for the V-shapes. However, undulations are not required. Instead, a central ledge or step is sufficient to create minor V-shapes (Figure 2.13d and Figure 2b from *Smith and Holt* [2010].

5.f Thoughts on ice flow

Each region exhibits variations from the classical theme of wind and insolation based trough migration. These differences have made it difficult to hypothesize one mechanism of formation for all visible features, and it is easy to seek alternative explanations. Besides wind transport, ice flow and internal creep have been postulated to explain what we see related to troughs, undulations, and large scale NPLD morphologies. However, we find that there is no stratigraphic evidence to support those claims. Furthermore, gross stratigraphic studies also find that ice flow is not consistent with the morphology of the NPLD [*Karlsson et al*., 2011]. Here we say about the relationship between troughs and the flow hypothesis.

Ice sheet modeling can account for the troughs in one of two ways: that the troughs existed during flow and were modified by it, or that the troughs are relative latecomers, having formed only after flow ceased. These models are predictive and testable with radar stratigraphy. For instance, *Fisher* [1993, 2000] made the case for an accublation model of sublimation and accumulation patterns allowing for the troughs to exist and remain open during flow. In this model, layers beneath the spiral troughs would

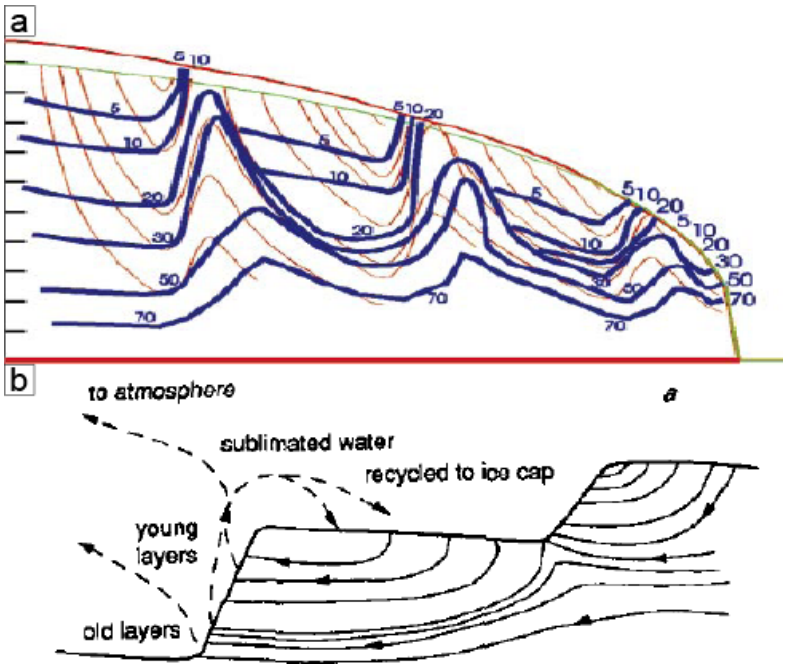

Figure 25: Cartoons depicting different types of predicted flow. *a) Troughs exist during flow modified from Fisher [2000]. Predicted flow lines and stratigraphy has upwelling beneath each trough. b) Accublation model modified from Fisher [1993]. Ice sublimes from the trough high side and is redeposited on the low side. This accounts for asymmetry but results in a stratigraphy inconsistent with radar observations.*

flow upward due to reduced overburden (Figure 2.25b). Our observations clearly indicate that NPLD troughs do not exhibit this stratigraphy. In fact, layers on the low side of a TMP are often offset and depressed beneath troughs, nearly opposite of what was predicted.

A second hypothesis suggested that trough topography would relax over time, eventually closing and becoming smooth [*Pathare and Paige*, 2005]. We find that the oldest troughs have existed throughout 1 km of deposition, approximately one half of the accumulation of the entire NPLD (Figure 2.9b). During the deposition of the same sequence an entire buried chasma, comparable in size to Chasma Boreale, was filled in [*Holt et al*., 2010] (Figure 2.8). Throughout the time required for all of this deposition, Region 1 troughs have grown in amplitude and cross sectional width, have increased in number, and have migrated as many as 90 km, greater than two trough wavelengths. These findings are incompatible with rapid trough relaxation and closure. While we

cannot rule out relaxation, it is not observed and must be comparatively slow in relation to other processes associated with migration.

Finally, in a study of gross topography, it has been suggested that Gemina Lingula flowed and reached steady-state ice sheet morphology before halting [*Winebrenner et al.*, 2008]. The steady-state hypothesis requires the surface to be a smooth dome during flow - one without troughs (or upwelling beneath troughs would occur). This implies that that the troughs formed due to incision after flow halted. However, trough migration is observed by SHARAD in Gemina Lingula (Figures 2.9d, 2.17, and 2.10). Furthermore, the discovery of buried troughs in Region 6 of Gemina Lingula (Figure 2.21) indicates that the current surface it not a result of flow, but one of deposition on top of an existing, non-smooth surface. This observation cannot be reconciled with the assumption of post-flow trough incision unless flow occurred prior to TIS-1, approximately 700 m beneath the current surface in Gemina Lingula. At this level Gemina Lingula is only 1000 m thick. Driving stresses on the smaller ice cap would be significantly less than present day stresses.

Based on previous work of bulk NPLD stratigraphy [*Karlsson et al.*, 2011] in combination with detailed trough related stratigraphy, there is no support for the flow hypothesis during the lifetime of NPLD troughs. We posit that if flow did occur on the NPLD, it was in sufficiently small amounts that it is undetectable with the resolution of SHARAD.

6 CONCLUSIONS

NPLD troughs are both fundamentally similar and rich in diversity. Every trough exhibits classical features, including layered high sides, banded low sides, asymmetric slopes, and albedo variations. Beneath the surface, SHARAD detects asymmetric accumulation patterns and trough migration paths at all troughs where observations can be made. Even though they can all be described similarly, regional and local differences make each unique. Troughs vary based on local and regional surface slopes, wavelengths, trough depths, trough age, presence of topographic undulations, presence of central promontories, and trough bottoms that reach bedrock. To better classify this diversity, we have divided the NPLD into eight regions. The boarders of each region separate troughs based on surface features and subsurface stratigraphy.

The troughs did not form all at the same time, and they can be divided into two generations. Generation 1 troughs reside in Regions 0, 1, 2, 3, 4, and 6. Radar evidence supports a gradual increase in number and longitudinal extent of Generation 1 troughs during deposition of more than 500 m, starting about 1000 m beneath the current surface. Generation 2 troughs are found in Regions 5 and 7a, corresponding to Gemini Scopuli. Onset of troughs in Region 5 was relatively rapid after a large erosion.

The troughs are not static features, and they evolve both independently based on local processes and as a group when considered by region. This evolution plays out over million year time scales. Some of the changes the troughs have undergone include increase in number (Figure 2.11), burial (Figure 2.21), change in wavelength (Figure 2.12b), evolution from compound to simple (Figures 2.9 and 2.23), or merging (Figure 2.14b).

Three common processes are sufficient to explain all of the features and varieties discussed in this paper: transport, insolation, and deposition. These processes are present in every region of the NPLD, but they are not uniform. Winds especially have variable

strengths based local and regional conditions. For example, Region 3 troughs, while at the same latitude as those in Region 1, are comparatively steeper and have reduced asymmetry patterns. They are also near to prominent topographic undulations. Each of those qualities is evidence for reduced wind intensity in Region 3. Region 5 and 7 troughs are steeper than those of other regions. *Pathare and Paige* [2005] noted that troughs near the margin are lower in elevation and latitude, which allow for warmer temperatures and increased insolation. With all of the variation we observe, no evidence is detected to support interpretations of other processes in trough evolution such as ice flow, volcanism, and tectonics.

The troughs evolved independently based on the known processes, but initial conditions set the state for trough formation. Several conclusions can be made from our survey: trough wavelength has an inverse relationship to regional initiation slope and latitude affects the amount of insolation received at each trough. Furthermore, Region 5 and 7 troughs formed on an eroded slope, in contrast to those in other regions. Several other physical properties are important to trough evolution: trough strike, albedo, high and low side slopes, depth, and wind patterns. These properties force the processes associated with evolution and are themselves modified by them: insolation, transport, and deposition.

Chapter 3: The Spiral Troughs of Mars as Cyclic Steps

ABSTRACT

We combine observations of stratigraphy, morphology, and atmospheric processes to relate the spiral troughs on Mars' polar layered deposits to a class of features known as cyclic steps. Cyclic steps are quasi-stable, repeating, and upstream-migrating bedforms that have been studied in terrestrial and submarine environments. The repeating pattern is bounded by hydraulic jumps, which act to stabilize the form. We use radar stratigraphy from the Shallow Radar (SHARAD) on Mars Reconnaissance Orbiter to examine trough evolution and constrain lateral transport. We examine visible images from the Thermal Emission Imaging System (THEMIS) and observe low altitude clouds that we interpret to be the result of katabatic jumps, i.e. the aeolian counterpart of hydraulic jumps in open channel flow. We then devise a theoretical framework for understanding the origin of the spiral troughs that agrees with ten criteria that should be explained for any scenario to satisfactorily model the spiral troughs. Finally, we use Froude and geometrical analysis to estimate the rate of upstream migration caused by katabatic winds for the spiral troughs.

1 INTRODUCTION

It has long been recognized that north polar layered deposits of Mars are fundamental to our understanding of atmospheric deposition, and thus climatic processes there [*Cutts and Lewis*, 1982; *Cutts et al*., 1976; *Fishbaugh and Hvidberg*, 2006b; *Hvidberg et al*., 2012; *Milkovich and Head*, 2005b]. Until recently, investigations have

focused on outcrops of exposed layers within the spiral troughs that cover the ice cap surface [*Fishbaugh et al*., 2010; *Howard et al*., 1982; *Milkovich and Head*, 2005b; *Squyres*, 1979]. However, the troughs are modified by wind, which affects the pattern of layer deposition [*Howard*, 2000; *Howard et al*., 1982; *Ng and Zuber*, 2006b; *Warner and Farmer*, 2008]. Thus, the outcrop record is not a straightforward exposure resulting from horizontal deposition. Instead, the layers must be interpreted in the context of local processes that include pre-existing morphology.

The spiral troughs found on the north and south polar layered deposits of Mars (NPLD and SPLD respectively) have been the source of much debate since their discovery during the Mariner 9 mission [*Murray et al*., 1972]. During the following four decades, many distinct hypotheses were developed for the formation of the spiral troughs [*Ivanov and Muhleman*, 2000; *Kolb and Tanaka*, 2001; *Ng and Zuber*, 2006b; *Pelletier*, 2004; *Weijermars*, 1986; *Zeng et al*., 2008b], but no hypothesis successfully combined the observed stratigraphy with a formation mechanism.

Subsurface data from the Shallow Radar (SHARAD) instrument onboard Mars Reconnaissance Orbiter [*Seu et al*., 2007c] provided a new method to test the varied hypotheses. Analysis of radar reflectors revealed that the troughs are constructional features, having migrated northward during deposition since their onset [*Smith and Holt*, 2010]. This finding revitalized a hypothesis of trough migration via ice transport by winds [Howard et al., 1982] and led to a better understanding of how the troughs developed. The story, however, remained incomplete.

In this paper we propose a new trough model that addresses trough initiation, migration, and all major physical characteristics of the spiral troughs. We then discuss ten criteria that are necessary to explain for a trough formation model to be successful. In general, the spiral troughs are more clearly expressed on the NPLD than the SPLD, and

our observations focus there; however, the ten criteria and our model apply to both poles. Our model employs constraints derived from remote sensing imagery and processes known to be active at the Martian poles today. In Section 3 we describe low altitude clouds observed above the troughs, and in Section 4 we interpret those clouds as evidence for katabatic jumps. In Section 5 we relate the spiral troughs in both hemispheres to a class of morphological features called cyclic steps, which have been studied on earth for decades. The governing fluid dynamics of cyclic steps is well understood, so their existence within the polar ice on Mars provides unique, scientifically useful insights into the development of the ice cap and into Mars'

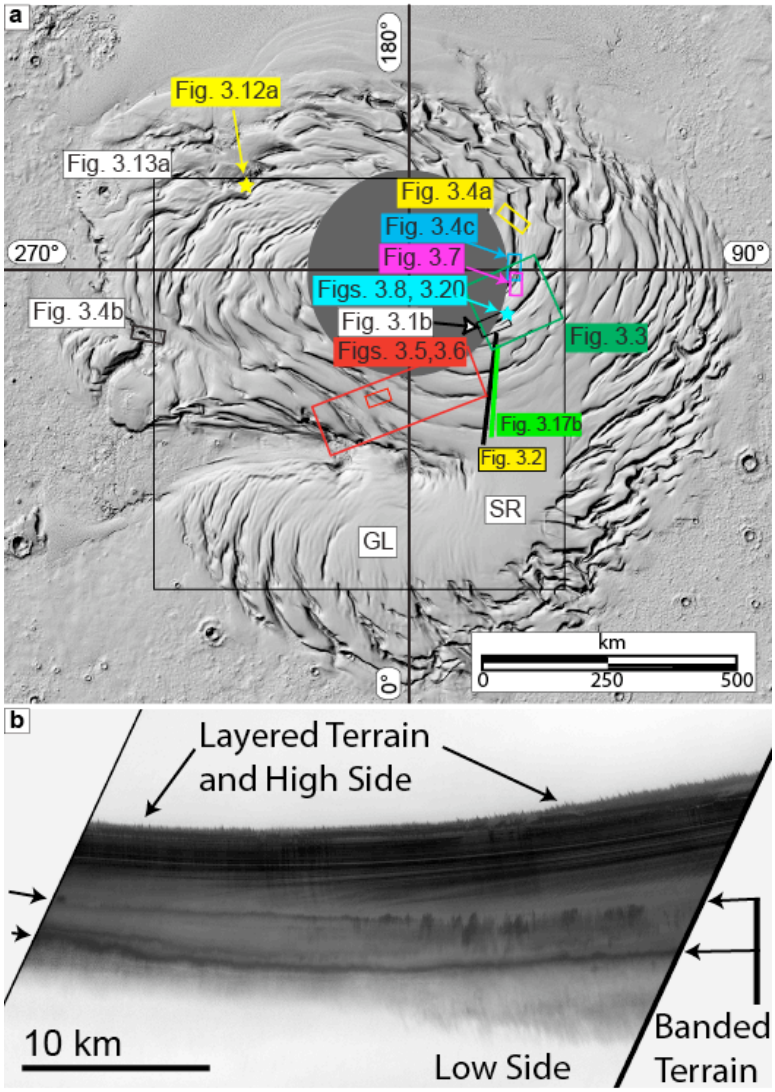

Figure 3.1: NPLD surface and trough image. *a) Shaded-relief NPLD surface from MOLA elevation data [Smith et al., 2001] showing morphology of troughs and footprint of figures for context b) CTX image P21_009266_2729_XN_87N307W taken during Mars Year 29 at L_s 100.4. Archetypal trough displays low-albedo eroded layers, medium-albedo banded terrain, and high-albedo inter-trough regions (top and bottom of image). Exposed layers on trough high side are the result of sublimation and mechanical removal by wind. Banded areas on trough low side exhibit thin feathery deposits that onlap inter-trough region.*

recent climate. In Section 6 we use this new interpretation and five years of observations to roughly estimate annual migration rates of NPLD troughs caused by winds. This framework allows us to better characterize atmospheric conditions at the poles of Mars.

2 BACKGROUND AND PREVIOUS OBSERVATIONS

2.1 Morphology

Most spiral troughs on the NPLD conform to a few basic observations. The troughs form an array of clockwise-bending depressions bounded by two walls that align sub-concentric to the north pole, offset by ~20° [*Howard*, 2000] (Figure 3.1a). The depressions are on average ~400 m deep near the interior and reach a maximum depth greater than 1000 m at the NPLD margin [*Pathare and Paige*, 2005]. The trough pattern is one of sub-parallel strike with a characteristic wavelength of between 20 and 70 km, and the lateral extent of a single trough may be from a few to many hundreds of km long [*Cutts et al*., 1979; *Howard*, 1978].

Troughs on Gemina Lingula deviate from the sub-concentric generalization (Figure 3.1a). This suggests that a longitudinally uniform process, such as insolation, is not solely responsible for gross trough morphology [Pathare and Paige, 2005]. Because of this variability in orientation, we reference the high and low sides of troughs throughout this paper, rather than equator-facing or pole-facing (Figures 3.1b and 3.2a).

The opposing trough walls are distinct based on albedo, texture, and slope. The high, generally equator-facing, side has the lowest albedo on the NPLD (Figure 3.1b) [*Cutts et al*., 1976; *Ng and Zuber*, 2006b]. It is characterized by layered terrain and a

relatively high percentage of dust. Although dust is known to obscure visible layers at the smallest scales, the presence of sharply delineated layers suggests that there is no thick lag obscuring or smoothing the entire surface [*Fishbaugh et al*., 2010; *Herkenhoff et al*., 2007; *Howard*, 2000]. Because of the ablation of volatiles on this surface, the dust originally part of the matrix must be mechanically removed, or a lag would obscure the layers. If thick enough, this lag would inhibit further ablation [*Howard*, 2000; *Warner and Farmer* 2008]. The low, generally pole-facing, side of a trough exhibits a different morphology, called banded terrain. Banded terrain is considered an irregular mantle that unconformably overlies adjacent terrain and has an albedo intermediate to the layered and inter-trough regions [*Howard et al*., 1982] (Figure 3.1b).

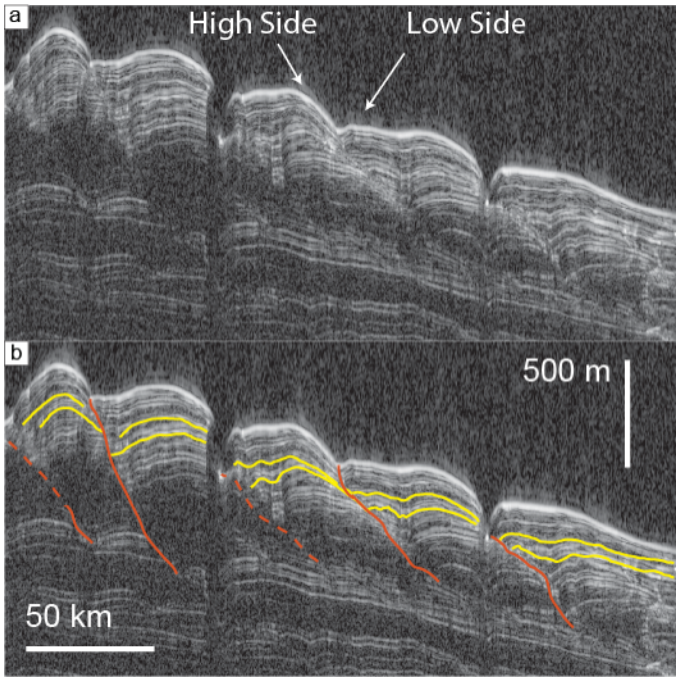

Figure 3.2: Portion of SHARAD radargram 1294501 crossing spiral troughs. *a) Stratigraphy associated with spiral trough migration is visible beneath the troughs. b) Same as a) with interpretation of reflectors to indicate Trough Migration Paths (TMP; orange) and thickness variations between reflectors (yellow) positively correlated across the TMPS (as in Smith and Holt, 2010). Troughs were originally lower and farther south and have risen during accumulation and northward migration. Asymmetric thickness across TMP boundary indicates transport of ice as described in the cyclic step model. Location indicated in Figure 3.1a. Vertical exaggeration ~ 80x.*

Besides albedo and texture differences, the trough wall slopes are asymmetric. Slopes range from 2° to about 15° on the high side, increasing with distance from the

north pole, while those on the low side are uniformly lower than their counterparts [*Pathare and Paige, 2005*].

Another feature of the NPLD associated with spiral troughs are smaller-scale, wavelike ridges and swales called "undulations" (Figure 3.3) [*Cutts et al*., 1979]. Where exhibited, undulations are found roughly strike-parallel adjacent to the low-side of troughs. Their wavelengths are or order 1 to 10 km, and amplitudes range from less than 10 to about 100 m [*Howard*, 2000].

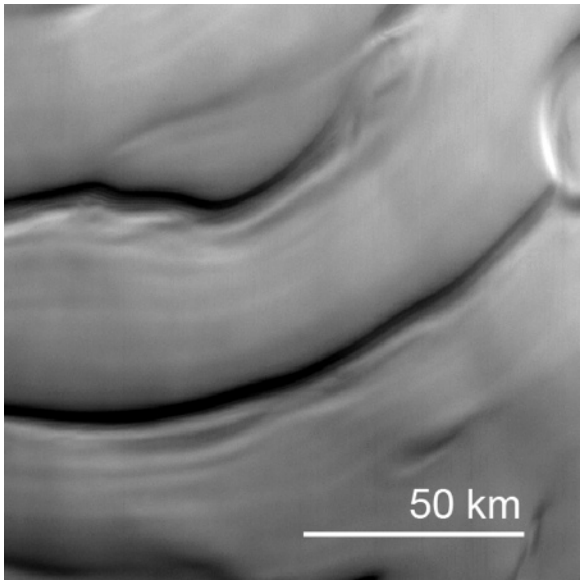

Figure 3.3: Troughs with undulations. *Mars Orbital Camera image M1800805 taken during Mars Year 28 at L_s 35.2. Topographic undulations align roughly parallel to, and on the low side of, NPLD troughs. Locations indicated in Figure 3.1a.*

2.2 Radar stratigraphy

The advent of SHARAD allowed scientists to test hypotheses of PLD evolution by probing beneath the surface [*Holt et al*., 2010b; *Phillips et al*., 2008a; *Putzig et al*., 2009; *Seu et al*., 2007a]. Radar reflectors serve as a proxy for visible stratigraphy and allow for quantitative measurements of subsurface layer geometries [*Christian et al*., in press; *Milkovich et al*., 2009]. Analysis of radar reflectors on the NPLD revealed discontinuities that extend downward from the bottom of the troughs into the ice [*Smith and Holt,* 2010] (Figures 1.2 and 3.2). *Smith and Holt* [2010] interpreted the discontinuities as bounding surfaces that represent trough migration paths (TMPs), indicating the former positions of eroded spiral trough high-side walls.

By mapping the TMPs, it was possible to determine the stratigraphic level at which the spiral troughs formed and thus the amount of accumulation that has occurred since their onset. *Smith and Holt* [2010] found evidence that the troughs near the NPLD margin at 90° E formed stratigraphically higher that the central troughs north of Chasma Boreale, implying that conditions were favorable for NPLD trough formation at least twice. Additionally, the total amount of migration undergone by individual troughs was measured for each region. The oldest troughs, those near Chasma Boreale, have migrated approximately 50 – 65 km during 550 – 700 m of accumulation, while the younger ones at 90° E have migrated between 15 and 25 km during ~360 m of accumulation.

Further analysis from SHARAD found that there is a correspondence of reflector separation (layer thickness) with horizontal distance from the TMP [*Smith and Holt,* 2010]. On the low side, reflector separation increases as it approaches the TMP. In contrast, high side layers thin as they approach the TMP (Figure 3.2). This relationship indicates one of two possibilities: that ice was deposited nonuniformly across a trough [*Pathare and Paige*, 2005]; or ice has been transported from the high side to the low side [*Howard et al*., 1982; *Howard*, 2000; *Smith and Holt*, 2010]. In any case, the examination of radar reflectors can quantify this asymmetry of net accumulation [*Smith and Holt*, in prep, 2011].

Finally, there are regional differences in TMP slopes and layer thickness variations. Such morphological differences are likely the result of initial conditions such as starting topography and atmospheric state [*Smith and Hol*t, 2011; in prep].

3 IMAGERY OF TROUGH CLOUDS

3.1 Observations in the north

As of this writing, 8,105 Thermal Emission Imaging System (THEMIS) images of the north polar region (northward of 82°) are available on Arizona State University's Mars Image Explorer for Mars Years 26-31 [*Christensen et al*., 2004]. Several hundred additional images exist from High Resolution Stereo Camera (HRSC) [*Neukum and Jaumann*, 2004], Mars Orbiter Camera (MOC) [*Malin et al*., 1998], Context Imager (CTX) [*Malin et al*., 2007], and the High Resolution Imaging Science Experiment (HiRISE) [*McEwen et al*., 2007], totaling approximately 8,500 optical observations for latitudes greater than 82° north.

We examined all of the images in the north polar region for evidence of atmosphere-surface interactions. Of those examined, ~380 images capture low-altitude clouds with an elongated structure. The earliest clouds each year were observed from L_s=24 to about L_s=60, during Mars' north polar spring (Figure 3.4a). These early-season clouds tend to be wispy and contrast with more opaque later seasonal clouds. Only a few, ~10, images of this type of cloud exist. Their origin is unknown but may be related to subliming carbon dioxide frost.

The majority of observed trough clouds occurs later in the season and appears to be strongly influenced by NPLD topography, specifically the troughs. We propose to name this type of near-surface cloud "trough clouds." They can be subdivided into 2 groups: transverse and parallel to the trough strike. Transverse clouds may be found either between or crossing troughs and are only exhibited in a few images. They orient roughly perpendicular to trough axes (Figure 3.4b). Parallel clouds, on the other hand, manifest near the bottom and low side of spiral troughs, parallel to their axes (Figures 3.4c and 3.5b). To date, trough-parallel clouds are observed in ~350 THEMIS VIS, one

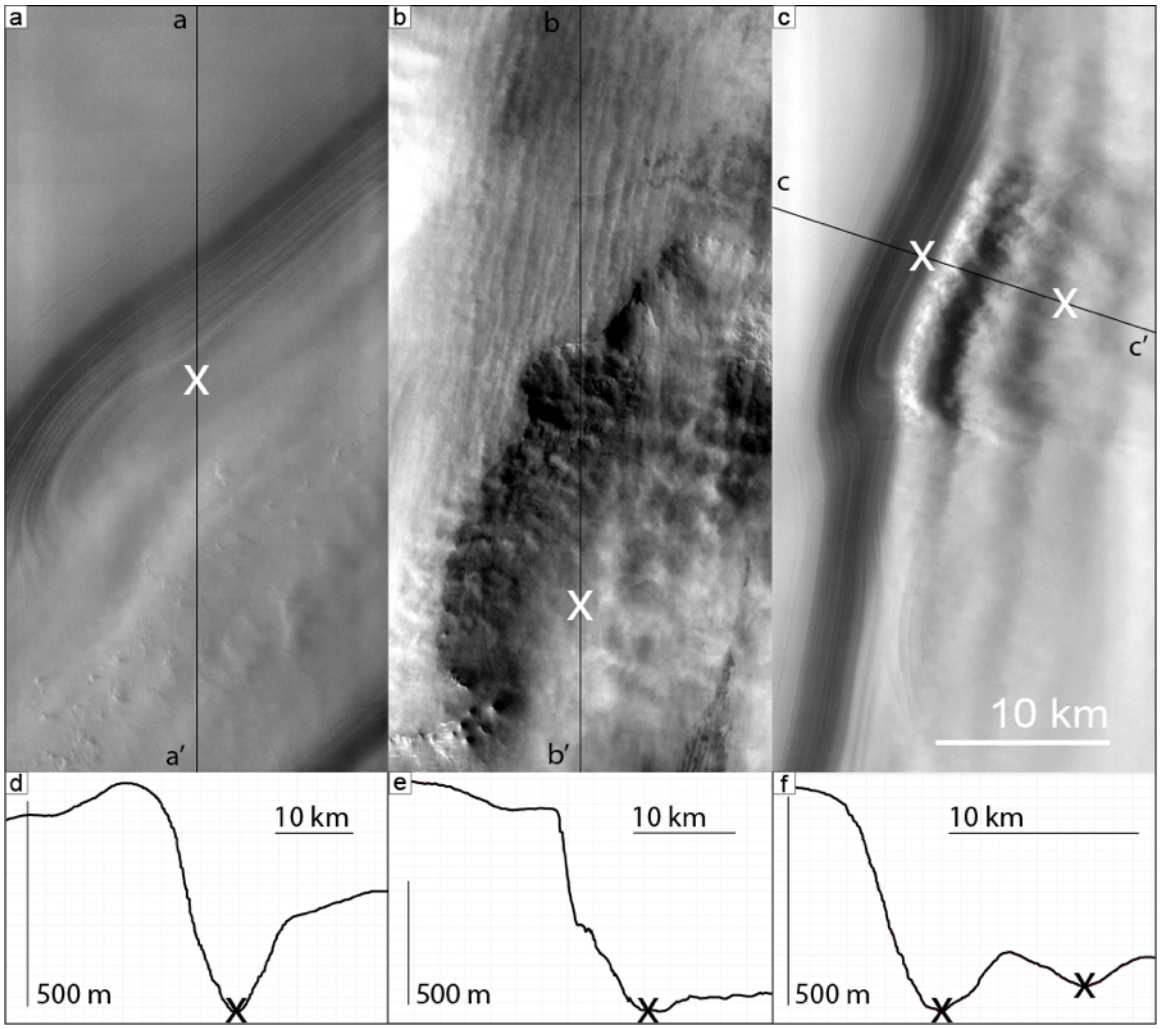

Figure 3.4: THEMIS VIS images of near-surface ice clouds. *a) V27668015 taken during Mars Year 29 at L_s 43.1, while CO_2 ice is still expected on the surface. Wispy clouds suggest sublimation from the surface. Vertical line for MOLA topographic profile in d). White X marks lowest elevation of the trough. b) V37081012 taken during Mars Year 30 at L_s 81.8. Linear clouds flowing downhill, sub-perpendicular to topography. The clouds interact with the surface, as evidenced by their change in structure across the top of the scarp. Vertical line for MOLA topographic profile in e). White X marks lowest elevation of the trough. c) Portion of V28743004 taken during Mars Year 29 at L_s 82: Trough-parallel clouds form near the bottom of a trough. Katabatic jump is visible at center, near the bottom of the trough (White X marks lowest elevation of trough). Clouds have undular pattern with a wavelength similar to topographic undulations. Slanted line for MOLA topographic profile in f). d) Topographic profile of vertical line in a). e) Topographic profile of vertical line in b). f) Topographic profile of vertical line in c). Black [white] X marks the lowest elevation in each profile. Locations shown in Figure 3.1a.*

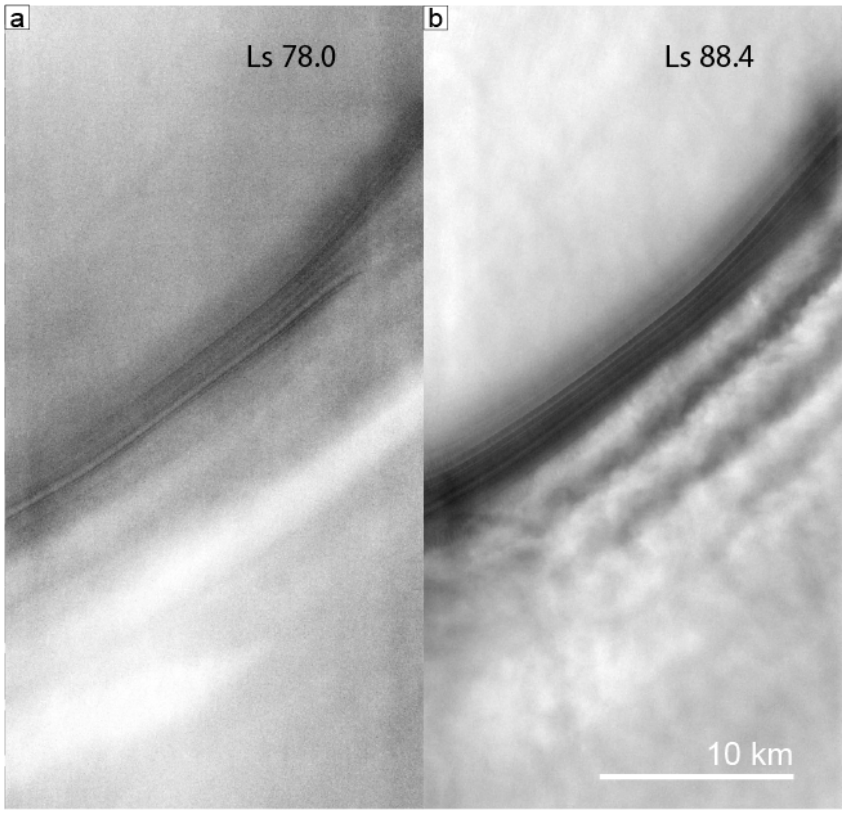

Figure 3.5: THEMIS observations of a trough with and without cloud cover. *a) Portion of THEMIS image V28633004 taken during Mars Year 29 at L_s 78.0. Seasonal frost covers the low side and a portion of the high side of the trough. b) Portion of THEMIS image V28920037 taken during Mars Year 29 at L_s 88.4, less than 5 hours prior to Figure 3.6a. Undular clouds cover the low side of the troughs. Footprint for a) and b) is the same. Locations in Figure 3.1a and 3.6 b.*

CTX, three MOC, and several HRSC images (Figure 3.6a) on the NPLD.

Figures 3.4c, 3.5b, and 3.6a share a further commonality besides the trough-parallel clouds. In these images, the parallel clouds exhibit undular, or wavelike structures. This morphology is observed in nearly 20% of images of trough-parallel clouds. The wavelengths of these patterns vary spatially around the NPLD from 1 to 9 km, the majority being 2 - 5 km. This wavelength is smaller than the cross sections of the troughs, which varies between 10 and 25 km.

Transverse linear streaks on the trough high side are also sometimes observed when parallel clouds are present (Figure 3.7). Linear streaks were previously observed in THEMIS V12432001 [*Warner and Farmer* 2008; *Smith and Holt*, 2010], but only four such images exist, ~1% of the total images with trough clouds. Separation of the streaks varies laterally in a single image and ranges from 250 to 500 m when observed.

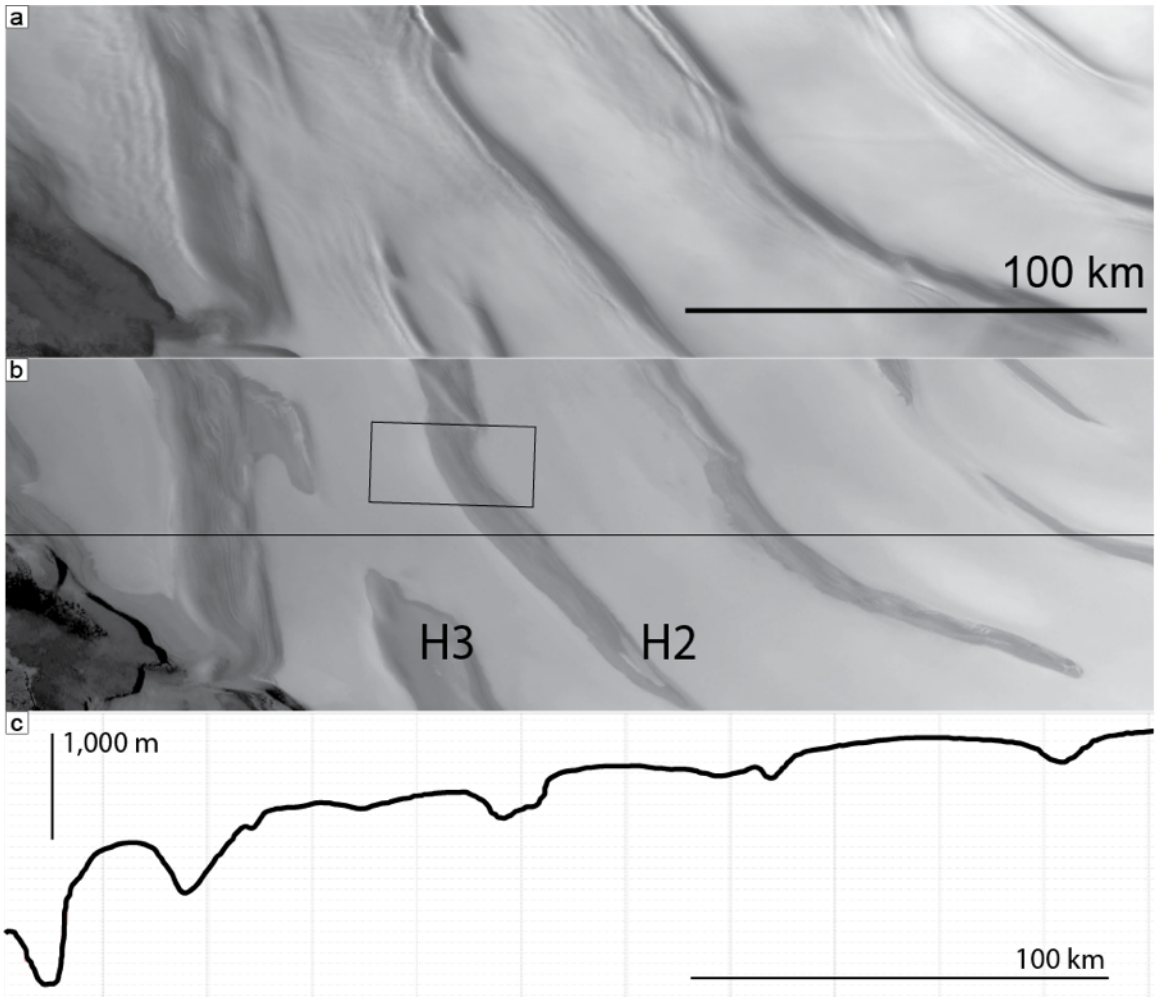

Figure 3.6: Troughs clouds north of Chasma Boreale. *a) Portion of H5741_0000_ND2 taken during Mars Year 29 at L_s 88.4, just 5 hours after Figure 3.5a. Undular trough clouds are visible at the bottom of at least 6 troughs over ~ 300 km. b) Portion of H1167_000_ND2 taken during Mars Year 27 at L_s 129.4. Same location as in a) but at a later time in the year. Clouds do not cover the surface. The contrast between a) and b) demonstrates temporary nature of trough clouds. Horizontal line is the approximate cross section corresponding to c). Rectangle is footprint of Figure 3.5. c) Topographic profile of horizontal line in b). More than 1000 m of elevation separate the northernmost trough from the southernmost trough. Because the clouds of a) are strongly affected by topography, it is unlikely that they reside at 4 km elevation [Whiteway et al., 2009]. Locations of a) and b) indicated in Figure 3.1a.*

3.2 Seasonality of NPLD cloud cover

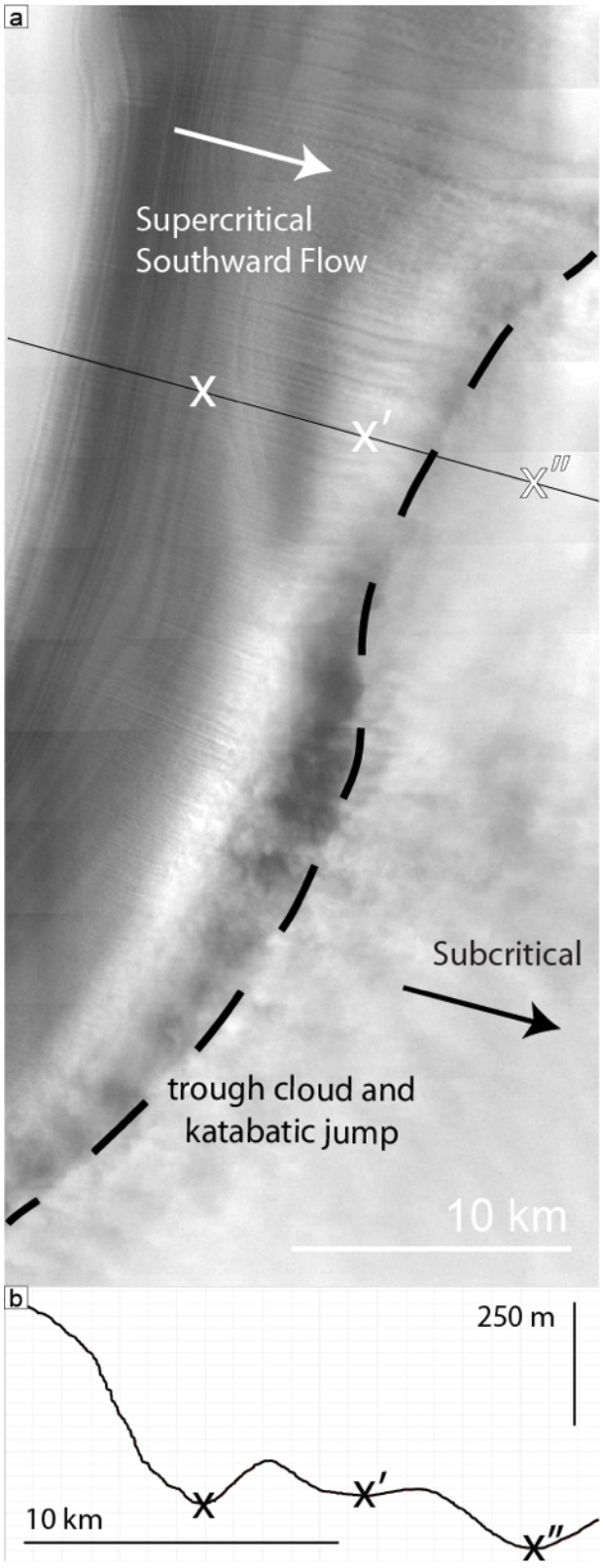

Figure 3.7: Trough cloud with linear streaks. *a) Portion of THEMIS VIS image V12295001 taken during Mars Year 27 at L_s 90.6. Winds enter the trough from the high side. The flow accelerates downhill towards the trough bottom (white Xs indicate local minimum elevations). The cloud shape is indicative of a katabatic jump separating subcritical and supercritical flow. Shadows and turbulence suggest that this is not part of the surface. Towards the high side from the katabatic jump, linear rolls are separated by 300 to 500 m. These rolls have shadows, indicating they reside at low elevations above the layered terrain. If the clouds were higher, the shadows would be displaced greatly from the individual roll. Fewer than 5 of the ~400 images of NPLD clouds exhibit linear rolls on the high side, exemplifying the rarity of this observation. b) Topographic profile of vertical line in a). Black X's mark the relatively lowest elevations in the trough and correspond to the White Xs in a). Location given in Figure 3.1a.*

The total number of observations is much greater for THEMIS than all other imaging instruments combined. Due to that and out need for high sampling frequency, our analyses are primarily based on these images. Occasionally, THEMIS images of the NPLD are acquired every two hours for up to twelve hours (Figure 3.8). Analysis of images across multiple years provides insight into the seasonal timing of cloud abundance

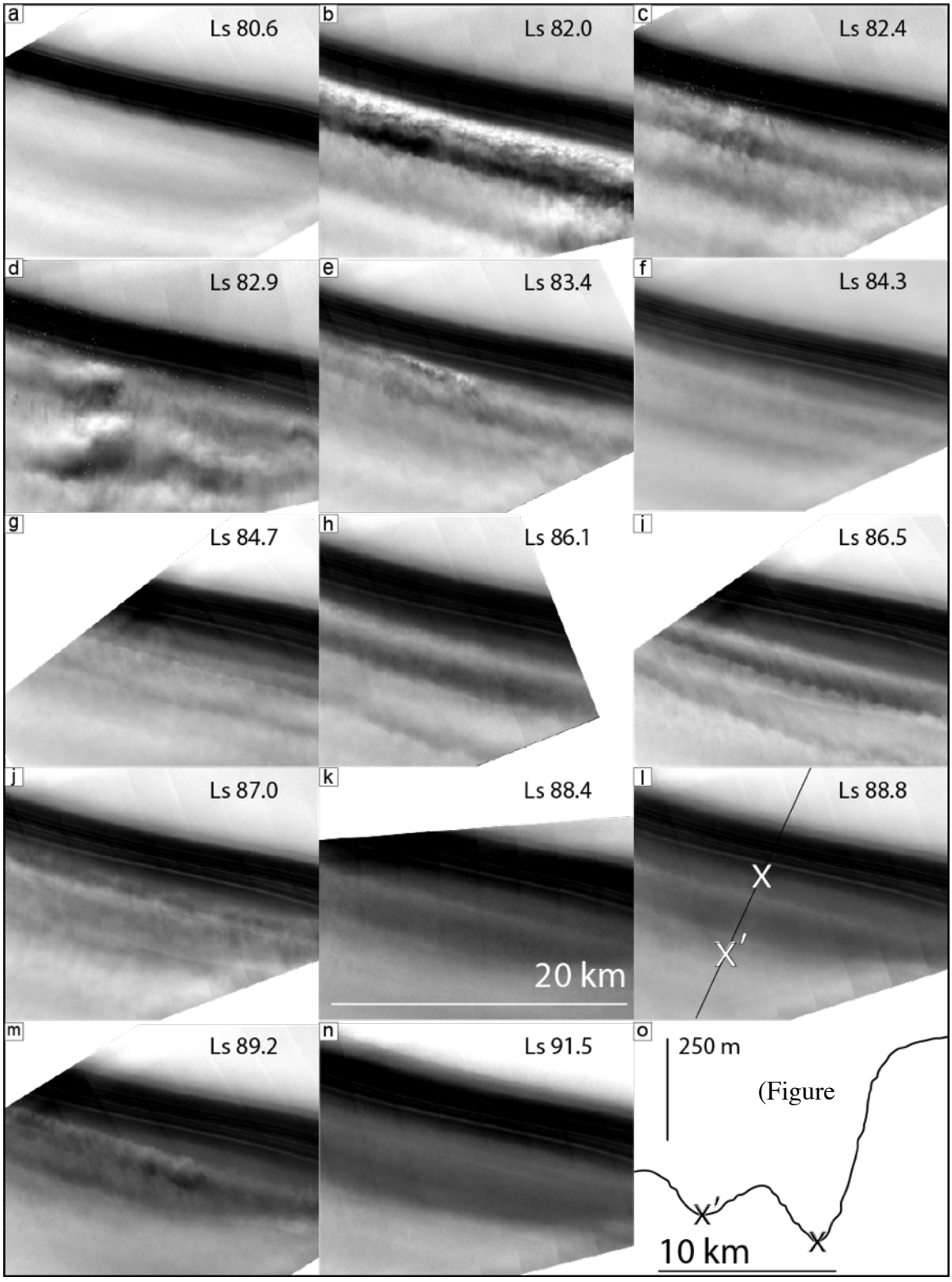
a
Ls 80.6
b
Ls 82.0
c
Ls 82.4
d
Ls 82.9
e
Ls 83.4
f
Ls 84.3
g
Ls 84.7
h
Ls 86.1
i
Ls 86.5
j
Ls 87.0
k
Ls 88.4
l
Ls 88.8
X
X′
20 km
m
Ls 89.2
n
Ls 91.5
o
250 m
(Figure
X′
X
10 km

Figure 3.8: Sequence of THEMIS images for trough during the cloud season. *a) through n) THEMIS images with same footprint: V28706003, V28744006, V28756004, V28769004, V28781003, V28806003, V28818007, V28856007, V28868003, V28881003, V28919037, V28931004, V28943004, V29006006 during Mars Year 29 from L_s 80.6 to L_s 91.5. Trough clouds exhibit strong morphological changes during this period. Images are individually stretched, making albedo changes difficult to detect; however, from a) to n) the low side of this trough gradually decreases albedo, while the high side changes little. The albedo change is the result of mantling from fresh deposition of ice and dust. o) Topographic profile of vertical line in l). Xs mark the local minimum elevations in the trough and correspond to the White Xs in n). See Figure 3.1a for location.*

3.9). All images capturing clouds were acquired between L_s 24 and L_s 102, with the first appearance of trough-parallel clouds at L_s 36.

Of the Mars years with available north polar THEMIS imagery, MY 26, 27, 28, 29, 30, and 31, there are 0, 52, 25, 133, 54, and 96 detections of trough clouds, respectively (Table 3.1). During MY 26 only 21 images were taken during the cloud season, hampering detection. For the date range between L_s 24 and L_s 102, MY 27 has 927; MY 28 has 559; MY 29 has 1622; MY 30 has 673; and MY 31 has 708 available images (Table 3.1). Combining all years for analysis, L_s range 80-90 has the highest frequency with over 180 observed clouds (Figure 3.9). L_s range 90-100 has ~70 detections, and 70-80 has ~50. There are no trough- parallel clouds detected after L_s 102.

Table 3.1: Number of trough cloud observations for Mars years 26 -31. *Total images; available images between L_s 24 and 102; images observing trough clouds; and percentage of images containing clouds during cloudy season.*

Mars year	Total Images	Ls 24 - 102	Trough Clouds	Percentage in Ls 34 - 98
26	177	21	0	0
27	2985	927	52	5.6
28	909	559	25	4.5
29	2101	1622	133	8.2
30	948	673	54	8.0
31	985	708	96	13.6
	8105	4510	360	

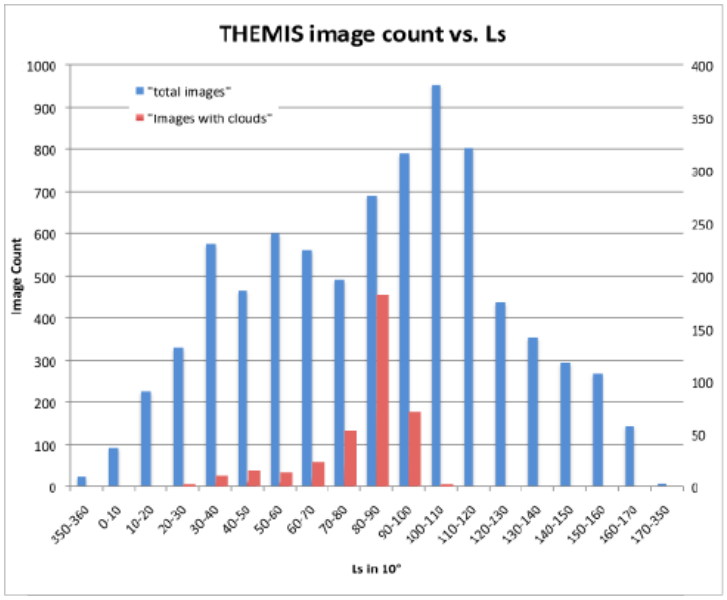

Figure 3.9: Temporal histogram of clouds. *8,108 THEMIS VIS images exist and were examined for latitudes north of 82° during Mars Years 26-31 (blue). More than 350 images capture clouds similar to those depicted in Figure 3.4 (red). Clouds imaged by THEMIS begin after L_s 24, peak between L_s 80 and 90, and end abruptly near L_s 100. The last trough cloud is observed at Ls 102.*

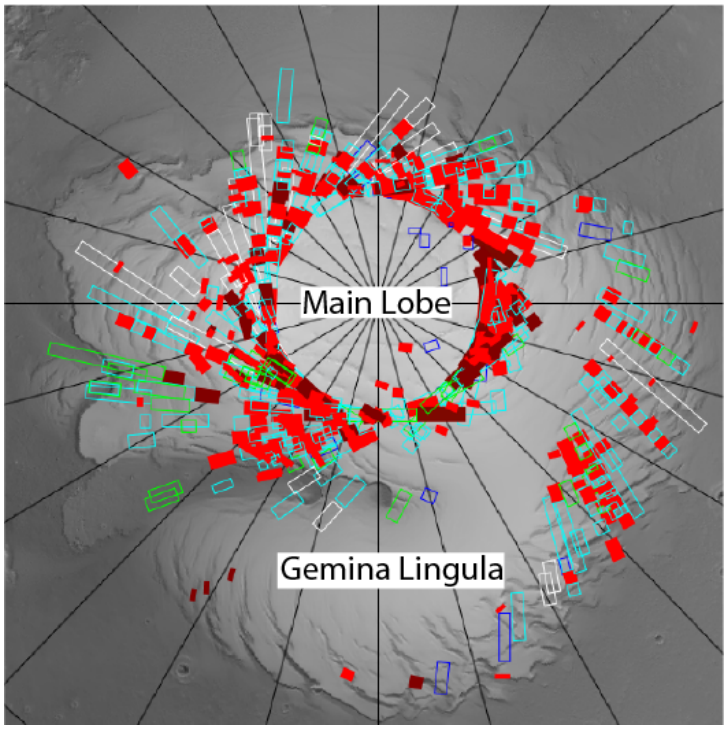

Figure 3.10: Location map of images with detected clouds on the NPLD. *Red boxes indicate locations of trough-parallel cloud. Dark red indicates undular clouds. Blue and green indicate general cloudiness and streaks, respectively. Gemina Lingula and the region extending to the main lobe have sparse detections. No images are available from THEMIS for latitudes north of ~ 87° before Mars Year 31.*

Most cloud events are only captured in a single image, but for the solar longitude range L_s 84.66 to 87.98 in Mars year 29, every visible wavelength image north of 86° contains trough-parallel clouds. Many others before and after also contain clouds. This extreme duration (a span greater than 200 hours) is only observed once in the four Mars years that have been examined. Images taken during this period from HRSC (Figure 3.6), THEMIS infrared bands and the Compact Reconnaissance Imaging

Spectrometers for MARS (CRISM) also capture this event.

The geographic pattern of trough cloud detections is show in Figure 3.10. During the five Mars years with sufficient imagery, most of the NPLD troughs experienced trough clouds. However, fewer detections were found in Gemina Lingula (GL; Figure 3.1) and in smaller regions at the margins near 90° E and 255° E. Relative infrequency of events at these locations or sampling bias may have contributed to this distribution of non-detection.

3.3 Observations in the south

More than 14,000 THEMIS images cover portions the SPLD, and a preliminary search has been undertaken. In a strategic survey, ~250 images containing trough-parallel clouds are found in Mars Years 26 – 29 (Figure 3.11). Fewer than 20 images capture transverse or wispy clouds.

Preliminary results indicate that, like on the NPLD, all of the trough-parallel clouds in the south are near topographic changes such as troughs, craters, and scallops (Figure 3.11b). They appear at L_s ranges, L_s 212 – 278, and 282-317. The early range corresponds to southern spring, which is similar to our findings in the northern cloud study. However, the later range of L_s does not have a northern equivalent. Clouds observed between L_s 282 and 317 are uniformly at higher elevations and nearer to the residual CO_2 ice cap than earlier clouds (Figure 3.11c). Trough clouds at the highest elevations on the SPLD may be CO_2 ice rather than H_2O ice.

4.1 Ice cloud formation

The clouds observed in Figures 3.4c, 3.5b, 3.6a, 3.7, and 3.8 are most likely composed of water ice crystals and some fraction of dust. A water ice composition is assumed because in late spring the temperatures in the north polar region are far too high

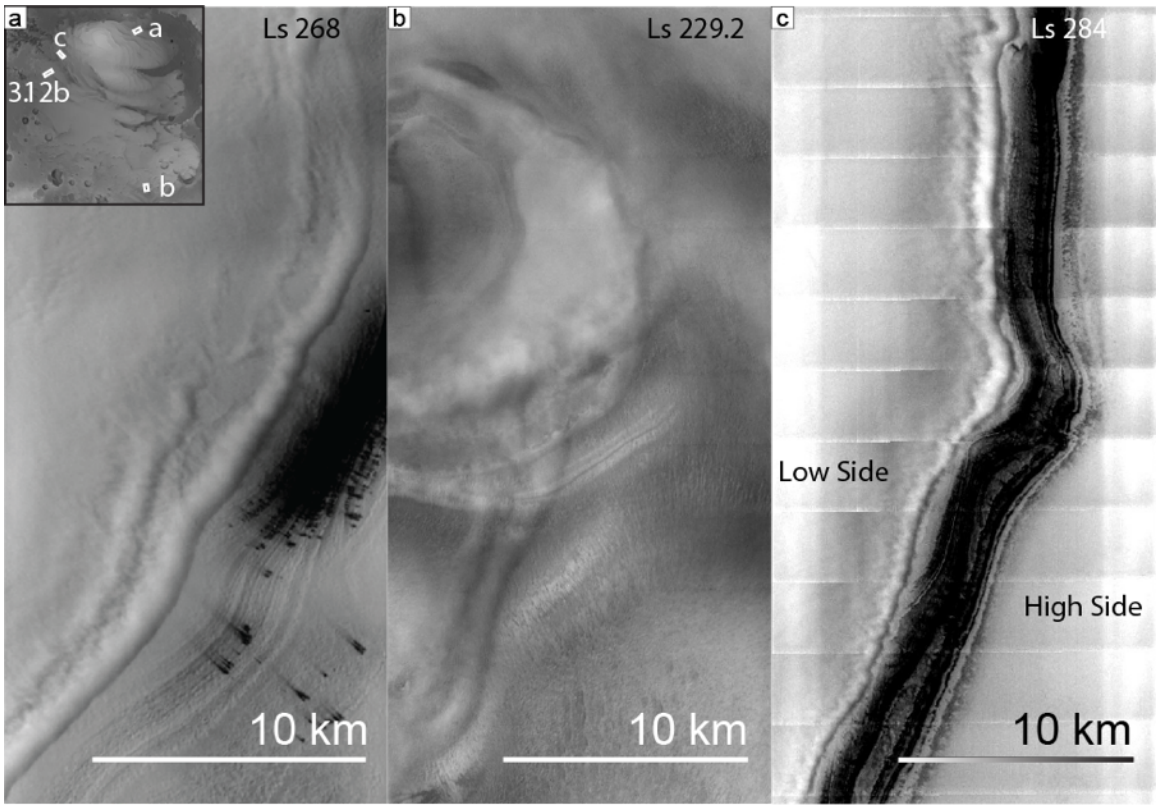

Figure 3.11: South polar trough clouds. *a) THEMIS VIS image V16249003 taken during Mars Year 27 at L_s 268. Trough clouds are found on the SPLD in southern spring and are manifested similar to those in the north. Wind streaks indicate wind direction from lower right towards upper left. b) Portion of THEMIS VIS image V07160010 taken during Mars Year 26 at L_s 229.2. Clouds form at katabatic jump near scalloped terrain of SPLD and have undular form, as observed for some NPLD troughs. c) Portion of THEMIS VIS image V08216005 taken during Mars Year 26 at L_s 284. Trough cloud, on low side, follows topography. Cloud changes from simple to undular jump (moving upward from bottom of the image), indicating slight changes in flow conditions and hence, Froude number. Locations indicated in inset of a).*

for solid CO_2 ice. The existence and properties of water ice clouds depend on several factors: ambient vapor concentration, pressure, temperature, and the number of cloud condensation nuclei [*Montmessin et al*., 2004; *Toon et al*., 1989]. While a discussion of ice cloud microphysics is beyond the scope of this paper, it is important to note some implications of clouds existence. In particular, conditions are met for enhanced sublimation of water from the surface, and ice crystals grow to sufficient size for an optically thick cloud to form. This implies that specific meteorological conditions are met to yield the formation of trough clouds.

We interpret the trough-parallel clouds as being primarily ice, but a previous interpretation suggested that they could be dust clouds [*Warner and Farmer* 2008]. We have no spectral analysis to contradict that claim, but the morphology of the

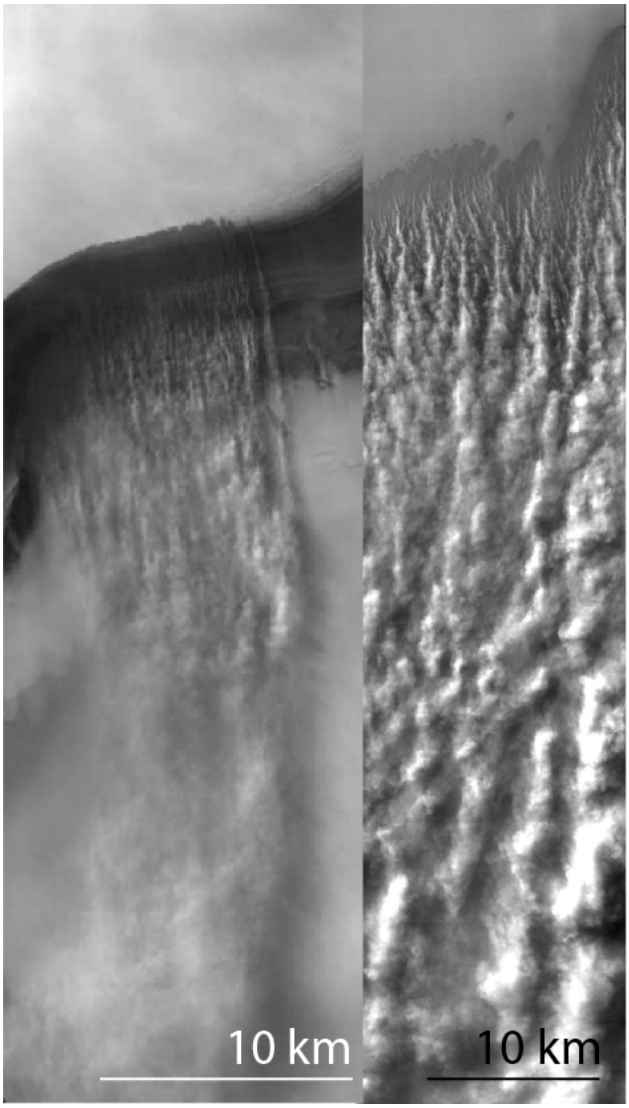

Figure 3.12: Elongated clouds emanating from trough high sides. *a) Portion of HRSC image H3670_000 taken during Mars Year 28 at L_s 135.9. b) Portion of THEMIS image V08874006 over SPLD taken during Mars Year 26 at Ls 316.3. The clouds in a) and b) are very distinct from the parallel trough clouds discussed in this paper, aligning perpendicular to troughs and extending tens of km beyond. Because they are so distinct, we don't consider them to be a part of the cyclic step story. They may be examples of dust plumes as described by Warner and Farmer [2008]. Location in of a) in Figure 3.1a and b) in Figure 3.11a inset.*

clouds goes against this argument. Trough clouds are typically elongated along-trough and have very little extent in the cross-trough direction (Figure 3.8b and 3.8m). This is consistent with cloud formation caused by wind and temperature disturbances associated with katabatic jumps (see section 4.3) rather than the purely aeolian erosion that yields dust clouds. We have detected other cloud morphologies on both poles that are more consistent with dust clouds (Figure 3.12). These clouds are elongated cross-trough for many tens of kilometers and are more frequent on the SPLD than the NPLD. As expected, the existence of dust clouds indicates the ability of wind to scour dust from a trough. The long extent of the clouds suggests that dust is not immediately redeposited and may be removed entirely from the cap, in agreement with spectral analysis of deposits [*Massé et al*., 2012].

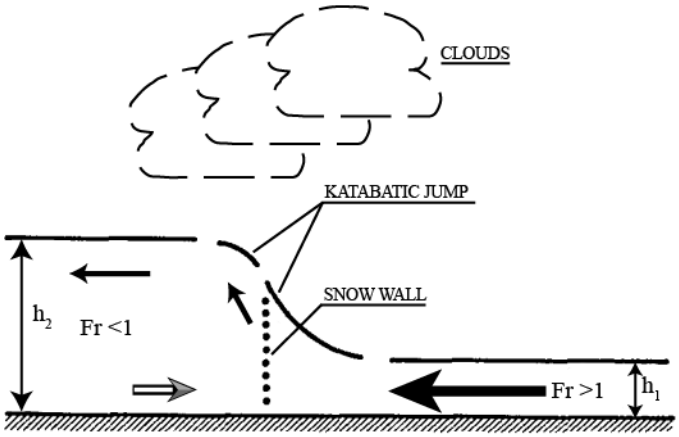

Figure 3.13: Cartoon depiction of aeolian katabatic jump in Antarctica. *Right to left, incoming flow is supercritical. Flow depth increases at the katabatic jump. Ice forms at snow line, and clouds form at site of katabatic jump. Downstream of the katabatic jump flow is subcritical. Arrows indicate flow direction. Reproduced with permission from Pettré and André [1991].*

Terrestrial clouds similar to the Martian trough clouds are found in Antarctica and often form elongated "walls of snow," especially close to large slope changes [*Lied*, 1964] (Figure 3.13). Those distinctive clouds result from a local enhancement of katabatic winds and formation of "katabatic jumps," also called Loewe effect [*Pettré and André*, 1991]. Strong perturbations of temperature, pressure, and wind velocity associated with this phenomenon could explain the formation of walls of snow. We propose that Martian trough clouds follow an analogous mechanism.

4.2 Katabatic Winds

Some of the most common winds on long regional planetary slopes are katabatic. These result from downhill flow of cold, dense air (radiatively cooled over the ice cap) beneath ambient, warmer air. Large elevation differences and temperature changes required to form these winds mean that they are most often found on Earth near elevated ice sheets. Ice sheets offer favorable conditions due to high thermal inertia and high albedo, both contributors for strong katabatic winds. Much effort has gone into studying such winds in Antarctica [*Ball*, 1956; *Lied*, 1964; *Pettré and André*, 1991].

The duration of katabatic winds on Earth has been recorded from several to tens of hours. Winds vary predictably in strength on both diurnal and seasonal time scales . Katabatic winds are strongest near the equinoxes, likely due to larger scale atmospheric phenomena occurring at that time. Diurnal variations are most directly linked to insolation. Wind direction is influenced both by the downhill katabatic acceleration and deflection by the Coriolis Force [Pettré et al., 1993].

Short radiative timescales and low thermal inertia of the Martian CO_2 atmosphere result in katabatic winds that are more frequent and intense on Mars than on Earth [*Gierasch and Sagan*, 1971; see *Spiga* [2011] for a comparative discussion]. This occurs in both polar regions and at lower latitudes. Katabatic wind strength and directions have been modeled on the NPLD during the springtime [*Spiga*, 2011; *Tyler and Barnes*, 2005]. Similarities exist between the modeled winds of Mars and those observed in Antarctica. For example, maximum velocities are found in both cases at the bottom of steep slopes, and local and regional topography affect the wind directions (Figure 3.14). In the model presented by *Spiga et al*. [2011] the maximum velocities attained by polar katabatic

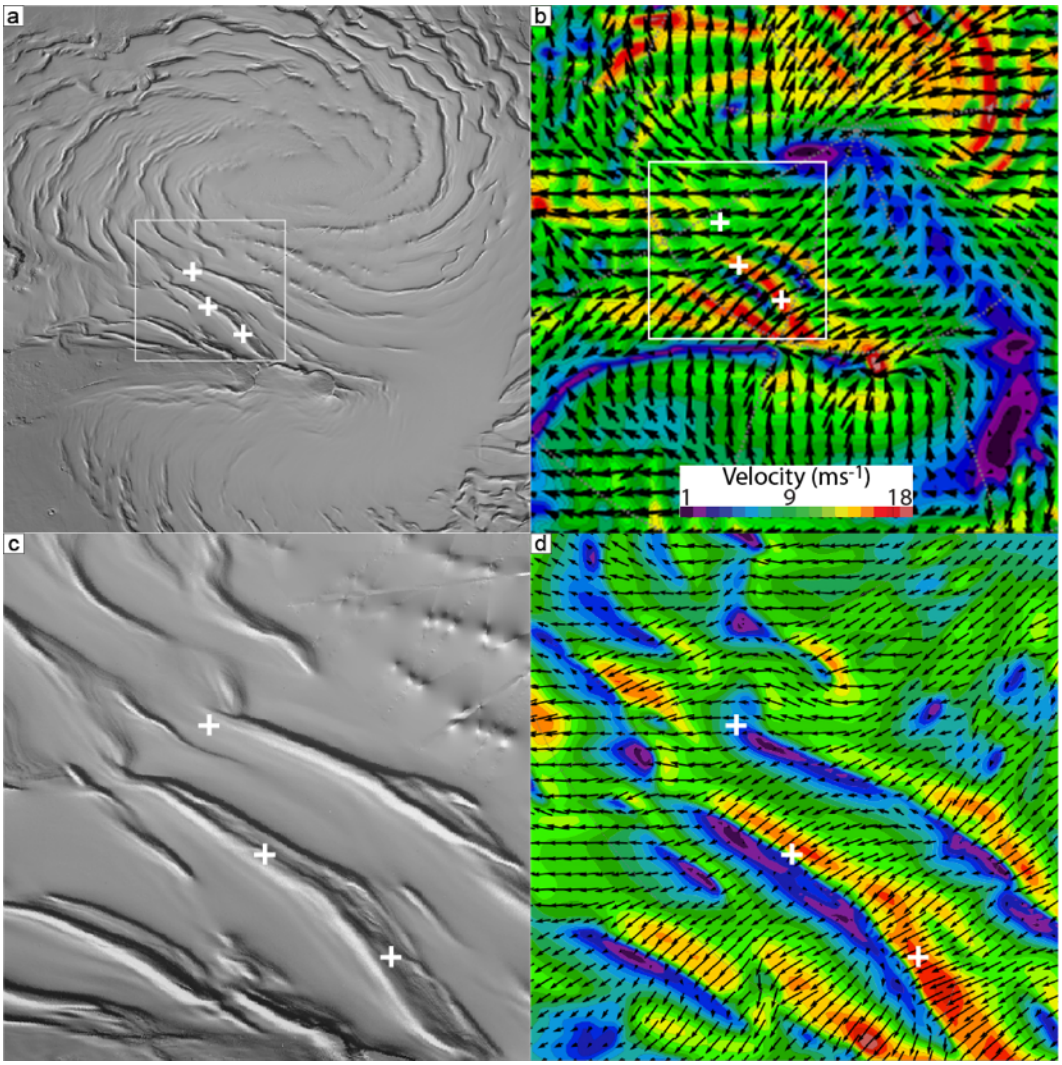

Figure 3.14: Locations and nested mesoscale model indicating velocities of katabatic winds on NPLD at L_s 50. *a) MOLA shaded topography of portion of NPLD corresponding to extent of mesoscale model Nest 2. Box indicates extent of c) and d). b) Nest 2 of mesoscale model with 6.7 km resolution per grid point. c) Extent of mesoscale model Nest 3 in shaded relief. d) Nest 3 with 2.2 km resolution. Winds 30 m above the surface reach speeds in excess of 18 ms^{-1} on the trough high side, locations associated with greatest removal of ice. Winds leaving the troughs on the low side are much slower, 1~3 ms^{-1} and are associated with areas of deposition. Color scale same for b) and d). Plus signs indicate the same location in each image.*

winds at the bottom of troughs were 10-12 m/s. Velocities on the low-side of troughs were near 4-6 m/s. Such a katabatic wind regime develops from the surface to about one kilometer above the surface. Those estimates represent the regional component of katabatic winds, obtained by a model with spatial resolution 10-20 km.

To better simulate the conditions on the NPLD, we used the same model with a spatial resolution of 2.2 km. This higher resolution simulation better represents the effects of topography and slopes and shows an enhancement of wind speed contrast across troughs. Wind velocities in excess of 18 m/s are modeled on trough high sides, while velocities as low as 1 m/s are modeled on the low sides (Figure 3.14d). Strong winds over the polar caps might also occur at other seasons due to large-scale atmospheric conditions [*Tyler and Barnes*, 2005], but clouds are not observed at those times, and it is unlikely that they contribute to the observed regularity of the trough features.

Katabatic winds act to increase sublimation from the surface in several ways. First, the downslope winds warm the local atmosphere due to adiabatic heating. Second, sensible heat is transferred into the NPLD surface [*Spiga et al.*, 2011]. *Spiga et al.* [2011] found that in normal conditions at L_s 60, as much as 15 W m^{-2} of energy were added to the surface – or approximately 6% of the total energy from insolation at summer solstice near the north pole (250 W m^{-2} at L_s 90) [*Laskar et al.*, 2002]. These are low estimates, given that local slope enhancements are too small to be resolved in the mesoscale model, and seasonal contrasts are not part of this study. Finally, moving, dry air has a direct effect on transfer coefficients of water vapor between the surface and the atmosphere.

4.3 Katabatic jumps

Lied [1964] and *Pettré and André* [1991] studied clouds in Antarctica that are similar in orientation and topographic setting to the trough clouds we find on the NPLD. The clouds were perpendicular to the katabatic flow and formed near changes in

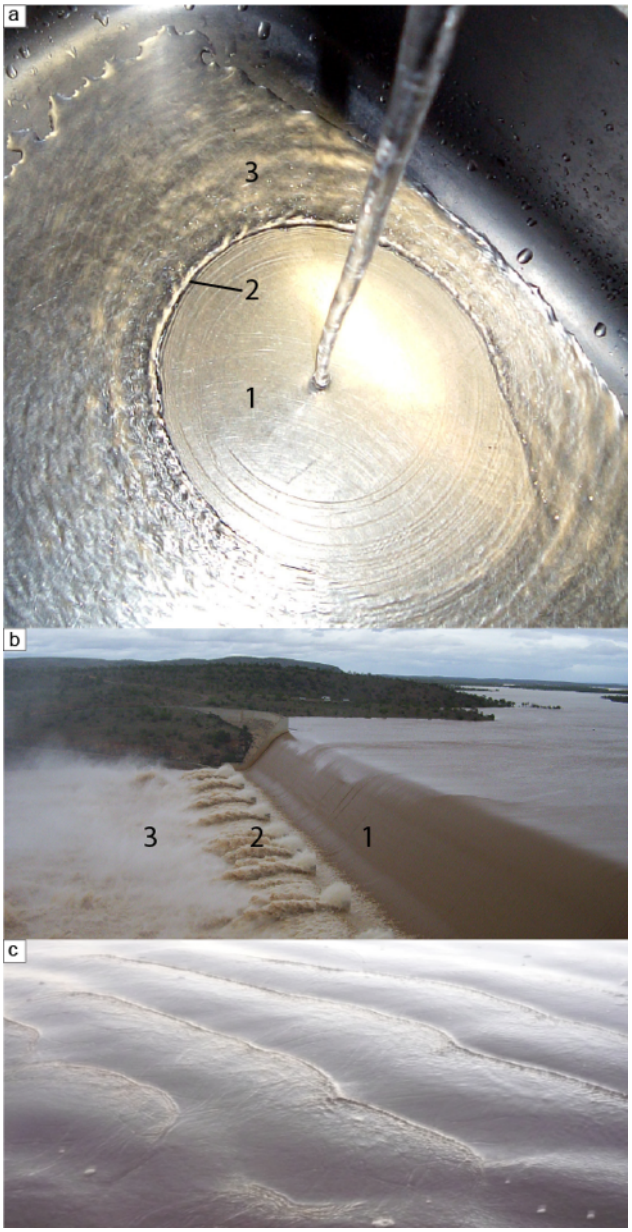

Figure 3.15 Terrestrial hydraulic jumps. *a) Hydraulic jump in a sink. Hydraulic jump forms even though there is no break in slope. b) Hydraulic jump beneath Burdekin Dam, Australia. Engineers design rivers below dams to reduce energy by slowing water in hydraulic jumps. 1) Fast-moving water leaves the source. 2) A hydraulic jump appears when the flow becomes unstable. 3) Water depth increases and water flow rates decreases downstream of the hydraulic jump. Image uploaded by Thuringowacityrep at en.wikipedia. Permission is granted to copy, distribute and/or modify this document under the terms of the GNU Free Documentation License Version 1.2. c) Series of repeating hydraulic jumps during return of wave on a beach. The cyclic step model uses repeating hydraulic jumps to explain the repetition of steps and the pattern of erosion and deposition. Photo taken by I.B.S. at Tan Tan Plage, Morocco.*

topography. The observed clouds appeared at a point the authors describe as a katabatic jump (Figure 3.13) and fall within the class of internal hydraulic jumps described by *Turner* [1979]. *Pettré and André* [1991] define a katabatic jump as "a narrow zone with large horizontal changes in wind speed, pressure, and temperature." While atmospheric flow speed and temperature decrease across a katabatic jump, pressure and flow thickness increase [*Lied* 1964]. *Pettré and André* [1991] observed velocities that decreased from ~20 ms^{-1} to ~5 ms^{-1} over a short distance and flow thicknesses that triple from 400 m to 1250 m.

We interpret the trough-parallel clouds in Figures 3.4c, 3.5b, 3.6a, 3.7a, 3.8, and 3.11 to be caused by katabatic jumps. The simplest model to derive first-order physical characteristics of katabatic jumps is based on an analogy with hydraulic jumps e.g. in rivers [*Ball*, 1956] (Figure 3.15). This is the model on which we base present discussions, but future work will involve high-resolution mesoscale modeling to refine our analysis.

In fluid dynamics, hydraulic jumps are defined as "discontinuous transitions from [Froude] supercritical to [Froude] subcritical flow in an open channel" [*Hager*, 1992]. Froude numbers (F_r) are mostly simply defined as the dimensionless ratio of fluid speed (U) to celerity (c), where celerity is the speed of propagation of a gravity wave in a fluid:

$$Fr = \frac{U}{c}$$

Equation 3.1

Supercritical flow has velocity greater than the celerity in a given fluid and is thus characterized by a Froude number >1. Subcritical flow moves slower than the celerity and has Froude number <1. Flows with Froude numbers >=1 do not transmit information upstream. In the case of two-phase flow, or a solid suspended in a fluid, the densimetric Froude number, Fr_d, is used. It is defined as:

$$Fr_d = \frac{U}{\sqrt{h \cdot g'}}$$

Equation 3.2

where h and g' are the flow thickness and reduced gravitational acceleration, respectively. In turn,

$$g' = \frac{g[(\rho_1 - \rho_2)\cdot C - (\rho_2 - \rho_3)\cdot (1 - C)]}{\rho_3} \qquad \text{Equation 3.3}$$

where ϱ_1 is the density of the sediment suspended in the flow, ϱ_2 the density of katabatic flow, ϱ_3 the ambient air in the absence of flow, and C is the volumetric concentration of sediment, expressed as m^3/m^3.

As for hydraulic jumps, the Froude number upstream of the katabatic jump is greater than 1, and the Froude number downstream is less than 1. Cloud morphologies in Figures 3.4c, 3.5b, and 3.6a allow for a more precise estimate of the high side Froude number. In those observations, the cloud has an undular or wavelike appearance. Several investigations have studied similar undulations in hydraulic jumps and found them associated with Froude numbers between 1.25 and 1.7 [*Andersen*, 1978; *Ohtsu et al*., 2001] . With Froude numbers < 1.25, the flow surface is smooth and unbroken, corresponding to a poorly defined undular jump. Froude numbers > 1.7 will exhibit sharp, well-defined jumps and become highly turbulent [*Ball*, 1957].

The majority of observed parallel troughs clouds, approximately 80%, do not have undular characteristics. This sets the lower bound of Froude number at 1.7 and leaves open the possibility of Froude numbers much higher. Froude numbers for winds above strong katabatic jumps on Earth have been measured, with values that range from 3.4 [*Pettré and André*, 1991] to 18 [*Ball*, 1957]. Froude numbers from our simulations reach ~5 (Equation 0 from *Pettré and André* [1991]); therefore we adopt $Fr_d = 5$ as an upper bound for katabatic flow on the NPLD, giving a range of 1.7 to 5. Froude numbers

between ~1 and 1.7 are also possible, but we observe conditions indicating such values relatively infrequently and treat them as special cases.

4.4 Flow depths

We interpret the transverse linear streaks visible in Figure 3.7 (and Figure 1.4) to be rolls (i.e., horizontal vortices) that align with the wind direction. Rolls occurring in natural systems have a ratio of separation to flow depth of ~1:2 [*Fedele and García*, 2009], allowing for a rough estimate of wind depth. Applying this rule to rolls separated by 300 - 500 m, we estimate a flow depth of 150 to 250 m and adopt 200 m for reference. Rolls are rarely observed, but there is no other method for obtaining flow depth by direct observation, so we rely on this estimate (and results from atmospheric modeling in calculations presented below).

Linear rolls may be used to estimate the flow depth of the incoming wind, but no measurements, either direct or indirect, are yet possible for the height of a katabatic jump on Mars. Instead, in this frame of our simplified hydraulic jump model, we rely on the Bélanger conjugate depth equation (Equation 3.4, Equation 9 *Pettré and André* [1991]), which specifies the ratio of thickness of flow post-hydraulic jump to that of the incoming flow [*Hager*, 1992; *Hand*, 1974]. That is,

$$\frac{h_2}{h_1} = \frac{\sqrt{1+8Fr_1^2}-1}{2}$$

Equation 3.4

where h_2 is the flow depth post-hydraulic jump, and h_1 and Fr_1 are the pre-jump flow depth and Froude number, respectively.

Applying the 1.7 to 5 range of Froude numbers and incoming flow depths of 200 m, the post-hydraulic jump depth is estimated to range from 400 m to 1300 m. This represents a flow depth ratio from post to pre-jump of ~2 – 6.5. Our simulations of the katabatic wind depths are consistent with these estimates.

4.5 Duration and frequency of clouds

Figure 3.6a displays trough clouds over at least six troughs, spanning an area of ~300 by 200 km, the largest area imaged with multiple trough clouds (all THEMIS observations cover a smaller area). The discovery of contemporaneous trough clouds in extended images suggests that a combination of specific large-scale, mesoscale, and local meteorological phenomena allows for their formation. Similar to findings from terrestrial studies [*Pettré et al*., 1993], we conclude that the duration of trough clouds can be several hours (and perhaps in exceptional conditions, several days) because slow, large-scale atmospheric processes play an important role. Meteorological modeling indeed shows that regional katabatic winds can be enhanced by large-scale weather systems such as baroclinic waves, planetary waves, and transients [*Tyler and Barnes*, 2005], which may explain the seasonality of katabatic jumps and trough cloud observations.

Direct comparison between multiple images of the same location is difficult due to lighting and other conditions, but detection of clouds is less ambiguous than other observations such as albedo or topography. In fact, the temporary nature of clouds makes their absence much easier to detect (Figures 3.5, 3.6, and 3.8). By examining sequential images over neighboring sites, we determine that typical clouds are often visible for 10 to

20 hours. One event in Mars Year 29 is observed in every image north of 86° for nearly 20 Martian Sols (Figure 3.8). While duration and intensity vary considerably, we adopt 10 hours to conservatively represent the duration of a standard event for future sections.

The frequency of storms may only be determined by examining a time series of images taken at the same location. This is difficult because observations of the same location are not often repeated on a short time scale; however, overlapping or adjacent images can be sufficient for making an estimate. In general, locations closer to the pole experience more events, while those between troughs, at lower elevations, or in low-slope regions will experience fewer. We find that at any given trough several events may be observed in one Mars year, but zero maybe be observed in another year. We therefore estimate, in an attempt to be conservative, that most troughs experience one trough cloud per year.

Making observations from orbit, especially of events that are short lived, can be expected to result in incomplete surveys. Until observations from the ground are possible, estimates of frequency will be based on few data points and sparse coverage. Additionally, sampling in this survey only spans 5 Mars years, leaving open the possibility that these were anomalous. Given the limitations and understanding that variations based on latitude are likely, we feel confident in estimating approximately one event of ~10 hours occurs at a typical site on the NPLD per year.

5 DISCUSSION AND CYCLIC STEP FRAMEWORK

5.1 Cyclic steps

Cyclic steps are described as "a train of upstream-migrating bed undulations bounded by hydraulic jumps" (Figure 3.15c) [*Kostic et al*., 2010; *Parker*, 1996]. Although not so named, they were first recognized as a distinct bedform by *Winterwerp et al*. [1992]. Fundamentally, cyclic steps are bedforms that exist due to the erosion, transport, and redeposition of sediment. Unlike dunes, where material is removed from the stoss slope and re-deposited on the lee, aeolian cyclic steps behave in the opposite manner. Nevertheless, the same properties exist in each: erosion occurs as accelerating winds pick up material, and deposition occurs at sites of decelerating winds. For example, katabatic jumps represent the point of sudden deceleration for winds at the bottom of troughs.

Cyclic steps are considered permanent, long-wave features, distinguishing them from their short-lived counterpart, antidunes. Antidunes are a train of smoothly rounded bedforms [*Hand*, 1974; *Hand et al*., 1972] that tend to be unstable and short lived [*Kostic et al*., 2010]. In cyclic steps, hydraulic jumps separate the fast moving, Froude-supercritical flow (red in Figure 3.16) from relatively slow moving Froude-subcritical

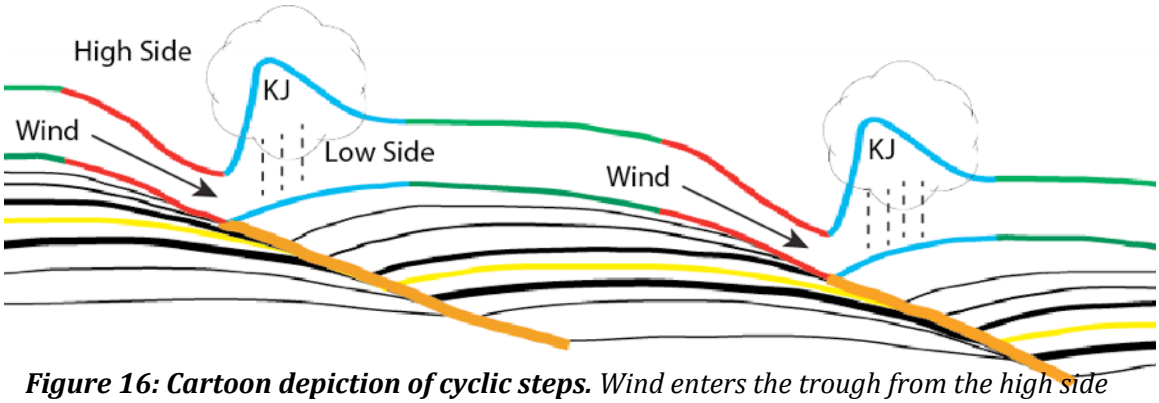

Figure 16: Cartoon depiction of cyclic steps. *Wind enters the trough from the high side and accelerates downhill. Red indicates sublimation enhanced by wind. Flow depth increases quickly at site of katabatic jump, and deposition beneath a cloud as snow or frost begins (blue). Green indicated subcritical flow and no change in elevation. Yellow depicts one stratigraphic level in the section. Exposed layers on the high side (red) and mantling associated with deposition (blue) depict asymmetric accumulation as cause of migration.*

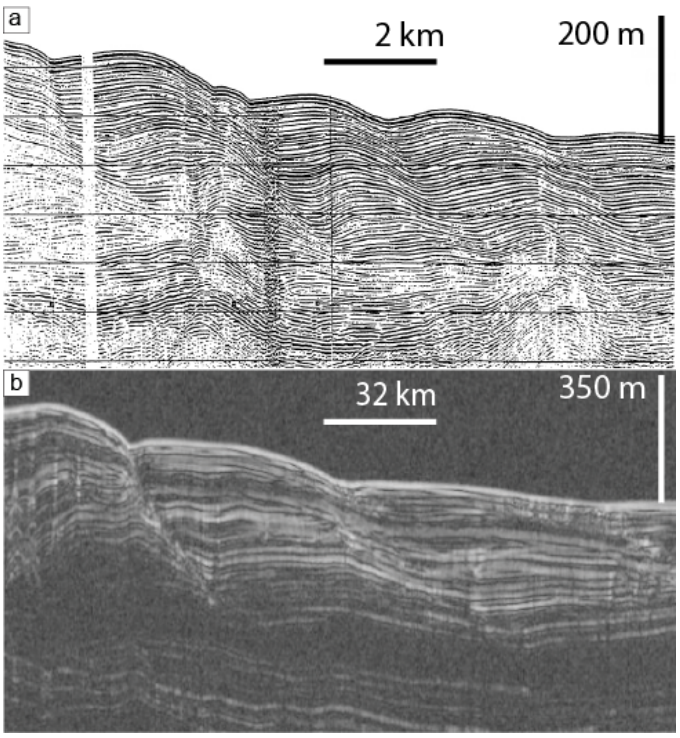

Figure 3.17: Stratigraphy of depositional cyclic steps. *a) Seismic image of sediment waves near continental slope at Var sedimentary ridge northwest of Italy [reproduced with permission from Migeon et al., 2000]. Layers are truncated in only a few spots, but upslope migration is clearly evident. Layer thickness variations are also readily apparent. b) Portion of SHARAD radargram 598301 near spiral troughs on the NPLD. Displayed stratigraphy has similar patterns to submarine sediment waves in a). The trough on the left has a well-delineated trough migration path, but the trough on the right looks more like a sediment wave. Different sublimation rates (possibly due to different wind speeds) on the high side may account for the contrast in stratigraphy. Location indicated in Figure 3.1a.*

flow (green in Figure 3.16) [*Kostic et al*., 2010]. At the hydraulic jump the flow rapidly decelerates upon encountering the adverse slope (blue in Figure 3.16). The process repeats upon entering another step.

2-D cyclic step models have been validated for terrestrial systems in flume experiments [*Spinewine et al*., 2009; *Taki and Parker*, 2005] and in numerical models [*Kostic and Parker*, 2006; *Sun and Parker*, 2005]. These steps can form under net erosional conditions [*Parker and Izumi*, 2000], net depositional conditions [*Kostic and Parker*, 2006] and conditions that are in equilibrium when averaged over the steps [Taki and Parker, 2005].

Terrestrial features attributed to hydraulic jumps and having similar stratigraphic and accumulation patterns to the spiral troughs are found in Antarctic ice [*Fahnestock et al*., 2000; *Frezzotti et al*., 2002; *Swithinbank et al*., 1988], subaerial streams (Figure 3.15c) [*Kostic et al*., 2010], and submarine sediments (Figure 3.17) [*Lee et al*., 2002;

Nakajima et al., 1998; *Normark et al*., 1980]. Features in submarine systems are called sediment waves and have been studied in detail [*Lee et al*., 2002; *Migeon et al*., 2000] (Figure 3.17a). They are classified as a subcategory of cyclic steps that exist in a depositional regime [*Kostic et al*., 2010]. Sediment waves have smaller amplitudes (by a factor of ~100) and wavelengths (by a factor of ~10) than the spiral troughs, but the topographic and stratigraphic similarities are striking (Figure 3.17) [*Frezzotti et al*., 2002; Smith and Holt, 2010]. In ice, features called megadunes also resemble the spiral troughs, and their origin has been linked to katabatic winds, but detailed studies of their formation have not yet been undertaken.

Models applied to net-depositional systems for sediment waves reproduce stacked morphologies and topographic patterns [*Fildani et al*., 2006] that are qualitatively similar to those observed in SHARAD data beneath the spiral troughs on the NPLD (Figures 3.2, 3.17). Sediment waves form when higher-density, sediment-laden water flows beneath the ambient fluid of normal density [*Kuenen*, 1951; *Mohrig and Marr*, 2003]. These flows, called turbidity currents, carry excess weight of sediment and accelerate downhill due to higher density, depositing the sediment at hydraulic jumps [*Parker et al*., 1996; Kostic et al., 2010]. In the Martian case, dense air, rather than water, flows directly over the surface as a katabatic wind, analogous to turbidity currents [*Zammett and Fowler*, 2007].

Erosional cyclic steps behave differently from their depositional counterpart. On Earth, they are most often observed as chute-pool morphologies or considered to be "discontinuous gullies" [*Reid*, 1989]. Even though they are exposed to supercritical flow, they evolve into a series of steps that migrate slowly upstream, and are bounded by hydraulic jumps, no sediment is deposited to leave a stratigraphic record. Only a morphology of evenly spaced, periodic headcuts (in two dimensions) will be exhibited

[*Parker and Izumi,* 2000]. Stratigraphy associated with erosional steps will not exhibit asymmetric accumulation or offset layering as seen in depositional systems.

Unlike in the depositional case where sediment is deposited at the hydraulic jump, suspended sediment remains in the flow to be carried past the system in the erosional case. The eroded material can be assumed to remain suspended load that is not redeposited after the hydraulic jump [*Kostic et al*., 2010]. As with the depositional cyclic steps, flume experiments [*Brooks*, 2001] and numerical models [*Parker and Izumi*, 2000] have verified these results for erosional steps in terrestrial environments. Because the flow characteristics are so similar, sediment supply is the primary difference between depositional and erosional cyclic steps.

5.2 Trough formation and Coriolis forcing

The NPLD spiral troughs are primarily constructional features as evidenced by the radar stratigraphy [*Smith and Holt,* 2010]. We suggest that the same processes observed today were operating when the troughs formed. In particular, katabatic winds, jumps, and trough clouds existed at the time of onset. Prior to trough formation, NPLD topography was smoother than today [*Smith and Holt,* 2010; in prep]. In flume experiments, cyclic steps and hydraulic jumps have been created on a smooth surface (Figure 5 from *Spinewine et al*. [2009]), much as the NPLD troughs may have began.

A katabatic jump forms as a condition dictated by flow constraints, in particular topography or atmospheric pressure. We propose that the effects of this jump are sufficient to make trough clouds, which in turn precipitate as snow or directly deposit the water vapor to the surface. Clouds typically form when either pressure increases or temperature decreases. *Lied* [1964] observed both of these qualities as he crossed the

katabatic jump. Walking through the jump from downstream, he measured "a sudden drop in pressure and immediate rise in temperature." If the incoming winds are saturated or nearly saturated with water vapor, clouds will form as the pressure increases and temperature drops coming into the jump.

Lied [1964] and *Pettré and Andre* [1991] detected a "wall of snow" at the site of a katabatic jump (Figure 3.13). If this snow reaches the surface, deposition occurs. This deposition of ice will eventually modify the topography to form a slope break that acts as a trigger for future katabatic jumps [*Spinewine et al*., 2009]. Thus a topographic feedback mechanism exists to steepen topography. Once this feedback exists, the relatively quick onset and persistence of trough stratigraphy observed by radar [*Smith and Holt*, 2010] can be explained.

Howard [2000] mapped the directions of wind streaks on the NPLD to determine wind vectors and found that the streaks align roughly perpendicular to the troughs. He concluded that topography is presently the primary influence on katabatic wind directions, with the Coriolis force exerting a secondary influence. This finding is in general agreement with our mesoscale modeling (Figure 3.14d). However, before the troughs formed, the NPLD was smoother [*Smith and Holt*, 2010]. At this time local topographic control would be less significant, allowing the Coriolis force to be the primary influence on direction. Thus, during trough onset, katabatic jumps, which are themselves nearly perpendicular to the winds, would have a spiral pattern determined by Coriolis deflection of downhill flow.

Smith and Holt [2010] observed that the NPLD spiral troughs are not all the same age, having formed on the NPLD at least twice. Surface age dates of the SPLD determined by crater counting statistics indicate that the troughs in the southern hemisphere are significantly older than even the oldest portion of the NPLD [*Herkenhoff*

and Plaut, 2000]. This observation implies that conditions were favorable for spiral troughs to form during multiple periods in Mars' past. However, there is no evidence supporting the existence of troughs at the earliest stages of either pole. We propose two mechanisms to explain this.

First, as with sediment waves and megadunes, the regional slope of the NPLD at the time of trough onset is a critical factor [*Fahnestock et al*., 2000; *Smith and Holt*, 2010]. Winds that flow down very shallow slopes will not become supercritical, precluding both katabatic jumps and significant wind induced sublimation. Atmospheric changes could also contribute to the necessary conditions for trough formation. A recent study found large volumes of CO_2 ice that were rapidly deposited and sequestered in the SPLD within the last several hundred thousand years [*Phillips et al*., 2011]. Prior to sequestration, the CO_2 ice was most likely in the atmosphere, suggesting that the atmosphere and wind intensities could change during the lifetime of troughs.

5.3 Exposures on trough walls, asymmetric accumulation, and layer offset

The contrast of the layer exposures and albedo on opposite trough walls can be directly attributed to cyclic step migration and katabatic jumps. As winds remove material from the trough high side, layers with high concentrations of dust are exposed [*Massé et al*., 2012]. *Masse et al*., [2012] found that greater than 80% ice is on the surface exterior to the trough, but the trough high side had as little 20% ice exposed beneath significant quantities of accumulated dust. Dust has a lower albedo than ice, so the combination of exposing dust and removing ice will decrease the overall albedo of the high side. Ice is removed in one of two ways, either sublimation or mechanical transport,

but dust is nonvolatile and only removed by mechanical transport during high intensity wind seasons.

On the opposite side of a trough, banded terrain overlies inter-trough material. The combination of intermediate albedo and irregular mantling associated with banded terrain is explained by the recent deposition of ice and dust that has been transported from upstream. The intermediate albedo of banded terrain is then the result of strong mixing between ice and dust, which will produce an albedo between that of the constituents.

Banded terrain is highly variable in albedo and location (Figure 3.1b). *Pettré and Andre* [1991] observed that katabatic jumps can move, or migrate during a single storm and that they often have a different location during subsequent storms. They determined that the location of a katabatic jump is based on the incoming flow properties. Therefore, the multiple bands observed at many troughs (Figure 3.1b) may be the result of variable katabatic jump locations (Figure 3.8).

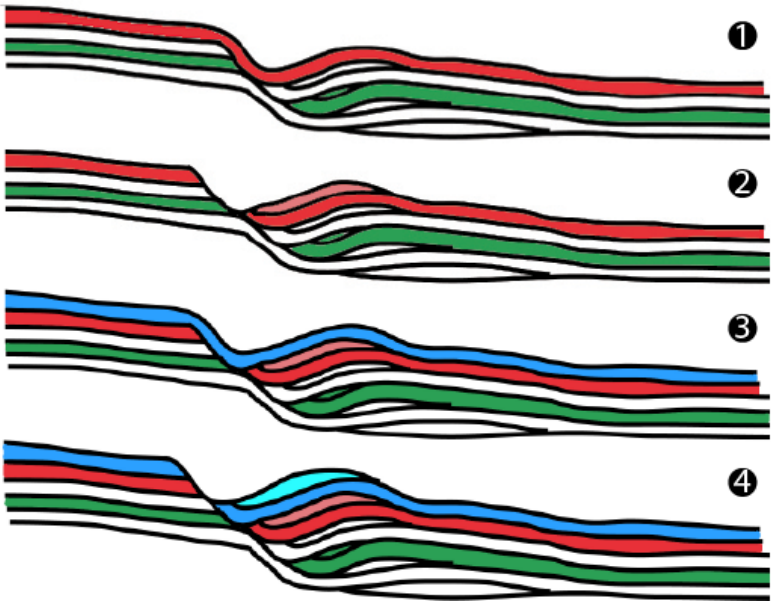

Figure 18: Cartoon of trough evolution. *(1) A layer is deposited uniformly in winter (red). (2) Subsequent winds transport material from high side to low side of trough. High side is thinned as low side is thickened. (3) and (4) repeat (1) and (2). After many steps a discontinuity will form where new layers onlap the eroded layers.*

Two consequences of erosion and redeposition on the opposite trough walls are an asymmetric accumulation of ice and an offset of time-equivalent layers (Figure 3.18). *Howard,* [1982] predicted this asymmetry and offset with optical observations, and *Smith and Holt*, [2010] confirmed it with radar observations. We propose that an alternating sequence of uniform deposition and transport created the stratigraphy that is observed. Deposition occurs in the winter, when temperatures are low and a seasonal frost covers the surface. Winter deposition would act as a blanket that covers troughs entirely (Figure 3.18b1 and 3.18b3). This is observed as a seasonal cap. Later, in spring, katabatic winds and trough clouds are active. They act to thin the new deposit on the high side (Figure 3.18b2 and 3.18b4). Given sufficient transport, the original blanket of snow will become discontinuous and offset. Freshly exposed, older material on the high side is also ablated, resulting in migration but not thinning. Over repeated cycles of deposition and transport the topography becomes amplified until reaching a steady state, as discussed in Section 5.2.

There is another hypothesis that can potentially explain the observations of asymmetric accumulation. Cold trapping of volatiles is known to occur on Mars at high latitudes due to lower temperatures [*Calvin and Titus*, 2008; *Clifford et al*., 2000] and on craters that receive non-uniform sunlight [*Fishbaugh and Head*, 2000]. It is therefore plausible that the spiral troughs act as insolation-induced cold traps and that the low side deposits are primarily created by this mechanism, but two arguments counter that interpretation.

First, accumulation on the low side, as predicted by cold trapping, should be found near the point of lowest temperature, or where insolation is least. However, thickened deposits, as observed by SHARAD, extend well past the troughs and far into the inter-trough region (Figures 3.2 and 1.3). The second point is related to albedo.

Banded terrain has an intermediate albedo to dust and ice. Cold-trapped materials are purely volatile and should have the same albedo as ice. In a case of transport without wind, dust would remain on the high side, leaving a lag that covered layered terrain completely, and a pure ice deposit with high albedo at the cold-trap region. Both the observed extended deposits and intermediate albedo are inconsistent with the cold trapping hypothesis. We find that invoking winds to transport the dust but not the ice is unnecessarily complicated and implausible. Furthermore, cold trapping of volatiles would not account for high side thinning. A much simpler explanation exists with the cyclic step model, which accounts for erosion on the high side and deposition on the low side by providing a mechanism of removal (wind transport) and deposition (snowfall or direct deposition) beneath the trough clouds.

5.4 Slopes and wavelength

The high side slopes of troughs are uniformly steeper than those on the low side [*Howard*, 2000; *Pathare and Paige*, 2005]. As discussed above, differing processes affect each slope. Katabatic winds are fastest near the bottom of the trough, having had a longer distance to accelerate. *Ng and Zuber* [2006] found that in a katabatic wind regime "the lower part of each scarp sublimates faster than the upper part." This is a consequence of faster winds than can accommodate higher vapor pressures and transfer more energy into the surface. The combination of increased capacity and enhanced sublimation makes the removal of material more likely. The high side tends to increase steepness, in turn accelerating winds to greater speeds, creating a positive feedback. However, in the seasons with sunlight, the lowest section of the equator-facing slopes remains in shadow for longer periods than the highest sections. Thus, throughout a

Martian year, insolation-induced sublimation is greatest near the top of the trough wall, tending to reduce the slope by a small amount. Insolation and wind driven sublimation are therefore competing mechanisms, acting as a check to steepening from wind ablation.

On the low side of the trough there is no competing mechanism. Snowfall from the cloud is predominantly at the trough bottom, near the katabatic jump, but takes some time to settle out. With weak low-side winds, the remaining snow will deposit downstream of the trough, thinning with increasing distance. This is substantiated by radar observations, which show the deposit to be thickest near the trough bottom and decrease with distance towards the low side (Figures 3.2 and 1.3) [*Smith and Holt*, 2010].

Spiral troughs in different regions have different wavelengths. This is best demonstrated by the contrast between troughs just north of Chasma Boreale (~0° E) with characteristic wavelength 40-50 km and those near the margin at 90° E with wavelengths of 20 to 30 km. Atmospheric modeling and flume experiments demonstrate that flows require some distance to accelerate and reach a supercritical state. That distance determines the position of the initial step. Given sufficient space to accelerate after a katabatic jump, the winds will form another, setting up a characteristic wavelength that continues until the regional slope changes or the edge of the ice cap is reached.

The relationship between regional slope (the slope on which cyclic steps form) and wavelength is well understood [*Sun and Parker,* 2005] and testable in flume experiments [*Yokokawa et al*., 2009]. Steeper regional slopes favor shorter wavelengths. Therefore the troughs north of Chasma Boreale, which began on a shallower regional slope than those at 90° E, should have a longer wavelength. *Smith and Holt* [in prep] detect this wavelength / slope correlation. They find that troughs north of Chasma Boreale have the longest wavelength on the NPLD. These troughs formed on a surface with average regional slope 0.19°. East of that, near the margin at 90°E, the troughs

formed on a surface with average slope 0.32°. The troughs between 180° and 270°E have a more variable but intermediate wavelength to the other two regions and are spaced between 30 and 40 km apart. Those troughs formed on a surface with average slope ~0.27°

5.5 Migration of spiral troughs

Howard et al. [1982] were the first to suggest that winds were an important component in trough migration and provided predictions of 3D stratigraphy that proved to be highly accurate. They described migration as the removal of material from the high side of a trough, as evidenced by wind streaks, and re-deposition of the material on the low side. Howard and colleagues were fundamentally correct in their interpretation, but did not have observations with high enough spatial or temporal resolution to observe active transport via winds. New, higher-resolution observations reveal that katabatic jumps provide the mechanism for alternating between accelerating and decelerating flow, or ablation and deposition.

By analyzing SHARAD radar, *Smith and Holt* [2010] supported the conclusions of *Howard et al*. [1982] and demonstrated that the oldest of the NPLD troughs have undergone as much as 700 m of deposition since their formation and have migrated ~50 km during that period. *Smith and Holt* [2010] isolated a bounding surface that traced the path of migration through time for many troughs on the NPLD. The bounding surface varies in steepness, indicating variability in the ratio of accumulation to migration. We interpret this to mean that there is no short-term steady state for migration. Instead, it is likely that the NPLD troughs have undergone alternating regimes of net deposition and

ablation throughout their history, with the long-term trend resulting in pronounced accumulation and migration.

Not every trough on the NPLD behaves the same, however. Besides temporal variations, regional and local conditions affect each trough [*Smith and Holt,* in prep]. Evidence for in-situ trough ablation at one trough near 250° E suggests that some locations have experienced incision in the past [*Rodriguez and Tanaka*, 2011]. *Smith and Holt* [in prep] find that this trough currently experiences migration, but former conditions may have been similar to those on the SPLD, where erosional cyclic steps are more prominent.

Overall, the SPLD troughs appear to behave differently than those on the NPLD. A test of the cyclic step model is to explain this discrepancy. Stratigraphic analysis from visible imagery suggests that a majority of troughs in the south formed during a period of ablation [*Kolb and Tanaka*, 2001], leaving no evidence for migration. Analysis of SHARAD radar images mostly agrees with that conclusion but finds a few locations exhibiting bounding surfaces and trough migration [supplementary section in *Smith and Holt*, 2010], adding to the puzzle. Thus, the majority of evidence supports the conclusion that at least some of the SPLD spiral troughs formed as erosional cyclic steps.

Parker and Izumi [2000] explain that in erosional regimes sediment entering the hydraulic jump bypasses the step rather than being deposited. The NPLD and SPLD undergo the same processes in this scenario, but the incoming sediment (water vapor) supply determines if the low side of a trough will experience accumulation (i.e. there is no deposition because ice crystals within clouds are not sufficiently large to reach the ground, therefore bypassing the katabatic jump.) Different dust concentration, temperatures, and pressures on the SPLD potentially explain this difference.

As with the north, the SPLD scenario is not uniform across the cap. At lower elevations on the SPLD, scalloped terrain exhibits a radar signature of asymmetric accumulation similar to the northern spiral troughs [*Grima et al*., 2011]. In addition, clouds associated with katabatic jumps are found in the scalloped terrain (Figure 3.11b), suggesting the likelihood of re-deposition of ice and migration.

Trough clouds are also observed at higher latitudes/elevations on the SPLD (Figure 3.11a), with the possibility of re-deposition. An explanation for the discrepancy between interpreted stratigraphy and the implications with observed clouds is not readably available, but it is possible that regional and temporal differences, like those on the NPLD, contribute to the variations observed on the SPLD.

5.6 Undulations

Various hypotheses have attempted to explain the origin of topographic undulations (Figure 3.3): viscous relaxation of troughs [*Pathare and Paige*, 2005], remnants of trough migration [*Squyres*, 1979], and the result of ice cap advance and retreat [*Cutts et al*., 1979]. The hypothesis that most closely approximates findings in this paper is one of standing waves emanating from the troughs [*Howard*, 2000]. While it is clear that undulations must be explained in the context of katabatic winds, cyclic step literature does not describe topographic undulations or hydraulic undular jumps.

We agree in principle with the explanation of *Howard* [2000]. Observations presented in earlier sections demonstrate that some trough clouds have undular characteristics (Figures 3.4c, 3.5b, 3.6a, 3.8, and 3.11b). Frequently, the wavelengths and locations of these undular jumps match those of topographic undulations. Thus it is plausible that undular jumps and clouds act as standing waves to deposit and create

undular topography. While the cyclic step model doest not directly predict the existence of topographic undulations downstream of troughs, the flow regime and undular clouds are consistent with depositional processes required to maintain the undulations.

5.7 Comparison of cyclic steps with previous models

The debate surrounding spiral troughs is primarily due to their complex structure and many unique features. In the previous sections we discussed ten observations that are integral to understanding trough evolution. Therefore, we propose a list of ten criteria that any trough formation and evolution hypothesis should address: 1) trough initiation; 2) large-scale spirals that have opposite sense in the northern and southern hemispheres (Figure 3.1) [*Cutts*, 1973]; 3) ablation of the equator-facing walls, exposing low-albedo layers [*Warner and Farmer* 2008]; 4) mantling deposits with intermediate albedo on the poleward slopes [*Howard et al*., 1982]; 5) offset layering as detected by SHARAD [*Smith and Holt*, 2010]; 6) asymmetric accumulation of ice across the troughs (Figure 3.2) [*Smith and Holt*, 2010]; 7) equator facing slopes that are uniformly steeper than pole-facing slopes [*Pathare and Paige*, 2005]; 8) different trough wavelengths occurring in different regions [*Pathare and Paige*, 2005]; 9) migration of the NPLD troughs as revealed by SHARAD [*Smith and Holt*, 2010], 10) purported lack of trough migration on the SPLD [*Kolb and Tanaka*, 2001]. Additionally, two other observations, indirectly related to the troughs should be explained: the troughs formed after 1/2 - 2/3 of the NPLD were deposited [*Smith and Holt*, 2010; in prep]; and the relationship of low-amplitude undulations to the spiral troughs. While many of the previous models provided mechanisms of formation or even predicted migration, they do not offer the same robustness in matching all of the criteria as the cyclic step model. Primarily, most models

of trough formation cannot account for evidence of asymmetric accumulation or offset layering, and the simplest models can only meet two or three of the criteria.

Ivanov and Muhleman, [2000] used albedo contrasts to explain trough formation due to sublimation. They found that trough walls with low albedo should sublime faster than the surrounding inter-trough regions. While this is most certainly true, it only accounts for formation and ablation of the equator-facing walls. Their model did predict slope asymmetries, although they were underestimated. They could not explain spirals or the onset of troughs midway through NPLD development. In this way they met criteria 1, 3, 7, and 10.

Another hypothesis proposed that lateral heat diffusion was the mechanism by which troughs formed [*Pelletier*, 2004]. This model predicted a spiral pattern for the troughs but was unsuccessful in explaining why the NPLD troughs would have opposing sense from the SPLD troughs. Related to stratigraphy, only the exposure of layers on the high side could be explained. Criteria 1 and 3 and part of criterion 2 were met in this model.

In situ erosion from wind was another proposed model for formation [*Kolb and Tanaka,* 2001; *Rodriguez and Tanaka*, 2011]. These models could employ the Coriolis force to explain the spirals, and winds could remove ice to form the troughs, but the resulting stratigraphy did not match NPLD troughs (Figure 1.3a). *Smith and Holt* [2010] discussed the stratigraphy observed with SHARAD and found it completely incompatible with in situ erosion, which only accommodates criteria 1, 2, 3, and 10. It cannot explain the wavelength differences between regions, asymmetric accumulation, or migration of the NPLD troughs.

Some models did not have formation mechanisms but were more successful at predicting the stratigraphy [*Squyres*, 1979]. *Squyres* [1979] used the observations of

exposed layered terrain on the high side and no exposures on the low side to predict a stratigraphy that was the result of migration. While this model included migration and ablation of the high side, it did not provide a formation mechanism or explain the spirals. Neither could this model explain thickened deposits on the low side of troughs (Figure 10 of that paper) as detected by SHARAD (Figures 13e and 1.3f). Alone, only Criteria 3, 5, and 9 were met. In combination with the formation mechanisms of *Ivanov and Muhleman*, [2000] or [*Pelletier*, 2004] criteria 1 or 2 could be added. As a caveat, there is significant variation in NPLD trough stratigraphy, and some troughs do have reduced asymmetry [Smith and Holt, in prep]. While this supports the model of *Squyres* [1979] and the conclusion that the troughs undergo variable amounts of migration due to wind and insolation, these examples do not represent the entire family of troughs.

Other models based on flowing ice predicted that given enough stress (and Coriolis forcing) the ice would fracture [*Weijermars*, 1986; *Zeng et al*., 2008]. These models offered a formation mechanism and proposed a method by which the troughs would spiral. Heuristically, these models may also account for the exposed layers on the high side and offset of layering observed. However, neither banded terrain nor asymmetric accumulation are explained. Also, these models relied on basal sliding and could not explain why the "fractures" would only extend part way through the ice. Only Criteria 1, 2, 3, 5, and 10 are met.

Ng and Zuber [2006] expounded on the *Squyres* [1979] model and offered several benefits over previous ideas. They explained that the spiral pattern was the result of Coriolis directed winds and gave a plausible mechanism of formation. They argued that winds were important for bringing in low albedo dust and depositing it in a spiral pattern. Once the dust was on the surface, preferential sublimation would occur where the albedo had been affected. Thus, spiral depressions would form due to sublimation on the

surface. Over time the depressions would become troughs. Their model combined the formation due to sublimation of *Ivanov and Muhleman*, [2000] with the migration due to sublimation of *Squyres* [1979]. Additionally, they loosely employed instabilities in the wind to explain the different wavelengths in different regions, and indirectly they could accommodate slope asymmetries. In this way they were able to create a scenario by which criteria 1, 2, 3, 5, 7, 8, and 9 were met. However, like *Squyres* [1979], they did not predict thickened low side deposits, nor could they account for intermediate albedo banded terrain or SPLD stationary troughs.

Thus the model of *Ng and Zuber* [2006] was very successful in explaining a majority of observations related to troughs. However *Ng and Zuber* [2006] had not observed their primary mechanism of formation: evidence of dust transport near the troughs. Detections of "dust storms" by *Warner and Farmer* [2008] might have provided that mechanism. *Warner and Farmer* [2008] interpret clouds near the troughs as removal of dust from the high side. *Warner and Farmer* [2008] likened this to the transport of material by winds. Their Figure 16 even had linear streaks near the high side to support their interpretation. They inferred the dust was being removed from the base of the equator-facing scarps and depositing it in the inter trough region. This would account for banded terrain on the low side. Unfortunately, the marriage of *Ng and Zuber's* [2006] model with *Warner and Farmer's* [2008] observations is not successful. The removal of dust from a trough is incompatible with dust being required to form a trough, and in this scenario, banded terrain would begin to form a second trough. To make this marriage successful, processes present today would have to be different from those that were present when the troughs formed.

Finally, we base many of our ten criteria on the observations of *Howard et al*., [1982], *Howard* [2000], and *Smith and Holt* [2010]. We believe that the stratigraphy they

observe is of critical importance in understanding trough evolution. Any model of formation that does not account for offset, asymmetric layering has not successfully described the troughs. The observations of *Howard et al*., [1982] and *Smith and Holt* [2010] demonstrated that the troughs were migrating as the result of transport from winds, but they had not yet explained the acceleration and deceleration associated with erosion and deposition. Furthermore, their hypothetical cross sections predicted the correct stratigraphy, but their processes were not sufficient to explain trough formation. It is only with the inclusion of repeating katabatic jumps in depositional (NPLD) or erosional (SPLD) regimes that criteria 1, 2, 3, 4, 5, 6, 7, 8, 9, and 10 can be met. Furthermore, undular jumps also offer an explanation for the undulations that are observed downstream from troughs. Finally, stratigraphic evidence for migrating troughs does not extend to the lowest portion of the polar layered deposits. A wind regime that changes periodically can account for the onset of troughs midway through NPLD development.

6 ESTIMATION OF RATES

6.1 Calculation of concentration and flux

Here we use two distinct methods to obtain the order of magnitude of flux of H_2O across the katabatic jump. These preliminary estimates will need to be refined in future work through either mesoscale meteorological modeling or high-resolution multispectral imagery.

The first method is to employ Froude analysis based on previous observations. Solving for the volumetric concentration of H_2O within the high side wind requires substituting Equation 3.3 into Equation 3.2 and reducing terms.

$$C = \frac{\frac{U^2 \cdot \rho_3}{Fr_d^{\,2} \cdot g \cdot h_1} - (\rho_2 - \rho_3)}{\rho_1 - \rho_3}$$

Equation 3.5

The H_2O concentration within the katabatic winds descending into a trough with parameters listed in Table 2 is ~$1x10^{-7}$ m^3/m^3 ($9x10^{-3}$ mol H_2O/mol air; we use both units for comparison in the rest of the paper). The calculated concentration represents the total amount of H_2O in the high side flow. This value is highly sensitive to specific inputs: for example, the ratio of velocity to densimetric Froude number is squared.

In terrestrial flows, deceleration is associated with deposition. Particles carried by air or water are often at the threshold of suspension. As the flow slows down it can no longer carry those particles, and they precipitate. We use this analogy to define the transition from net ablation to net deposition as the boundary of rapid deceleration, or the katabatic jump. Creating this boundary enables the estimate of H_2O concentration below the jump. Equation 3.6 calculates the flux, Φ, across this boundary [*Ball*, 1956].

$$\Phi = U_1 \cdot h_1 \cdot C_1 = U_2 \cdot h_2 \cdot C_2$$

Equation 3.6

Conservation requires that flux of particles entering the boundary must equal the flux of particles leaving it, ~$3.6x10^{-4}$ m^2s^{-1}mol/mol. Low side flow depth was estimated from Equation 3.4 to be ~1300 m. Using 4 ms^{-1}, a velocity consistent with estimates from

ρ1 (g/cm3)	ice	916
ρ2 (g/cm3)	laden air	0.0250
ρ3 (g/cm3)	ambient air	0.0247

	supercritical	subcritical
Fr	5	0.31
U	18	3
g	3.72	3.72
h	200	1318
C	9.8E-08	8.9E-08
Flux	3.5E-04	3.5E-04

	low estimate	high estimate
Fr1	1.7	5
Fr2	0.1	0.9
U	14	20
h1	150	250
h2	400	1300

Table 3.2: Values used as inputs into equations in this study. *Densities of laden air and ambient air are taken from Mars Climate Database web interface (c) LMD/OU/IAA/ESA/CNES [http://www-mars.lmd.jussieu.fr/mars/access.html]. Lower Froude numbers are estimated from the existence of undular clouds, and higher Froude numbers are estimated from the mesoscale atmospheric model. Flow velocities are taken from the atmospheric model. h_1 is estimated from Figure 3.7, and h_2 is from the Bélanger Equation. Concentration and Flux are calculated from Equations 3.5 and 3.6, respectively.*

Spiga et al. [2011] and Section 4 of this paper, the post-hydraulic jump concentration of water molecules is ~7×10^{-8} m^3/m^3 (5.5×10^{-3} mol/mol), ~0.7 times the value pre-jump.

As a first test to the cyclic step model, we apply the low-side calculated values to Equations 3.2 and 3.3 to determine the densimetric Froude number below the hydraulic jump. The result, ~0.45, is consistent with the range of published Froude numbers below terrestrial hydraulic jumps with two-phase flow [e.g. *Kostic et al*., 2010], supporting the framework for this estimation.

Our second method for estimating water ice concentration in a katabatic jump takes advantage of the fact that in many cases visible trough clouds are associated with this phenomenon. Since the clouds appear optically thick in THEMIS images (Figure 3.6), we assume that their optical depth is at least 1. From this we are able to obtain an

order of magnitude of the quantity of water ice within such a cloud (see formula in the caption of Figure 10 in *Spiga and Forget* [2009]).

We assume the size of ice particles is about 10 μm (a conservative estimate between the common size encountered in Martian water-ice clouds [*Madeleine et al.*, 2012] and the fast-falling ice particles detected by [*Whiteway et al.*, 2009]). We also assume that the extinction coefficient is ~2. The vertical extent of trough clouds is probably around 200 m given the depth of the katabatic layer. This yields a mass mixing ratio for water ice within the trough clouds of about $2x10^{-3}$ kg/kg or a volumetric mixing ratio of about $5x10^{-3}$ mol/mol and corresponds to a total mass of ice particles within trough clouds of ~7 precipitable microns (or ~$7x10^{-3}$ kg m^{-2}). The concentration calculated in this way provides a check for H_2O concentrations calculated by the first method. Not all of the ice will reach the ground, but only the flux of H_2O across the katabatic jump is required for further calculations.

Pathare and Paige [2005] found a conservative estimate of sublimation over the entire NPLD at 190 precipitable microns per year. This number is a cap-wide average and should be considerably higher over the low albedo spiral troughs than the inter-trough regions. Nevertheless, it is about 27 times what we find necessary for an optically thick cloud to form. Therefore, we find it reasonable that very powerful winds acting over a short time can contribute to the annual sublimation by a factor of 1/27 or ~4%. If sublimation estimates were available for the spiral troughs, the percentage would certainly go down.

It is important to note that the equations in this section are highly sensitive to input parameters. Our parameters were chosen to be conservative estimates, therefore choosing a cloud optical depth greater than 1, or a slightly higher velocity in Equation 3.5 (both possible scenarios) results in a much greater concentration of H_2O and thus a

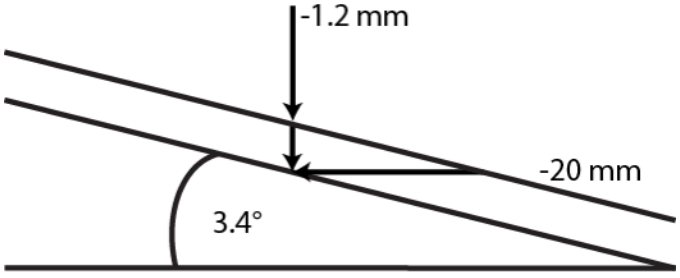

Figure 19: Cartoon depicting geometry of trough high-side erosion. *Conservative estimates of migration are one 10-hour wind event per year. During that time ~1.2 mm of ice is removed from the high side. On a slope of 3.4°, this equates to ~20 mm scarp retreat or migration per year. Faster winds or longer durations will increase the migration rate.*

greater flux of across the katabatic jump.

6.2 Migration and accumulation rates

In order to estimate the total amount of water mass that crosses a hydraulic jump, we multiply the flux with the duration derived earlier. 13 m^3/m of ice along a flow path is transported during a storm of 10 hours. Assuming a high side slope of length 11 km [*Pathare and Paige*, 2005] yields 1.2 mm of ablation along that slope (Figure 3.19). Over an area 25 km wide (approximate extent of trough cloud in Figure 3.5b), the volume of ice that passes through the hydraulic jump is: $3x10^5$ m^3. Assuming no porosity, the mass of that much ice is $3x10^8$ kg. These numbers seem quite large, but over an area of greater than 300 km^2 it represents only one mm of ablation, quite a small amount. HiRISE detects surface changes during the katabatic wind season (Figure 3.20). Noticeable in Figure 3.20 is a marked increase in surface texture on the trough high side. One millimeter of erosion should not be detectible with the 25 cm resolution of HiRISE. Thus we infer either that more than 1 mm of material is eroded, or enhanced surface texture reveals non-uniform ablation with some parts experiencing no erosion while others experience more, for an average of 1 mm.

The slope of the high side must be considered in order to estimate scarp retreat during any given storm. Using data from the Mars Orbiter Laser Altimeter (MOLA) [*Smith et al*., 2001], *Pathare and Paige* [2005] measured a range of high side slopes on

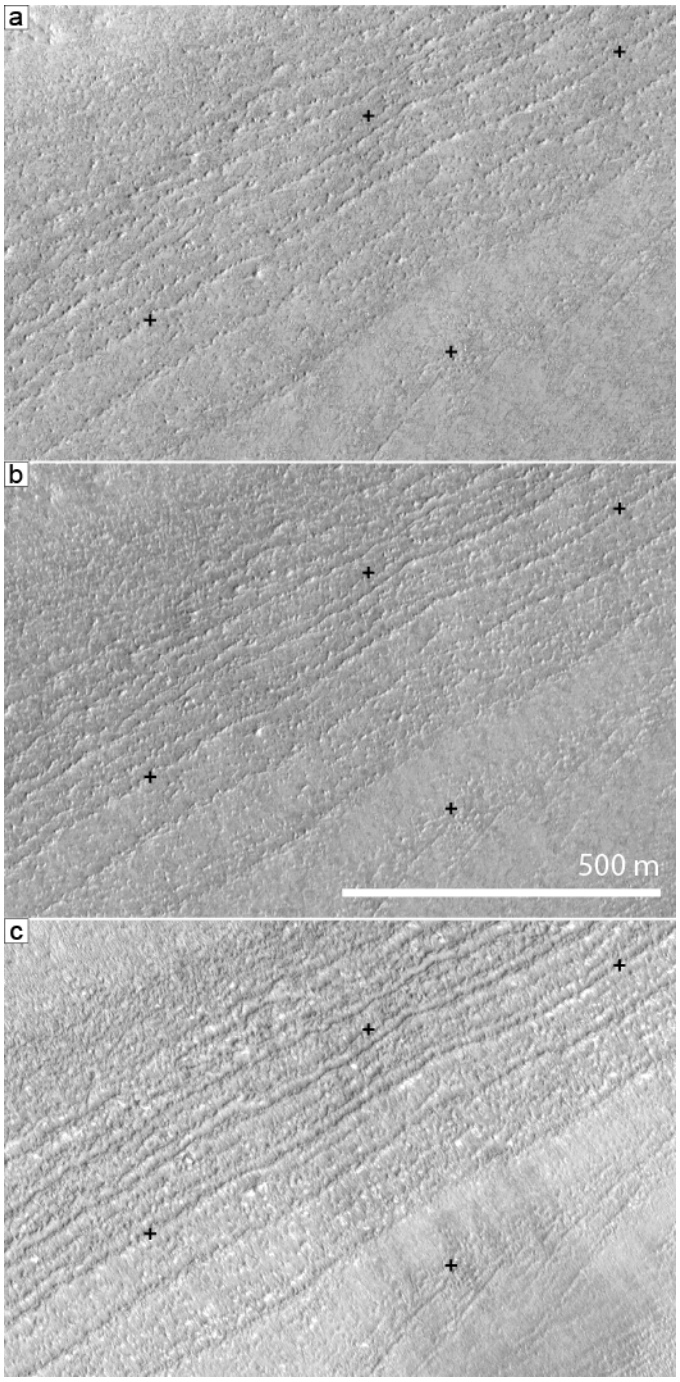

Figure 3.20: HiRISE images detect enhanced surface texture during katabatic wind season. *a) ESP_027056_2670 taken during Mars Year 31 at L_s 48, prior to katabatic wind season. Surface has subdued texture, and no wind streaks are present. b) ESP_026054_2670 taken during Mars Year 31 at L_s 71, before peak of katabatic wind season. Little change is observed from earlier image. c) ESP_025368_2670 taken during Mars Year 31 at L_s 105, soon after katabatic wind season. Trough high side slope has visible wind streaks and enhanced surface texture, consistent with the removal of a mantling surface layer. All images were taken at the same emission angle to reduce parallax. Location indicated by star in Figure 3.1a.*

interior troughs between 2.0° and 14.5°. The slopes for their H2 and H3 troughs (shown in Figure 3.6c) are 3.1, and 3.4° respectively. Adopting 3.4°, and assuming the entire 11 km slope eroded uniformly, the high side slope retreats 20 mm (Figure 3.19). Since we assume only one ten-hour jump event per year as determined in Section 4.4, we find an annual migration rate for polar troughs of about 20 mm per year.

Smith and Holt [2010] used SHARAD reflectors to measure ~50 km of horizontal trough migration at the H2 and H3 troughs of Pathare and Paige [2005]. The time

required to migrate 50 km at 20 mm per year is ~2.5×10^6 Mars or ~4.7×10^6 Earth years. Hence the age of the spiral troughs determined by this analysis is greater than the estimated age of the NPLD, ~4×10^6 Earth years [*Levrard et al*., 2007]. Based on ice accumulation rates and depth of initiation, the troughs were estimated to have formed between 5×10^5 and 2.5×10^6 Earth years ago [*Smith and Holt*, 2010], a factor between 2 and 10 younger than our estimate.

Our calculations are made in the context of the cyclic step model: we made the implicit assumption that trough migration is due entirely to katabatic wind transport and ignored other processes. Previous studies have determined that in addition to winds, insolation would remove ice from the high side slope [*Howard*, 2000]. Hence high side migration will be supplemented during the summer season, when temperatures are warmer. Our constraints in this study are not precise enough to determine exactly how much migration is due to wind or sun, yet our estimates tend to show that wind transport played a major role in the history of migration of polar troughs.

Nevertheless, there are factors in our calculations that can greatly modify the migration rate (and thus age of the troughs) in order to find younger ages. The best constraints available from radar, imagery, and atmospheric models have been used for these analyses, but the chosen inputs may be altered within the modeled and observed limits. For example, if we assume 2 katabatic jump events per year instead of 1, we obtain an age consistent with previous estimates. Likewise, another factor requires only a slight adjustment; changing the wind speed in Equation 3.5 from 18 to 20 m/s more than doubles the H_2O concentration, resulting in a trough age of 2×10^6 Earth Years.

Finally, if we apply the ratio of migration to accumulation as determined by *Smith and Holt* [2010] to our wind-only model, we find that between 0.22 and .28 mm of ice per Mars year (or .12 - .15 mm per Earth Year) accumulated since the troughs initiated. This

number is lower than published accumulation estimates of between 0.28 and 1.2 mm/yr [*Fishbaugh and Hvidberg*, 2006b; *Herkenhoff and Plaut*, 2000] but is within a factor of 2 to the lower estimate, reconcilable with a slightly higher migration rate.

7 CONCLUSIONS

Any hypothesis that attempts to describe the formation and evolution of spiral troughs of the Martian polar layered deposits must be able to explain all of the available observations related to their morphology and stratigraphy. To date, no model has successfully accounted for all of the trough features. The cyclic step model is especially compelling because a katabatic jump explains all atmospheric and stratigraphic observations of a single trough, and repeating katabatic jumps deflected by the Coriolis force account for the gross spacing and orientation of the troughs. This model is also supported by observations of active processes and meteorological modeling.

The cyclic step model outlined by *Parker* [1996], provides the foundation for explaining all ten of the following criteria: 1) formation mechanism; 2) large-scale spirals that have opposite sense in opposite hemispheres [*Cutts,* 1973]; 3) ablation of the equator facing walls exposing low-albedo layered terrain [Warner and Farmer 2008]; 4) irregular mantling of "banded terrain" material, with intermediate albedo on pole facing slopes [*Howard et al*., 1982]; 5) offset layering as detected by SHARAD [*Smith and Holt*, 2010]; 6) asymmetric accumulation of ice across the trough [*Smith and Holt*, 2010]; 7) larger surface slopes on the equator-facing walls than on the pole facing walls [*Pathare and Paige,* 2005]; 8) different trough wavelengths in different regions on the NPLD [*Pathare and Paige*, 2005; *Smith and Hol*t, in prep]; 9) migration of the NPLD troughs [*Smith and Holt*, 2010]; and 10) apparent lack of trough migration on the SPLD [*Kolb*

and Tanaka, 2001]. Furthermore, we find that the topographic undulations discussed by *Cutts et al.,* [1979] can be linked to spiral trough formation and trough clouds.

Because these features match predictions so well, it is possible to use flow modeling related to the Froude Number to describe the conditions at the NPLD and to derive order of magnitude analytical solutions for migration and accumulation rates. While highly dependent on input parameters and qualified assumptions, these analyses represent a new method for estimating migration of troughs and accumulation of ice at the NPLD, independent of previous methods based on assumed accumulation rates. Using discussed constraints, we calculate an annual migration rate directly related to winds of ~20 mm per year and an average ice accumulation of 0.12 - 0.15 mm per Earth Year. When better data, the inclusion of insolation, or improved models are available, this framework can be easily adapted to include up-to-date analysis.

Furthermore, this model is testable on the decadal time scale. Observations from the highest resolution visible instrument, HiRISE, can observe at the sub-meter scale. Therefore, detecting changes in elevation in areas of high activity may be a reality over just a few years. During that time, the monitoring of aeolian activity and surface changes will continue. With future observations we will be able to increase the reliability of the estimates contained in this paper.

Our investigations provide a significant step to understanding the processes that control spiral trough formation and evolution, but there remains much work to do, such as a broader SHARAD survey to detect variability of troughs in more locations [*Smith and Holt*, in prep]. Besides finding images of trough clouds in coming years and higher resolution atmospheric modeling, there are remaining questions to be addressed. What is the contribution of sublimation from insolation on the high side? Can we better understand the relationship between katabatic jumps and the formation of trough clouds?

What physical conditions are met for the clouds to form? Lastly, can we differentiate between snowfall and frost buildup on the trough low-side? These questions will all be addressable in detail in future investigations when more data are available.

A challenge for the future is the development of a numerical model of cyclic steps on Mars that a) explains their initiation as a stability problem and b) predicts the spiral troughs observed on Mars. This model will have to take into account the Coriolis force, along with the mechanisms which give birth to jumps within the katabatic flow, and describe sublimation and deposition of ice rather than erosion and deposition of sediment. We believe that such a model is within reach.

Chapter 4: Aeolian Processes as Drivers of Landform Evolution on Mars' South Pole

4.1 Introduction

Mars' polar layered deposits are composed of primarily water ice and dust [*Fishbaugh et al*., 2010; *Grima et al*., 2009; *Hvidberg et al*., 2012]. Studies have shown that beyond their bulk properties, the surfaces are shaped mostly by a few external processes: wind transport, atmospheric deposition, and insolation induced sublimation [*Smith et al*., in review]. These processes have been attributed to the formation of the large spiral troughs and other landforms on the polar caps, including scallops, chasms, and wirebrush terrain [*Howard*, 2000]. Based on arguments of morphology, it has been suggested that the SPLD scalloped terrain is one of the most likely to have been influenced by aeolian processes. Yet, other process have been invoked to explain some of these features: basal melting [*Fishbaugh and Head III*, 2002], tectonics [*Grima et al*., 2011], and viscous ice flow [*Fisher et al*., 2002].

Recent evidence on the north polar layered deposits (NPLD) has shown that winds and atmospheric deposition were the primary forces in the construction of the spiral troughs and Chasma Boreale [*Holt et al*., 2010; *Smith and Holt*, 2010]. Observations of low altitude clouds, atmospheric modeling, and surface morphology [*Smith et al*., in review] in addition to radar stratigraphy [*Smith and Holt*, in prep] support this conclusion, but no studies have provided the same detailed combination of techniques on the south polar layered deposits (SPLD). We hypothesize that features on the SPLD can be explained by the same processes as the well-studied NPLD features.

To test our hypothesis, we synthesize several datasets where possible. Using similar methods to *Smith et al.,* [in review], we employ mesoscale atmospheric modeling, topographic analysis, analysis of subsurface stratigraphy with the shallow radar

instrument (SHARAD), and optical data that observes both the surface and atmospheric phenomena. We demonstrate through the detection of trough clouds, or clouds that are located within and near troughs, that enhanced sublimation and subsequent redeposition are present on the SPLD during spring and summer. Furthermore, radar detections of subsurface reflectors reveal stratigraphies that show the pattern of ablation and accumulation near these features.

Global climate and mesoscale models have been developed for many years to predict atmospheric circulation and clouds with great success. In particular, NPLD features related to winds have been studied in detail [*Brothers et al*., 2013; *Massé et al*., 2012; *Smith et al*., in review], yet few, or no, studies have attempted to relate the landforms on the SPLD to modeled winds. We employ the first high resolution, 20 km grid, mesoscale model of currents on the SPLD so support the hypothesis that winds are of primary importance in the surface evolution of the SPLD. The model was developed at and provided by the Laboratoire de Meterologie Dynamique (LMD) [*Spiga and Forget*, 2009].

4.2 Background

The variety and complexity of features on both poles has led to a wide range of formation hypotheses. Competing hypotheses have provided evidence for several arguments, but some hypotheses have the advantage of including processes that are known to be active on the surface, both in the present and the past. Others account for formation by introducing more exotic processes that have not been directly observed but could result in similar features.

Previous work suggested that only three processes were required to form all of the non-impact features on both poles: wind transport, sublimation from insolation, and atmospheric deposition [*Howard*, 2000]. On the NPLD, optical imagery provided evidence of ice transport in the form of wind streaks and erosion. Topography and

photographs detected surface morphologies consistent with aeolian bedforms in depositional environments, and exposed stratigraphy was postulated to be the result of migration for several features [*Blasius et al*., 1982; *Howard*, 2000; *Howard et al*., 1982]. Subsequent work detected subsurface stratigraphies that indicated migration for NPLD troughs [*Smith and Holt*, in prep, 2010] and low altitude clouds capable of returning ice from the atmosphere to the surface [*Smith et al*., in review].

While the spiral troughs are abundant on both poles, SPLD troughs have more variety in morphology than NPLD troughs. Some of the variety includes smaller features that resemble troughs in cross section but only extend some tens of km: gull winged scallops. The "gull-wing" like scarps with asymmetric ridges resemble barchan dunes in a bimodal wind regime [*Howard*, 2000]. While it is uncommon, the asymmetric ridge is not unique to scallops. SPLD troughs at high latitudes exhibit a similar morphology with ridges on their higher side, and explanations for this morphology require more attention. The scallops have crescent shapes in map view and exhibit asymmetric cross sectional profiles [*Grima et al*., 2011]. In addition, the scallops frequently exhibit a raised edge, creating a transverse ridge. *Howard* [2000] attributed the transverse ridges to a long-term bimodal wind regime, one where the majority of the morphology develops in downslope flow from the pole, but the ridge forms during secondary, upslope flow.

The idea of migrating mega-bedforms is not the only one that includes winds on the SPLD. Others have concluded that the spiral troughs and scallops are carved features forming due to in situ erosion [*Kolb and Tanaka*, 2001; *Rodriguez and Tanaka*, 2011]. This idea is has strong supporting evidence in certain locations, especially in Promethia Lingula and near the wirebrush terrain. Where these troughs exist, subsurface stratigraphic analysis should agree. *Smith and Holt* [in prep] demonstrate that few or no NPLD troughs are purely erosional, but they left open the question for the SPLD. Another investigation discovered trough clouds on the south pole, suggesting that the same processes of migration occur on both poles [*Smith et al*., in review]. Those findings were preliminary and not well constrained spatially.

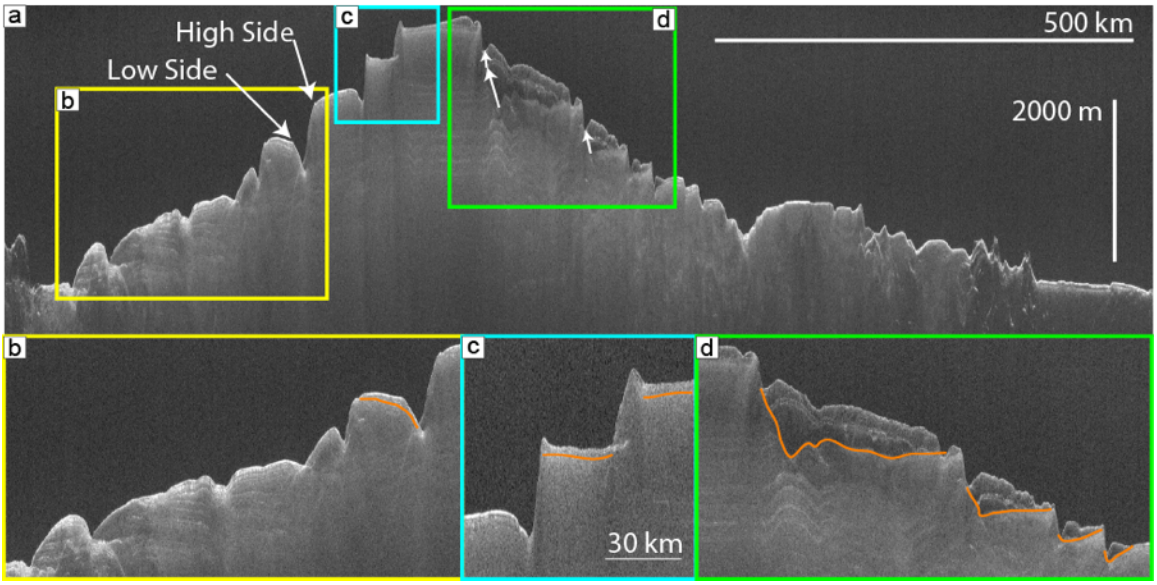

Figure 4.1: Radar observations of the SPLD*: a) Radargram 2759301, crossing the SPLD. High side and low side slopes are based strongly on topography and loosely on latitude. Ground track in Figure 4.2c. b) Portion of Figure 4.1a. Orange line delineates deposition occurred after the formation of these troughs. c) Portion of Figure 4.1a. Two Australe Mensa troughs have highly asymmetric cross sections and reversing ridges on the high side. Layering on both sides of the trough indicates deposition. d) Portion of Figure 4.1a. CO2 deposits detected by Phillips et al., [2008] fill in older troughs. The shape of the troughs is highly asymmetric, similar to those observed in 4.1c. Migration has occurred (white arrows in 4.1a)*

Atmospheric models are capable of predicting wind directions and intensities for many Martian days or seasons. Mesoscale models have provided context for understanding wind patterns on the north pole [*Smith et al*., in review; *Spiga et al*., 2011], but few if any south polar studies have compared modeled wind patterns to evidence from exposures on the surface. Locally, mesoscale models have sufficient resolution to reflect medium scale topographic influences, including spiral troughs and scallops. These models may be predictive or supportive of hypotheses that rely primarily on aeolian processes to describe the features on the poles.

Descriptions of trough orientation can often be inadequate. The troughs are not circumpolar, so their corresponding slopes do not always point "equatorward" or "poleward." Additionally, the terrain on each slope varies by location, so characterizations of morphology or exposure are fundamentally limited to the individual

trough being examined. This is especially true for the SPLD, where troughs are more diverse than on the NPLD. Due to these limitations, we adopt the nomenclature utilized by *Smith et al.,* [in review], who separated the trough's slopes by high side and low side, based strongly on topography and loosely on latitude (Figure 4.1).

4.3 METHODS

4.3.1 Optical Imagery

As of this writing, more than 14,200 publically available Thermal Emission Imaging System (THEMIS) images capture portions of the SPLD [*Christensen et al.*, 2004]. We analyze these images to find near surface trough clouds. The SPLD is not symmetric about the south pole, so regions of interest are bounded to include the entire SPLD south of -80°. For longitudes between 90 and 220, we also examine images between -80° and -71° (Figure 4.2).

Other instruments are useful for detecting clouds at higher resolutions and across more area. To supplement our THEMIS survey, we examine imagery from the High Resolution Stereo Camera (HRSC) [*Neukum and Jaumann*, 2004], Mars Orbital Camera (MOC) [*Malin et al.*, 1998], Context Imager (CTX) [*Malin et al.*, 2007], and High Resolution Imaging Science Experiment (HiRISE) [*McEwen et al.*, 2007]. Occasionally, images detect multiple clouds at the same time. This detection allows for better approximations for cloud properties.

Our survey is modeled after the one conducted by *Smith et al.,* [in review] for the NPLD. *Smith et al.,* [in review] examined every image of the NPLD in an effort to characterize low altitude clouds that interacted with the surface. They found approximately 350 THEMIS images contained clouds of various forms. The majority of those clouds were aligned parallel to and above the bottom of spiral troughs. *Smith et al.,*

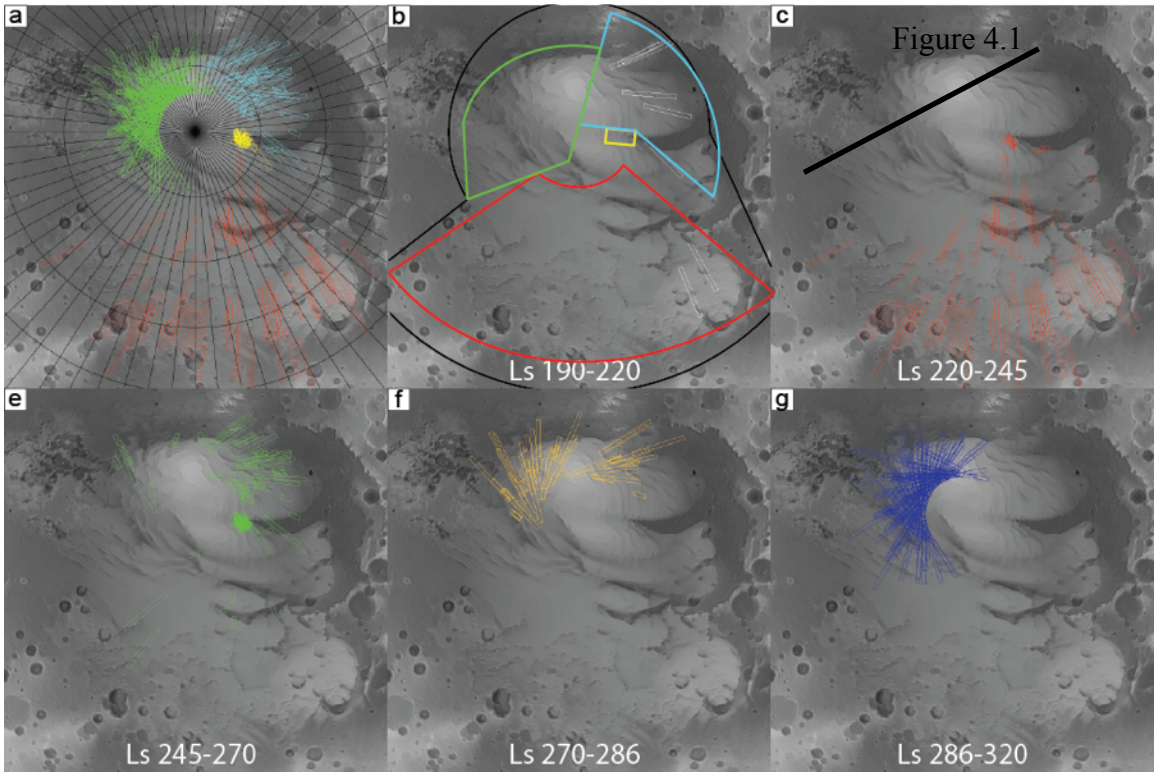

Figure 4.2: Footprints of SPLD trough clouds over MOLA basemap. *a) Four regions are determined by the timing of trough cloud appearances. Red: Region 1. Yellow: Region 2. Blue: Region 3. Green: Region 4. b) Clouds detected in Ls range 190-220 in white. Footprints of the four regions are in matching colors to 4.2.a. Black outline is survey area for entire SPLD. c) Clouds detected in Ls range 220-245. Black line indicates ground track of radargram 2759301 in Figure 4.1a. e) Clouds detected in Ls range 245-270. f) Clouds detected in Ls range 270-286. g) Clouds detected in Ls range 286-320. No clouds outside of Region 4 are detected after Ls 286.*

[in review] extended their survey to the SPLD in a preliminary effort and found trough clouds at various locations on the SPLD.

Here we continue their SPLD work and expand temporal and spatial examinations of images. We add Mars year 31 (MY31) and expand the time window of the survey previously conducted. We also incorporate the larger area described above. Some lessons were learned during the survey of *Smith et al*., [in review], and we modify the procedure for efficiency. Instead of examining every image of the SPLD, our survey is more targeted.

We designed our initial sampling to include a time period that is approximately complementary with the NPLD detection of clouds, from Ls ~30 to ~100. That

corresponds to Ls ~210 to ~ 280 in the southern hemisphere. Clouds were detected at the ends of this inadequate time period, and an expanded search grew to include dates as early as Ls 190 and as late as Ls 330 for all of the SPLD.

4.3.2 Radar observations

SHARAD has been operating since late 2006 [*Seu et al*., 2007]. The instrument sends a signal that increase from 15 to 25 MHz in order to have a vertical resolution of about 15 m in free space and ~ 9 m in ice. SHARAD records many traces, or 1D plots of intensity and time in order to generate a radargram (Figure 2.6). A signal transmitted from the dipole antenna reflects off of interfaces of changing permittivity, ε, and is received by the same antenna. We use radargrams to observe and interpret subsurface features within the PLD.

Since reaching orbit, approximately 11,500 observations of Mars have been collected by SHARAD. The abundance of observations, especially near the south pole, is useful for analysis. Occasionally, we utilize both repeated and crossing observations to increase confidence in interpretations. Repeated observations are important for checking against artifacts of processing or low signal strength, things that may hamper an individual observation. Crossing observations are important for eliminating ambiguous interpretations. By examining from multiple orientations, our view of subsurface geometries is expanded. Furthermore, multiple observations of a target help to separate side reflections, or reflections from targets other than the one of interest, from scientifically interesting subsurface reflections, a critical first step of interpretation. Due to their often-undesirable nature, reflections recorded by SHARAD from non-nadir objects are considered “clutter”.

Clutter cannot be removed from a radargram, but it can be mitigated. By comparing predicted clutter in a synthetic radargram to actual SHARAD observations, one can determine which part of the signal is subsurface and desired [*Holt et al*., 2008]

(Figure 2.6). A synthetic radargram is calculated from surface topography in the form of Mars orbiter laser altimeter (MOLA) digital elevation models [*Smith et al*., 2001]. The synthetic radargram only predicts what reflections the instrument will receive from the surface. Thus, information in the actual radargram that is not simulated is accepted as scientifically interesting subsurface reflections. In our survey we employ clutter mitigation techniques for all observations and present radargrams that are the most favorable for interpretation.

4.3.3 Atmospheric modeling

To simulate atmospheric conditions on the SPLD, we use a dynamical core mesoscale model developed at the Laboratoire de Meterologie Dynamique (LMD) [*Spiga and Forget*, 2009]. This model has the power to simulate Martian conditions from global scale to tens of meters, including scales appropriate for sampling topographic features such as spiral troughs and scallops.

In our simulations we chose an area of ~1800 km by 1800 km centered on 86° south and 173° east. The grid is 100 by 100 cells, yielding a resolution of ~18 km per cell. At this resolution we are able to resolve the large chasma and general topography of the SPLD, but smaller features, such as scallops and spiral troughs are not resolved in our simulations. Because the intent of this initial study is to focus on regional wind patterns and variations on the seasonal and diurnal scales, our simulations are adequate for this initial atmospheric study. In order to understand local effects of topography on the atmosphere, future work will focus on individual features.

Our model is not yet capable of predicting the locations of clouds, especially near topographic features as small as spiral troughs. Future work, including increased resolution and a water cycle, will hopefully allow us to predict not only the locations, but the composition, frequency, duration, and volume of trough clouds. Those answers will be integral into understanding migration and evolution of mesoscale features on the PLD.

4.4 OBSERVATIONS OF SPLD CLOUDS.

Similar to the study of trough clouds on the NPLD [*Smith et al*., in review], we examine optical imagery for evidence of low altitude clouds on the SPLD. The SPLD is physically larger in aerial extent and elevation range than the NPLD [*Smith et al*., 1999]. Due to these differences, clouds are detected over greater latitudinal ranges and over a longer season. Furthermore, SPLD topographic features are more diverse than features on the NPLD. Spiral trough morphology varies greatly, as do 10 km scale scallops and craters that are not found on the NPLD. The increased diversity of features results in more variable trough cloud structure.

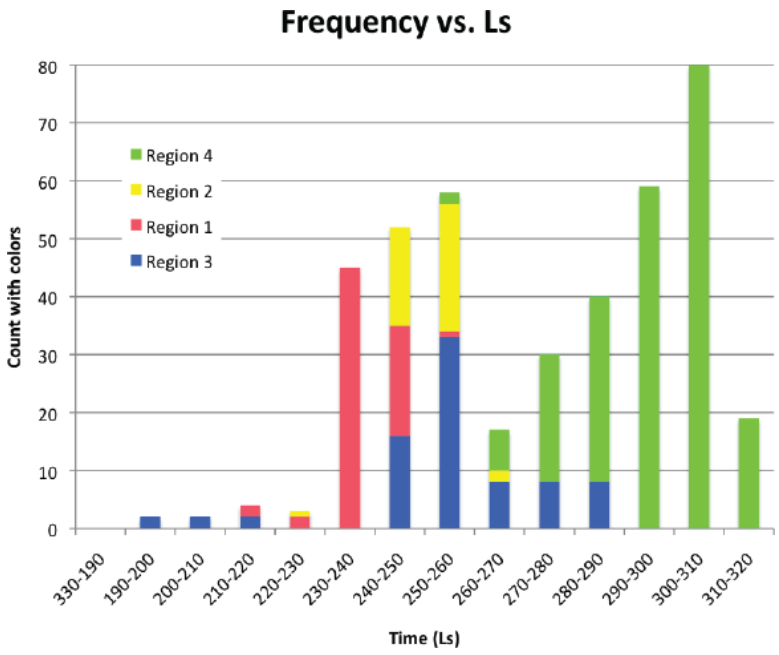

Figure 4.3: Histogram of trough cloud detections in each region. *Clouds are detected from Ls 198 until Ls 318. This 120° Ls range is twice the Ls range of ~60° for the NPLD: from ~Ls 40 until Ls 102, 12° after summer solstice. Region 4 clouds are imaged until Ls 318, 48° after summer solstice, significantly longer than the NPLD.*

We combine observations from five Mars years, MY26, MY26, MY28, MY29, and MY30 to garner the best statistics possible. Besides physical differences, there were large variations between the number and coverage of photos between years. SPLD observations decreased significantly each year (Table 1). During the date range 190-320, MY27 had the most images with more than 4400. MY26 had ~3600 for the same

range. By MY28 fewer than 1500 images were taken in that period. MY29 and MY30 had ~750 and ~450, respectively. Furthermore, MY29 and MY30 campaigns were highly focused, and coverage was limited to only a few targets.

Given the various differences, clouds at the SPLD and NPLD also have common characteristics. Spatially, trough clouds are found near topographic changes at both poles, especially near decreasing slopes. Temporally, large numbers of clouds are detected towards the end of spring and early summer (Figure 4.3).

Many SPLD clouds are found in mid-spring until early summer, ~ Ls 220 – 280, similar to observed clouds on the NPLD [*Smith et al*., in review]. However, SPLD trough clouds are observed both earlier and later than their NPLD counterparts. Four images detect trough clouds prior to Ls 210, as early as Ls 198. At the other end of the season trough clouds are observed until Ls 318, well into summer. The total season is ~120° Ls, far greater than the ~60° Ls of the NPLD. Trough clouds detected between Ls 280 and 318 are unique to southern summer. No trough clouds are detected on the NPLD after Ls 102 [*Smith et al*., in review].

Besides the addition of a second, later season, trough clouds are detected at locations that vary spatially in correspondence to date (Figure 4.1a, b, c, d, e, f). Therefore, we divide the SPLD into four regions loosely based on the timing of detected clouds and loosely based by elevation (Figure 4.1b). In general, clouds at lower latitudes occur earlier in the spring, and clouds of higher latitudes appear later. The four regions contain 69, 42, 74, and 230 clouds.

Region 1 corresponds to Ultima Scopuli and Ultima Lingula, in the range 120° - 235° east and 70° - 83.5° south. ~70 trough clouds are found in this region between Ls 210 and 254, for a total duration of 44° of Ls. The bulk of detections (63) are between Ls 229 and Ls 245. Only 4 images capture clouds in Region 1 after Ls 245, so this region sees the most activity in the early part of the cloudy season.

Region 2 is much smaller than any of the other regions. It is distinguished by being at the head of Chasma Australe and exists in a range of latitude from 85° to 110° and longitude from 85.5° to 87° south. Outside of Region 4, this region has the highest

density of observations. More than 40 clouds are detected there, and detections span from Ls 225 through Ls 268. Prior to Ls 243 only one cloud is detected, so a more concise range is Ls 243 – Ls 268, or about 25° of Ls. Region 2 contains clouds during a transition period between Region 1 and Region 3.

Region 3 experiences trough clouds over a longer duration. Region 3 has a higher latitude than Region 1, between 80° and 86.5° south. It ranges from 5° to 110° east. The majority of Region 3 clouds are captured between Ls 241 and Ls 295, for a duration of 54° Ls. However, another date range contains clouds 7 in Region 3: Ls 198 through Ls 228. These are the earliest detected clouds on the SPLD. Between Ls 228 and Ls 241 no clouds are found in Region 3.

Finally, Region 4 stands alone. This region primarily contains Australe Mensa and the residual CO2 ice cap but extends to the margin near 83°. All detections of trough clouds after Ls 286 are found in Region 4, or ~150 images. The 80 remaining Region 4 trough clouds are detected as early as Ls 250. Between Ls 250 and Ls 265, only 5 clouds are imaged. Between Ls 265 and Ls 295 another >70 observations contain clouds. This overlaps with Region 3 but not with Region 1 and only ~5 days with Region 2. The vast majority of Region 4 trough clouds are at high latitudes, and only a few are found near the margin. Those are found during the earliest part of Region 4's window of detection.

Further evidence for the localization of cloud formation on the SPLD is found in the dearth of detections in Promethei Lingula (except the head of Chasma Australe) and Australe Scopuli. No trough clouds are found in the vast, smooth plains between Australe Mensa and Ultima Scopuli. South of ~88° there is no THEMIS coverage to seek clouds.

4.5 RADAR AND TOPOGRAPHIC DATA

4.5.1 Spiral troughs

Spiral troughs on the SPLD vary greatly from region to region and are often distinctly different from those on the NPLD. For example, in Promethei Lingula, the troughs appear to be primarily erosional features, with little evidence for migration (Figure 6 from *Kolb and Tanaka* [2001]). These troughs are broad, having wider cross sections and lower depth-to-width ratio than troughs elsewhere, including on the NPLD. Nearby, in Australe Sulci, where wirebrush terrain dominates, there is considerable evidence for erosion, supporting the eroded trough interpretation.

While some troughs have clear evidence of erosion, troughs in Australe Lingula are generally more complicated (Figure 4.1b). The variability here begins when comparing troughs at high and low latitudes, the latter showing evidence for migration. At low latitudes, trough low sides display accumulation, while high sides have been eroded. The slopes of these lower troughs are much more symmetric than those closer to the pole.

Higher latitude troughs in Australe Lingula are very asymmetric (Figure 4.1c). The two highest troughs have only small depressions and may be mistaken for scarps rather than troughs. These troughs have step-like cross sections with steep high sides and sub-horizontal low sides. High side layered terrain is exhibited, but there is only little evidence for deposition on the low side. (Figure 4.4) [*Smith et al*., 2013]. Another contributing factor to the asymmetry is reversing ridges [*Howard*, 2000]. Unlike troughs elsewhere on the SPLD and NPLD, the high side of these troughs is raised more than 50 m above the surrounding terrain, immediately above (latitudinally) the high side scarp.

Those higher elevation troughs deviate strongly from the well-studied, classical troughs previously described [*Howard et al.*, 1982; *Smith and Holt*, in prep]. They have clearly exposed layering on the high side slope, but across, on the low side, the surface gives little indication of migration nor erosion (Figure 4.4). Radar and optical evidence demonstrate that erosion was not the final state of the troughs,

unlike those of Promethei Lingula. Instead, the lack of exposed layering on the low side in optical imagery indicates that deposition has occurred relatively recently, although a previous erosional state cannot be ruled out (orange in Figures 4.1c and 4.4) Excluding the asymmetric ridge and discontinuity at the trough, Figure 4.1c shows deposits of nearly uniform thickness on either side of the trough.

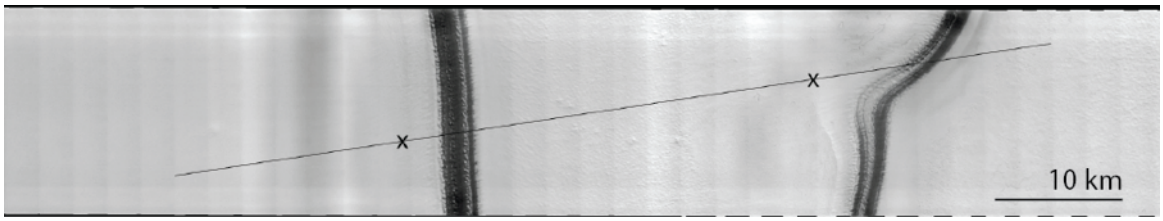

Figure 4.4: THEMIS Vis image 16611013 of SPLD asymmetric troughs. *Ground track corresponds to Figure 4.1c. Lowest local elevations marked by Xs. Layers are exposed on the high side, but no evidence for erosion exists on the low side.*

4.5.2 Residual cap troughs

The troughs near SPLD's residual cap again behave differently from troughs elsewhere on the SPLD and NPLD. Filled with CO2 ice [*Phillips et al*., 2011], these troughs have been modified from their original morphology (Figure 4.1d). Prior to infill, these troughs had strikingly similar morphologies to the two highest troughs of Australe Mensa. They took a mostly stair shape and had minimal depressions near their lowest point (orange in Figure 4.1d).

Currently, these troughs do exhibit depressions, but they are smaller in depth and in cross section than they were before being filled. We call these secondary troughs. The CO2 ice was at one point (post deposition) likely to have been much more smooth than at present. Current topography has then been shaped by sublimation. It was only after infill that the secondary troughs took the current shape (Figure 4.5).

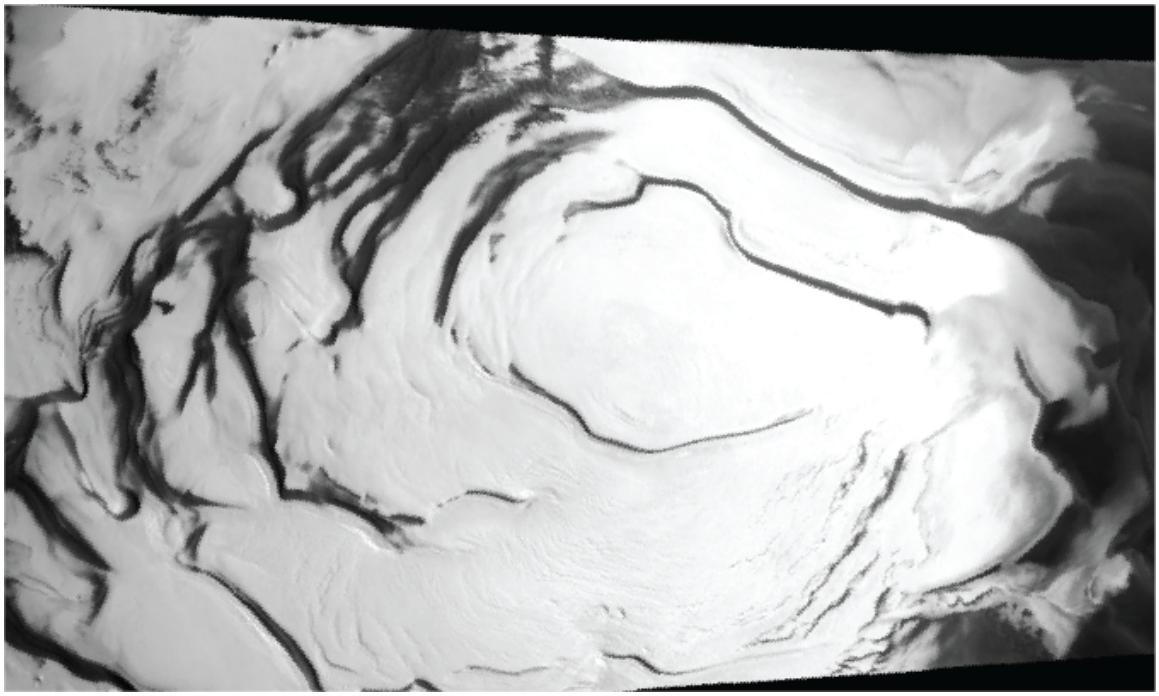

Figure 4.5: Optical image of the SPLD residual ice cap (corresponding to Region 4). *Large scale spiral troughs are observed. In addition, where CO2 ice was detected by Phillips et al., [2012] only secondary troughs exist.*

Additionally, SHARAD detects multiple reflectors within, above, and below the CO2 ice. These reflectors clearly indicate that the current location of the largest troughs is further south than the reflector directly below it (Figure 4.1d). Thus deposition was accompanied by migration, similar to the NPLD, but unlike on the NPLD, the deposition was not water ice. Topographically, these troughs are very small. However, they are laterally extensive and spiral, similar to other troughs on the SPLD (Figure 4.5).

4.5.3 Scallops

Within Ultima Scopuli, the largest region of the SPLD by areal extent, many "gull-wing" shaped troughs exist. These crescent shaped troughs exhibit layered terrain on the high side and occasionally exhibit banded terrain on the low side (Figure 4.6).

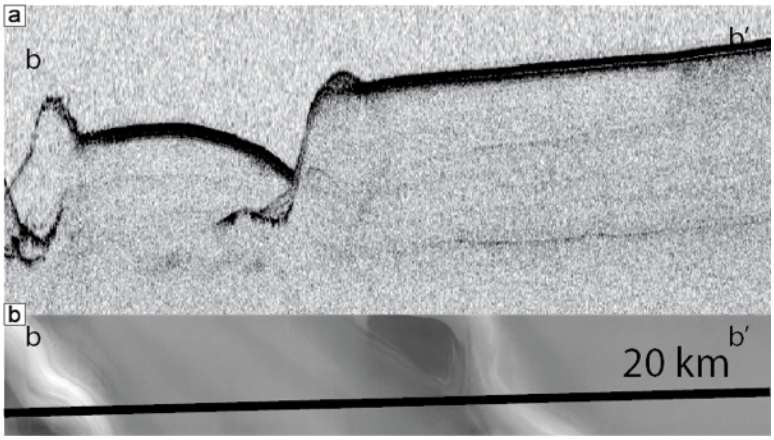

Figure 4.6: Radar and optical imagery of scallops in Region 1*. a) Portion of radar image 244901 crossing two scallops. Internal reflectors are reminiscent of NPLD troughs, but asymmetric ridges are very different. Ridges are created by winds that flow contrary to those that formed the scallops. b) THEMIS vis image V08651005. Ground track gives location of a). Layers are exposed on the scallop high sides, but darker, mantled material may be on the low side.*

Many have cross sections similar to NPLD troughs; however, there are also many exceptions. Scallops that have asymmetric ridges, similar to troughs near Australe Mensa, are abundant (Figure 4 from *Grima et al*., [2012]).

For their "gull-winged" shape, these troughs resemble barchan dunes and are nicknamed "scallops." It has been hypothesized that the scallop's uniqueness results from their relatively limited size. Individual scallops are tens of km in extent. When conjoined, they can reach distances greater than 100 km. Contrast that to NPLD troughs, which are extensive sometimes for 600 km [*Howard et al*., 1982], and the scallops are significantly smaller than the well-developed NPLD troughs. Thus the amount of migration for scallops must be small relative to their size.

Scallops have been hypothesized to form as a result of local tectonic processes, i.e. the basement lowers, causing fracture in the ice and exposed high side layering [*Grima et al*., 2011]. This explanation could potentially explain the change in elevation across a trough, but it cannot explain the abundant asymmetric ridges. *Howard* [2000] offered an explanation that included winds. He saw the asymmetric ridges as being analogous to those created on terrestrial dunes during bimodal wind regimes. In this scenario, the scallops would form during prolonged winds (perhaps thousands or more years). Afterward, in the current or recent wind regime, the winds reversed, causing a

retreat of material. Therefore, the SPLD has complicated, and possibly reversing, wind regimes on many year time scales.

4.6 SPLD MESOSCALE MODEL

Previous examinations of SPLD features have been limited to topographic and photographic observations. The morphology of troughs and scallops, especially those with asymmetric ridges, is a fascinating question. Various hypotheses have been employed to understand both the medium scale features and the reversing ridges including wind [*Howard*, 2000] and tectonics [*Grima et al*., 2011]. To offer more insight into processes affecting the features, we employ a mesoscale atmospheric model designed at the Laboratoire de Meterologie Dynamique.

The simulations run within the model are comparable to those that have been conducted on the NPLD [*Smith et al*., in review]. We utilize a 20 km grid spacing centered at 89S 173E in a region large enough to cover the entire SPLD (1000 x 1000 km). Outputs of wind speed, wind direction, and temperature are output every hour for an equally divided "24 hour" Mars day. We simulate the conditions at several points throughout spring and summer, including these Ls dates 220, 260, 290, and 320.

The results of the simulations are striking. Unlike simulations on the NPLD, [*Smith et al*., in review] for all seasons the SPLD winds vary in direction and velocity quite rapidly within a single day (Figure 4.7). In fact, the simulated mesoscale winds may reverse direction within a single hour. During one day the winds alternate from having katabatic to an adiabatic properties. This reveals complex wind states at different locations on the SPLD, sometimes contrary to expected results. In other words, the winds flow uphill as often as they flow downhill.

Adiabatic winds are not modeled on the NPLD in our simulations. Within a single day the winds deviate velocity vectors by only a few degrees making them in effect unimodal (Figure 3.14). This is true for all dates that we have simulated. The deviation

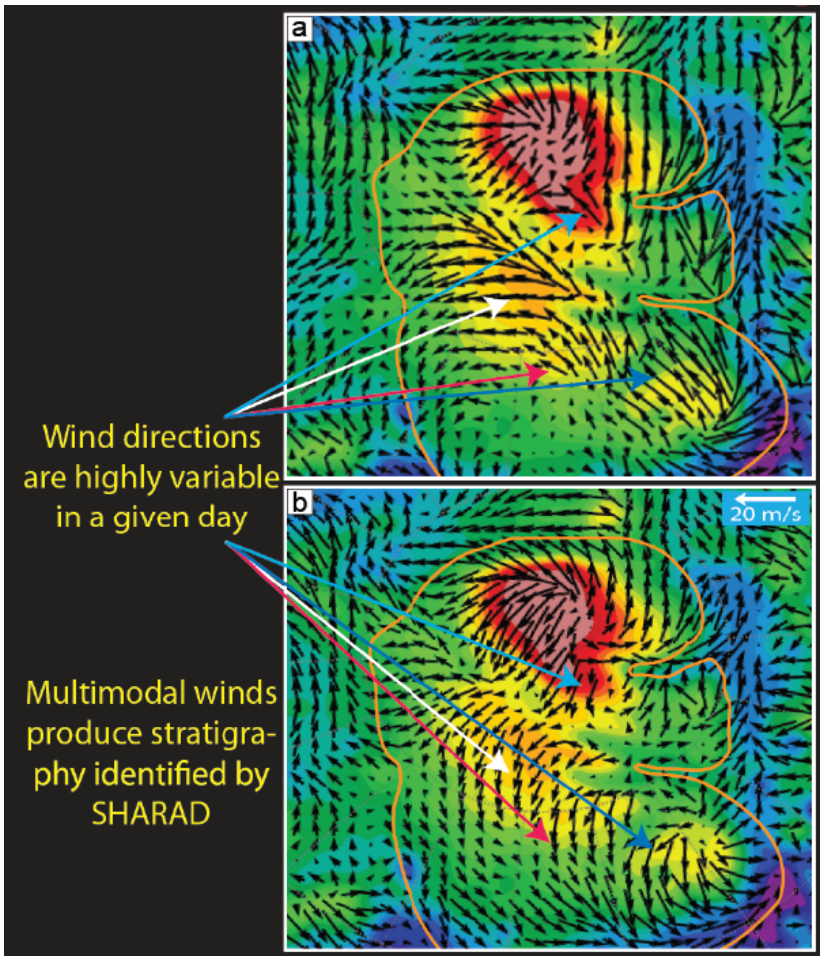

Figure 4.7: Results from mesoscale wind modeling. *a) Wind vectors from 50 m altitude overlay colorized topography at Ls 223 around 7:00. b) same as a) but at 20:00. Vectors are highly variable throughout one Martian day. Changing, and variable winds may be responsible for the stratigraphy and morphology of features identified in this paper. Orange outlines the SPLD extent.*

from NPLD to SPLD winds is likely explained as the result of large topographic forces beyond the SPLD margin. In particular, winds in the southern hemisphere, especially near the south polar, are directly driven by currents from Hellas and Argyre basins. Indirectly, albedo variations resulting from those currents can cause local effects [*Colaprete et al.*, 2005].

The difference between NPLD unimodal winds and SPLD multimodal winds will certainly have an effect on ice accumulation. In the current regime, SPLD ice on the surface is not likely to have long term stability. This ice can be transported across the surface to deposit in a more stable location. Stabile regions include those with reduced wind speeds, pole-facing slopes, and high albedo regions.

4.7 DISCUSSION

The results of wind modeling with observations of clouds indicates that the SPLD is a very active place. Significant variations exist on a diurnal timescale (Figure 4.7) and on seasonal scales (Figure 4.2). Especially compelling is the observation that trough clouds are found at different locations (latitudes) as the season progresses.

Latitudinal differences may account for the dates of clouds found in Regions 1-3, but Region 4 has a unique property. First, when compared to the NPLD, Region 4 clouds are manifest well beyond the expected date range, and except for a few clouds detected at the SPLD margin, Region 4 clouds also appear much later than all other SPLD trough clouds. S*mith et al.,* [in review] noticed this disparity and suggested that the formation of these clouds and their timing may be related to CO2 properties. This offers a plausible explanation. The highest latitudes should warm later in the season. Downhill, katabatic winds, required to form clouds at the bottom of troughs, should be more prominent near CO2, especially during sublimation.

THEMIS coverage of the SPLD varies greatly by year, so our statistics will not be as robust as for the NPLD, where coverage was more evenly spread: temporally and spatially. Nevertheless, available data suggests that the four regions are distinct, with only minor overlap in seasonality.

The troughs themselves offer a greater diversity than on the NPLD, and local processes are likely the cause. For NPLD troughs, which demonstrate variability to a lower degree than those in the south, studies have concluded that wind transport, atmospheric deposition, and sublimation from insolation were the three primary forces involved in formation [*Howard*, 2000; *Smith et al.*, in review]. NPLD troughs do occasionally exhibit purely erosional characteristics (as opposed to patterns of erosion and deposition associated with migration), and some locations exhibit evidence for reduced intensity winds [*Smith and Holt*, in prep], but the variations do not include deviations from the set of three process; only the ratio of the three varies.

It is therefore not surprising that eroded and buried troughs are found on the SPLD, along with troughs that have been found to migrate. The number of trough-like scallops may be more surprising, as with asymmetric ridges, since neither feature has been described on the NPLD. Nevertheless, we argue that the same three processes can also explain these features and others on the SPLD: wind, sublimation, and deposition.

Large scale trough and scallop morphologies, in combination with intermediate scale asymmetric ridges tell of wind regimes that vary in time [*Howard*, 2000]. We favor a scenario for the formation of these features in which large structures are created by persistent, unimodal winds or winds of one overwhelming primary direction and subsequent winds are in an antiparallel or sub-antiparallel direction for a shorter duration. Our atmospheric simulations demonstrate that, unlike on the NPLD, wind directions are highly variable within a single day. This in itself does not prove our favored scenario, but it does lend credence to the idea that SPLD winds are neither uniform in orientation nor in direction.

Troughs and scallops form during the longer period, growing via the three processes. Transport, the most important difference between features that migrate and those that remain constant in position, occurs in places where katabatic jumps and trough clouds manifest. At higher latitudes, repeating katabatic jumps create either erosional (on Promethia Lingula) or depositional cyclic steps (on Australe Lingula and Australe Mensa) to form spiral troughs.

Asymmetric ridges, on the other hand, form by the same processes as the troughs but during a reversal of the wind regime. Ridges are smaller in size and mass than usual low side deposits (near banded terrain), requiring significantly less time to form than troughs. Trough clouds are occasionally observed on the high side of a feature, evidence for this reversal to the standard scheme.

For a first estimate of the time required to form ridges, we invoke the transport rates calculated for the NPLD troughs [*Smith et al.*, in review]. Mass flux of active NPLD troughs was on the order of 10 – 20 m^3/m of ice per year. The 2 dimensional volume of the SPLD ridges, is on the order of $2x10^5$ m^3/m. At the rate determined for NPLD

troughs it would take 10^5 Mars years to create the asymmetric ridges. Observations of SPLD trough clouds that only endure 5 years are insufficient to support this interpretation confidently. Additional work defining the frequency and duration of clouds at individual features is required. More detailed atmospheric modeling will supplement that effort.

The presences of ridges is very telling. If the multimodal winds were balanced in strength, the ridges would never have formed. Therefore, the story is one of both short and long term variability. In this paper we focus on short term variability, but work simulating SPLD winds at other obliquities and states is underway. The combination of gross morphological structure and knowledge of reversing winds is strong evidence for wind transport that has changed primary direction during thousands of years or perhaps longer time scales.

Works Cited

Andersen, V. M. (1978), Undular hydraulic jump, *Journal of the Hydraulics Division*, *104*(8), 1185–1188.

Ball, F. K. (1956), The theory of strong katabatic winds, *Australian Journal of Physics*, *9*(3), 373–386.

Ball, F. K. (1957), The katabatic winds of Adélie Land and King George V Land, *Tellus*, *9*(2), 201–208.

Black, H. P., and W. Budd (1964), Accumulation in the region of Wilkes, Wilkes Land, Antarctica, *Journal of Glaciology*, *vol.5*(Issue 37), pp.3–15.

Blasius, K. R., J. A. Cutts, and A. D. Howard (1982), Topography and stratigraphy of Martian polar layered deposits, *Icarus*, *50*(2-3), 140–160.

Brooks, P. C. (2001), Experimental study of erosional cyclic steps, University of Minnesota.

Brothers, T. C., J. W. Holt, and A. Spiga (2013), Orbital radar, imagery, and atmospheric modeling reveal an aeolian origin for Abalos Mensa, Mars, *Geophysical Research Letters*, n/a–n/a, doi:10.1002/grl.50293.

Byrne, S. (2009), The Polar Deposits of Mars, *Annu. Rev. Earth Planet. Sci.*, *37*(1), 535–560, doi:10.1146/annurev.earth.031208.100101.

Calvin, W. M., and T. N. Titus (2008), Summer season variability of the north residual cap of Mars as observed by the Mars Global Surveyor Thermal Emission Spectrometer (MGS-TES), *Planetary and Space Science*, *56*(2), 212–226, doi: 10.1016/j.pss.2007.08.005.

Campbell, B. A., N. E. Putzig, L. M. Carter, and R. J. Phillips (2011), Autofocus Correction of Phase Distortion Effects on SHARAD Echoes, *IEEE Geoscience and Remote Sensing Letters*, *8*(5), 939 –942, doi:10.1109/LGRS. 2011.2143692.

Christensen, P. R. et al. (2004), The Thermal Emission Imaging System (THEMIS) for the Mars 2001 Odyssey Mission, *Space Science Reviews*, *110*(1/2), 85–130, doi:10.1023/B:SPAC.0000021008.16305.94.

Christian, S. W., J. W. Holt, S. Byrne, and K. E. Fishbaugh (in press), Integrating Radar Stratigraphy with High Resolution Visible Stratigraphy of the North Polar Layered Deposits, Mars., *Icarus*.

Clifford, S. M. et al. (2000), The state and future of Mars polar science and exploration, *Icarus*, *144*(2), 210–242.

Colaprete, A., J. R. Barnes, R. M. Haberle, J. L. Hollingsworth, H. H. Kieffer, and T. N. Titus (2005), Albedo of the south pole on Mars determined by topographic forcing of atmosphere dynamics, *Nature*, *435*(7039), 184–188, doi:10.1038/nature03561.

Cutts, J. A. (1973a), Nature and origin of layered deposits of the Martian polar regions, *Journal of Geophysical Research*, *78*(20), 4231–4249.

Cutts, J. A. (1973b), Wind erosion in the Martian polar region., *J. Geophys. Res.*, *78*.

Cutts, J. A., and B. H. Lewis (1982), Models of climate cycles recorded in Martian polar layered deposits, *Icarus*, *50*(2-3), 216–244.

Cutts, J., K. Blasius, G. Briggs, M. Carr, R. Greeley, and H. Masursky (1976), North polar region of Mars: Imaging results from Viking 2, *Science*, *194*(4271), 1329–1337.

Cutts, J., K. Blasius, and W. Roberts (1979), Evolution of Martian polar landscapes-Interplay of long-term variations in perennial ice cover and dust storm intensity, *Journal of Geophysical Research*, *84*(B6), 2975–2994.

Dillon, W. P., W. W. Danforth, D. R. Hutchinson, R. M. Drury, M. H. Taylor, and J. S. Booth (1998), Evidence for faulting related to dissociation of gas hydrate and release of methane off the southeastern United States, *Geological Society London Special Publications*, *137*(1), 293.

Fahnestock, M. A., T. A. Scambos, C. A. Shuman, R. J. Arthern, D. P. Winebrenner, and R. Kwok (2000), Snow megadune fields on the East Antarctic Plateau: extreme atmosphere-ice interaction, *Geophysical Research Letters*, *27*(22), 3719–3722.

Fedele, J. J., and M. H. García (2009), Laboratory experiments on the formation of subaqueous depositional gullies by turbidity currents, *Marine Geology*, *258*(1–4), 48–59, doi:10.1016/j.margeo.2008.11.004.

Fildani, A., W. R. Normark, S. Kostic, and G. Parker (2006), Channel formation by flow stripping: large-scale scour features along the Monterey East Channel and their relation to sediment waves, *Sedimentology*, *53*(6), 1265–1287, doi:10.1111/j.1365-3091.2006.00812.x.

Fishbaugh, K. E., S. Byrne, K. E. Herkenhoff, R. L. Kirk, C. Fortezzo, P. S. Russell, and A. McEwen (2010), Evaluating the meaning of "layer" in the martian north polar layered deposits and the impact on the climate connection, *Icarus*, *205*, 269–282, doi:10.1016/j.icarus.2009.04.011.

Fishbaugh, K. E., and J. W. Head III (2002), Chasma Boreale, Mars: Topographic characterization from Mars Orbiter Laser Altimeter data and implications for mechanisms of formation, *Journal of geophysical research*, *107*(E3), 5013.

Fishbaugh, K. E., and J. W. Head (2005), Origin and characteristics of the Mars north polar basal unit and implications for polar geologic history, *Icarus*, *174*(2), 444–474.

Fishbaugh, K. E., and C. S. Hvidberg (2006a), Martian north polar layered deposits stratigraphy: Implications for accumulation rates and flow, *Journal of Geophysical Research-Planets*, *111*(E6), E06012.

Fishbaugh, K. E., and C. S. Hvidberg (2006b), Martian north polar layered deposits stratigraphy: Implications for accumulation rates and flow, *Journal of Geophysical Research-Planets*, *111*(E6), E06012.

Fishbaugh, K., and J. Head (2000), North polar region of Mars: Topography of circumpolar deposits from Mars Orbiter Laser Altimeter(MOLA) data and evidence for asymmetric retreat of the polar cap, *Journal of geophysical research*, *105*(E 9), 22455–22486.

Fisher, D. A. (1993), If Martian Ice Caps Flow: Ablation Mechanisms and Appearance, *Icarus*, *105*(2), 501–511.

Fisher, D. A. (2000), Internal Layers in an "Accublation" Ice Cap: A Test for Flow, *Icarus*, *144*(2), 289–294.

Fisher, D. A., D. P. Winebrenner, and H. Stern (2002), Lineations on the "White" Accumulation Areas of the Residual Northern Ice Cap of Mars: Their Relation to the "Accublation" and Ice Flow Hypothesis, *Icarus*, *159*(1), 39–52.

Frezzotti, M., S. Gandolfi, and S. Urbini (2002), Snow megadunes in Antarctica: sedimentary structure and genesis, *J. Geophys. Res*, *107*(4344), 10–1029.

Gierasch, P., and C. Sagan (1971), A preliminary assessment of Martian wind regimes, *Icarus*, *14*(3), 312–318, doi:10.1016/0019-1035(71)90003-0.

Grima, C., F. Costard, W. Kofman, B. Saint-Bézar, A. Servain, F. Rémy, J. Mouginot, A. Herique, and R. Seu (2011), Large asymmetric polar scarps on Planum Australe, Mars: Characterization and evolution, *Icarus*, *212*(1), 96–109, doi: 10.1016/j.icarus.2010.12.017.

Grima, C., W. Kofman, J. Mouginot, R. J. Phillips, A. Hérique, D. Biccari, R. Seu, and M. Cutigni (2009), North polar deposits of Mars: Extreme purity of the water ice, *Geophysical Research Letters*, *36*(3), L03203.

Hager, W. H. (1992), *Energy dissipators and hydraulic jump*, Springer.

Hand, B. M. (1974), Supercritical Flow in Density Currents, *Journal of Sedimentary Research*, *44*(3), 637–648, doi: 10.1306/74D72AB3-2B21-11D7-8648000102C1865D.

Hand, B. M., G. V. Middleton, and K. Skipper (1972), ANTIDUNE CROSS-STRATIFICATION IN A TURBIDITE SEQUENCE, CLORIDORME FORMATION,

GASPÉ, QUEBEC, *Sedimentology*, *18*(1-2), 135–138, doi:10.1111/j.1365-3091.1972.tb00009.x.

Head, J. W., J. F. Mustard, M. A. Kreslavsky, R. E. Milliken, and D. R. Marchant (2003), Recent ice ages on Mars, *Nature*, *426*, 797–802.

Herkenhoff, K. E., S. Byrne, P. S. Russell, K. E. Fishbaugh, and A. S. McEwen (2007), Meter-scale morphology of the north polar region of Mars, *Science*, *317*(5845), 1711.

Herkenhoff, K., and J. G. Plaut (2000), Surface Ages and Resurfacing Rates of the Polar Layered Deposits on Mars, *Icarus*, *144*(2), 243–253, doi:10.1006/icar.1999.6287.

Holbrook, W. S., D. Lizarralde, I. A. Pecher, A. R. Gorman, K. L. Hackwith, M. Hornbach, and D. Saffer (2002), Escape of methane gas through sediment waves in a large methane hydrate province, *Geology*, *30*(5), 467–470.

Holt, J. W., K. E. Fishbaugh, S. Byrne, S. Christian, K. Tanaka, P. S. Russell, K. E. Herkenhoff, A. Safaeinili, N. E. Putzig, and R. J. Phillips (2010a), The construction of Chasma Boreale on Mars, *Nature*, *465*(7297), 446–449, doi:10.1038/nature09050.

Holt, J. W., K. E. Fishbaugh, S. Byrne, S. Christian, K. Tanaka, P. S. Russell, K. E. Herkenhoff, A. Safaeinili, N. E. Putzig, and R. J. Phillips (2010b), The construction of Chasma Boreale on Mars, *Nature*, *465*(7297), 446–449.

Holt, J. W., M. E. Peters, S. D. Kempf, D. L. Morse, and D. D. Blankenship (2006), Echo source discrimination in single-pass airborne radar sounding data from the Dry Valleys, Antarctica: Implications for orbital sounding of Mars, *Journal of Geophysical Research-Planets*, *111*(E6), E06S24.

Holt, J. W., A. Safaeinili, J. J. Plaut, J. W. Head, R. J. Phillips, R. Seu, S. D. Kempf, P. Choudhary, D. A. Young, and N. E. Putzig (2008), Radar Sounding Evidence for Buried Glaciers in the Southern Mid-Latitudes of Mars, *Science*, *322*(5905), 1235.

Howard, A. D. (1978), Origin of the stepped topography of the Martian poles, *Icarus*, *34*(3), 581–599.

Howard, A. D. (2000), The Role of Eolian Processes in Forming Surface Features of the Martian Polar Layered Deposits, *Icarus*, *144*(2), 267–288.

Howard, A. D., J. A. Cutts, and K. R. Blasius (1982), Stratigraphic relationships within Martian polar cap deposits, *Icarus*, *50*(2-3), 161–215.

Hvidberg, C. S., K. E. Fishbaugh, M. Winstrup, A. Svensson, S. Byrne, and K. E. Herkenhoff (2012), Reading the climate record of the martian polar layered deposits, *Icarus*, *221*(1), 405–419, doi:10.1016/j.icarus.2012.08.009.

Ivanov, A. B., and D. O. Muhleman (2000), The Role of Sublimation for the Formation of the Northern Ice Cap: Results from the Mars Orbiter Laser Altimeter, *Icarus*, *144*(2), 436–448, doi:10.1006/icar.1999.6304.

Karlsson, N. B., J. W. Holt, and R. C. A. Hindmarsh (2011), Testing for flow in the north polar layered deposits of Mars using radar stratigraphy and a simple 3D ice-flow model, *Geophysical Research Letters*, *38*(24), n/a–n/a, doi: 10.1029/2011GL049630.

Kolb, E. J., and K. L. Tanaka (2001), Geologic History of the Polar Regions of Mars Based on Mars Global Surveyor Data II. Amazonian Period, *Icarus*, *154*(1), 22–39.

Kolb, E. J., and K. L. Tanaka (2006), Accumulation and erosion of south polar layered deposits in the Promethei Lingula region, Planum Australe, Mars, *International Journal of Mars Science and Exploration*, *2*, 1–9.

Kostic, S., and G. Parker (2006), The response of turbidity currents to a canyon–fan transition: internal hydraulic jumps and depositional signatures, *Journal of Hydraulic Research*, *44*(5), 631, doi:10.1080/00221686.2006.9521713.

Kostic, S., O. Sequeiros, B. Spinewine, and G. Parker (2010), Cyclic steps: A phenomenon of supercritical shallow flow from the high mountains to the bottom of the ocean, *Journal of Hydro-environment Research*, *3*(4), 167–172.

Kuenen, P. H. (1951), Properties of turbidity currents of high density, *Turbidity currents and the transportation of coarse sediments to deep water*, 14–33.

Laskar, J., B. Levrard, and J. F. Mustard (2002), Orbital forcing of the Martian polar layered deposits, *Nature*, *419*(6905), 375–377.

Lee, H., B. Edwards, and M. Field (1981), Geotechnical analysis of a submarine slump, Eureka, California, in *Offshore Technology Conference*.

Lee, H. J., J. P. . Syvitski, G. Parker, D. Orange, J. Locat, E. W. . Hutton, and J. Imran (2002), Distinguishing sediment waves from slope failure deposits: field examples, including the'Humboldt slide', and modelling results, *Marine geology*, *192*(1-3), 79–104.

Levrard, B., F. Forget, F. Montmessin, and J. Laskar (2007), Recent formation and evolution of northern Martian polar layered deposits as inferred from a Global Climate Model, *Journal of geophysical research*, *112*(E6), E06012.

Lied, N. T. (1964), Stationary hydraulic jumps in a katabatic flow near Davis, Antarctica, 1961, *Aust. Meteor. Mag*, *47*, 40–51.

Madeleine, J.-B. et al. (2012), Aphelion water-ice cloud mapping and property retrieval using the OMEGA imaging spectrometer onboard Mars Express, *Journal of Geophysical Research (Planets)*, *117*, doi:10.1029/2011JE003940.

Malin, M. C. et al. (1998), Early Views of the Martian Surface from the Mars Orbiter Camera of Mars Global Surveyor, *Science*, *279*(5357), 1681–1685, doi: 10.1126/science.279.5357.1681.

Malin, M. C. et al. (2007), Context Camera Investigation on board the Mars Reconnaissance Orbiter, *Journal of Geophysical Research: Planets*, *112*(E5), n/a–n/a, doi:10.1029/2006JE002808.

Massé, M., O. Bourgeois, S. Le Mouélic, C. Verpoorter, A. Spiga, and L. Le Deit (2012), Wide distribution and glacial origin of polar gypsum on Mars, *Earth and Planetary Science Letters*, *317–318*, 44–55, doi:10.1016/j.epsl.2011.11.035.

McEwen, A. S., E. M. Eliason, J. W. Bergstrom, N. T. Bridges, C. J. Hansen, W. A. Delamere, J. A. Grant, V. C. Gulick, K. E. Herkenhoff, and L. Keszthelyi (2007), Mars reconnaissance orbiter's high resolution imaging science experiment (HiRISE), *Journal of Geophysical Research: Planets (1991–2012)*, *112*(E5).

Migeon, S., B. Savoye, and J. C. Faugeres (2000), Quaternary development of migrating sediment waves in the Var deep-sea fan: distribution, growth pattern, and implication for levee evolution, *Sedimentary Geology*, *133*(3-4), 265–293.

Milkovich, S. M., and J. W. Head (2005a), North polar cap of Mars: Polar layered deposit characterization and identification of a fundamental climate signal, *J. Geophys. Res*, *110*.

Milkovich, S. M., and J. W. Head (2005b), North polar cap of Mars: Polar layered deposit characterization and identification of a fundamental climate signal, *J. Geophys. Res*, *110*.

Milkovich, S. M., and J. J. Plaut (2008), Martian South Polar Layered Deposit stratigraphy and implications for accumulation history, *Journal of Geophysical Research-Planets*, *113*(E6), E06007.

Milkovich, S. M., J. J. Plaut, A. Safaeinili, G. Picardi, R. Seu, and R. J. Phillips (2009), Stratigraphy of Promethei Lingula, south polar layered deposits, Mars, in radar and imaging data sets, *Journal of Geophysical Research-Planets*, *114*(E3), E03002.

Mohrig, D., and J. G. Marr (2003), Constraining the efficiency of turbidity current generation from submarine debris flows and slides using laboratory experiments, *Marine and Petroleum Geology*, *20*(6-8), 883–899, doi:10.1016/j.marpetgeo.2003.03.002.

Montmessin, F., F. Forget, P. Rannou, M. Cabane, and R. M. Haberle (2004), Origin and role of water ice clouds in the Martian water cycle as inferred from a general

circulation model, *J. Geophys. Res.*, *109*(E10), E10004, doi: 10.1029/2004JE002284.

Murray, B. C., L. A. Soderblom, J. A. Cutts, R. P. Sharp, D. J. Milton, and R. B. Leighton (1972), Geological framework of the south polar region of Mars, *Icarus*, *17*(2), 328–345.

Nakajima, T., M. Satoh, and Y. Okamura (1998), Channel-levee complexes, terminal deep-sea fan and sediment wave fields associated with the Toyama Deep-Sea channel system in the Japan Sea, *Marine Geology*, *147*(1-4), 25–41, doi: 10.1016/S0025-3227(97)00137-0.

Neukum, G., and R. Jaumann (2004), HRSC: the High Resolution Stereo Camera of Mars Express, *Mars Express: the Scientific Payload*, *1240*, 17–35.

Ng, F. S. L., and M. T. Zuber (2006a), Patterning instability on the Mars polar ice caps, *Journal of Geophysical Research-Planets*, *111*(E2), E02005.

Ng, F. S. L., and M. T. Zuber (2006b), Patterning instability on the Mars polar ice caps, *Journal of Geophysical Research-Planets*, *111*(E2), E02005.

Nittrouer, C. (2007), *Continental Margin Sedimentation: From Sediment Transportto Sequence Stratigraphy*, International Association of Sedimentologists, John Wiley & Sons, Ltd, Oxford.

Normark, W. R., G. R. Hess, D. A. V. Stow, and A. J. Bowen (1980), Sediment waves on the monterey fan levee: A preliminary physical interpretation, *Marine Geology*, *37*(1-2), 1–18, doi:16/0025-3227(80)90009-2.

Nunes, D. C., and R. J. Phillips (2006), Radar subsurface mapping of the polar layered deposits on Mars, *Journal of Geophysical Research-Planets*, *111*(E6), E06S21.

Ohtsu, I., Y. Yasuda, and H. Gotoh (2001), Hydraulic condition for undular-jump formations, *Journal of Hydraulic Research*, *39*(2), 203–209, doi: 10.1080/00221680109499821.

Parker, G. (1996), Some speculations on the relation between channel morphology and channel-scale flow structures, *Coherent flow structures in open channels*, 429–432.

Parker, G., and N. Izumi (2000), Purely erosional cyclic and solitary steps created by flow over a cohesive bed, *Journal of Fluid Mechanics*, *419*, 203–238.

Pathare, A. V., and D. A. Paige (2005), The effects of martian orbital variations upon the sublimation and relaxation of north polar troughs and scarps, *Icarus*, *174*(2), 419–443.

Pelletier, J. D. (2004), How do spiral troughs form on Mars?, *Geology*, *32*(4), 365–367.

Pettré, P., and J. C. André (1991), Surface-pressure change through Loewe's phenomena and katabatic flow jumps- Study of two cases in Adelie Land, Antarctica, *Journal of the atmospheric sciences*, *48*, 557–571.

Phillips, R. J. et al. (2008a), Mars north polar deposits: Stratigraphy, age, and geodynamical response, *Science*, *320*(5880), 1182.

Phillips, R. J. et al. (2011a), Massive CO2 ice deposits sequestered in the south polar layered deposits of Mars, *Science*, *332*(6031), 838–841.

Phillips, R. J. et al. (2011b), Massive CO2 Ice Deposits Sequestered in the South Polar Layered Deposits of Mars, *Science*, *332*(6031), 838–841, doi:10.1126/science.1203091.

Phillips, R. J., M. T. Zuber, S. E. Smrekar, M. T. Mellon, J. W. Head, K. L. Tanaka, N. E. Putzig, S. M. Milkovich, B. A. Campbell, and J. J. Plaut (2008b), Mars North Polar Deposits: Stratigraphy, Age, and Geodynamical Response, *Science*, *320*(5880), 1182.

Picardi, G., J. J. Plaut, D. Biccari, O. Bombaci, D. Calabrese, M. Cartacci, A. Cicchetti, S. M. Clifford, P. Edenhofer, and W. M. Farrell (2005), Radar soundings of the subsurface of Mars, *Science*, *310*(5756), 1925–1928.

Putzig, N. E., R. J. Phillips, B. A. Campbell, J. W. Holt, J. J. Plaut, L. M. Carter, A. F. Egan, F. Bernardini, A. Safaeinili, and R. Seu (2009), Subsurface structure of Planum Boreum from Mars Reconnaissance Orbiter shallow radar soundings, *Icarus*, *204*(2), 443–457.

Reid, L. M. (1989), Channel incision by surface runoff in grassland catchments, University of Washington.

Rodriguez, J. A. P., and K. L. Tanaka (2011), Evidence for In-Situ Trough Erosion in Planum Boreum, Mars, *Fifth International Conference on Mars Polar Science and Exploration*, *1323*, 6015.

Seu, R., R. J. Phillips, G. Alberti, D. Biccari, F. Bonaventura, M. Bortone, D. Calabrese, B. A. Campbell, M. Cartacci, and L. M. Carter (2007a), Accumulation and Erosion of Mars' South Polar Layered Deposits, *Science*, *317*(5845), 1715.

Seu, R., R. J. Phillips, D. Biccari, R. Orosei, A. Masdea, G. Picardi, A. Safaeinili, B. A. Campbell, J. J. Plaut, and L. Marinangeli (2007b), SHARAD sounding radar on the Mars Reconnaissance Orbiter, *Journal of Geophysical Research-Planets*, *112*(E5), E05S05.

Seu, R., R. J. Phillips, D. Biccari, R. Orosei, A. Masdea, G. Picardi, A. Safaeinili, B. A. Campbell, J. J. Plaut, and L. Marinangeli (2007c), SHARAD sounding radar on the Mars Reconnaissance Orbiter, *Journal of geophysical research*, *112*(E5), E05S05.

Smith, D. E., M. T. Zuber, H. V. Frey, J. B. Garvin, J. W. Head, D. O. Muhleman, G. H. Pettengill, R. J. Phillips, S. C. Solomon, and H. J. Zwally (2001), Mars Orbiter Laser Altimeter: Experiment summary after the first year of global mapping of Mars, *Journal of Geophysical Research-Planets*, *106*(E10).

Smith, D. E., M. T. Zuber, S. C. Solomon, R. J. Phillips, J. W. Head, J. B. Garvin, W. B. Banerdt, D. O. Muhleman, G. H. Pettengill, and G. A. Neumann (1999), The global topography of Mars and implications for surface evolution, *Science*, *284*(5419), 1495.

Smith, I. B., and J. W. Holt (in prep), SHARAD detection of regional spiral trough diversity,

Smith, I. B., and J. W. Holt (2010), Onset and migration of spiral troughs on Mars revealed by orbital radar, *Nature*, *465*(7297), 450–453, doi:10.1038/nature09049.

Smith, I. B., and J. W. Holt (2011), Implications for Current and Past atmospheric Conditions of Mars from Radar Stratigraphic Studies of Spiral Troughs in the North Polar Layered Deposits, in *Mars Atmosphere: Modelling and observation*, vol. -1, pp. 439–442.

Smith, I. B., J. W. Holt, A. Spiga, and A. D. Howard (2013), Aeolian Processes as Drivers of Landform Evolution on the South Pole of Mars, *LPSC 44*, *Abst. 1240*.

Smith, I. B., J. W. Holt, A. Spiga, A. D. Howard, and G. Parker (in review), The Spiral Troughs of the Mars Polar Layered Deposits as Cyclic Steps, *Journal of Geophysical Research: Planets*.

Soderblom, L. A., M. C. Malin, B. Murray, and J. Cutts (1973), Mariner 9 observations of the surface of Mars in the north polar region, *Journal of Geophysical Research*, *78*(20), 4197–4210.

Spiga, A. (2011), Elements of comparison between Martian and terrestrial mesoscale meteorological phenomena: Katabatic winds and boundary layer convection, *Planetary and Space Science*, *59*(10), 915–922, doi:10.1016/j.pss.2010.04.025.

Spiga, A., and F. Forget (2009), A new model to simulate the Martian mesoscale and microscale atmospheric circulation: Validation and first results, *J. Geophys. Res.*, *114*(E2), E02009, doi:10.1029/2008JE003242.

Spiga, A., F. Forget, J. B. Madeleine, L. Montabone, S. R. Lewis, and E. Millour (2011), The impact of martian mesoscale winds on surface temperature and on the determination of thermal inertia, *Icarus*.

Spinewine, B., O. E. Sequeiros, M. H. Garcia, R. T. Beaubouef, T. Sun, B. Savoye, and G. Parker (2009), Experiments on Wedge-Shaped Deep Sea Sedimentary

Deposits in Minibasins and/or on Channel Levees Emplaced by Turbidity Currents. Part II. Morphodynamic Evolution of the Wedge and of the Associated Bedforms, *Journal of Sedimentary Research*, *79*(8), 608 –628, doi: 10.2110/jsr.2009.065.

Squyres, S. W. (1979), The evolution of dust deposits in the Martian north polar region, *Icarus*, *40*(2), 244–261.

Sun, T., and G. Parker (2005), Transportational cyclic steps created by flow over an erodible bed. Part 2. Theory and numerical simulation, *Journal of Hydraulic Research*, *43*(5), 502–514.

Swithinbank, C., K. Brunk, and J. Sievers (1988), A glaciological map of Filchner-Ronne ice shelf, Antarctica, *Annals of glaciology*, *11*, 150–155.

Taki, K., and G. Parker (2005), Transportational cyclic steps created by flow over an erodible bed. Part 1. Experiments, *Journal of Hydraulic Research*, *43*(5), 488, doi:10.1080/00221680509500147.

Tanaka, K. L., and C. M. Fortezzo (2012), Geologic map of the north polar region of Mars: U.S. Geological Survey Scientific Investigations Map 3177, [online]

Tanaka, K. L., J. A. P. Rodriguez, J. A. Skinner, M. C. Bourke, C. M. Fortezzo, K. E. Herkenhoff, E. J. Kolb, and C. H. Okubo (2008), North polar region of Mars: Advances in stratigraphy, structure, and erosional modification, *Icarus*, *196*(2), 318–358.

Toon, O., G. Ferry, R. P. Turco, J. Jordan, and J. Goodman (1989), Physical processes in polar stratospheric ice clouds, *Journal of Geophysical Research*, *94*(D9), 11–359.

Turner, J. S. (1979), *Buoyancy effects in fluids*, Cambridge University Press. [online]

Tyler, D. J., and J. R. Barnes (2005), A mesoscale model study of summertime atmospheric circulations in the north polar region of Mars, *J. Geophys. Res.*, *110*(E6), E06007, doi:10.1029/2004JE002356.

Warner, N. H., and J. D. Farmer (2008), Importance of aeolian processes in the origin of the north polar chasmata, Mars, *Icarus*, *196*(2), 368–384.

Weijermars, R. (1986), The polar spirals of Mars may be due to glacier surges deflected by Coriolis forces, *Earth and Planetary Science Letters (ISSN*, *76*(3-4), 227–240.

Whiteway, J. A. et al. (2009), Mars water-ice clouds and precipitation, *Science*, *325*(5936), 68.

Winebrenner, D. P., M. R. Koutnik, E. D. Waddington, A. V. Pathare, B. C. Murray, S. Byrne, and J. L. Bamber (2008), Evidence for ice flow prior to trough

formation in the martian north polar layered deposits, *Icarus*, *195*(1), 90–105.

Winterwerp, J. C., W. T. Bakker, D. R. Mastbergen, and H. van Rossum (1992), Hyperconcentrated sand-water mixture flows over erodible bed, *Journal of Hydraulic Engineering*, *118*(11), 1508–1525.

Yokokawa, M., K. Okuno, A. Nakamura, T. Muto, Y. Miyata, H. Naruse, and G. Parker (2009), Aggradational cyclic steps: sedimentary structures found in flume experiments, in *Proceedings of the 33rd IAHR Biennial Congress*, pp. 5547–5554.

Zammett, R. J., and A. C. Fowler (2007), Katabatic winds on ice sheets: A refinement of the Prandtl model, *Journal of the atmospheric sciences*, *64*(7), 2707–2716.

Zeng, Z., N. E. Putzig, H. Xie, S. J. Birnbaum, S. F. Ackely, and L. Liu (2008a), Evidence of Fractures in NPLD and Their Significance to the Formation of Martian Polar Spiral Troughs, in *Lunar and Planetary Institute Science Conference Abstracts*, vol. 39, p. 2179.

Zeng, Z., N. E. Putzig, H. Xie, S. J. Birnbaum, S. F. Ackely, and L. Liu (2008b), Evidence of Fractures in NPLD and Their Significance to the Formation of Martian Polar Spiral Troughs., *Anon. 39th LPSC. League City: LPI*, *2179*.